DUAL MECHANISM NONLINEAR RESPONSE OF SELECTED METAL ORGANIC CHROMOPHORES

By

JOHN D. PEAK

A DISSERTATION PRESENTED TO THE GRADUATE SCHOOL
OF THE UNIVERSITY OF FLORIDA IN PARTIAL FULFILLMENT
OF THE REQUIREMENTS FOR THE DEGREE OF
DOCTOR OF PHILOSOPHY

UNIVERSITY OF FLORIDA

2007

Report Documentation Page

Form Approved
OMB No. 0704-0188

1. REPORT DATE	2. REPORT TYPE	3. DATES COVERED
01 OCT 2007	**N/A**	**-**

4. TITLE AND SUBTITLE	5a. CONTRACT NUMBER
Dual Mechanism Nonlinear Response Of Selected Metal Organic Chromophores	5b. GRANT NUMBER
	5c. PROGRAM ELEMENT NUMBER
6. AUTHOR(S)	5d. PROJECT NUMBER
	5e. TASK NUMBER
	5f. WORK UNIT NUMBER
7. PERFORMING ORGANIZATION NAME(S) AND ADDRESS(ES) **University Of Florida**	8. PERFORMING ORGANIZATION REPORT NUMBER
9. SPONSORING/MONITORING AGENCY NAME(S) AND ADDRESS(ES) **AFIT/ENEL WPAFB, OH**	10. SPONSOR/MONITOR'S ACRONYM(S)
	11. SPONSOR/MONITOR'S REPORT NUMBER(S)

12. DISTRIBUTION/AVAILABILITY STATEMENT
Approved for public release, distribution unlimited

13. SUPPLEMENTARY NOTES

14. ABSTRACT

15. SUBJECT TERMS

16. SECURITY CLASSIFICATION OF:			17. LIMITATION OF ABSTRACT	18. NUMBER OF PAGES	19a. NAME OF RESPONSIBLE PERSON
a. REPORT	b. ABSTRACT	c. THIS PAGE			
unclassified	**unclassified**	**unclassified**	**UU**	**145**	

Standard Form 298 (Rev. 8-98)
Prescribed by ANSI Std Z39-18

The views expressed in this dissertation are those of the author and do not reflect the official policy or position of the United States Air Force, Department of Defense, or the U.S. Government.

This dissertation is dedicated to Cameron and Kelsey for their unconditional love and support

ACKNOWLEDGMENTS

First, I would like to acknowledge Cameron and Kelsey. I am extremely blessed to have two such wonderful children. Being apart from you for so long while completing this part of my education was not easy. Both of you have grown fast and have matured well beyond your years. I am very proud of you both. To my parents, I know you don't really understand what I do or why I do it, but you have always freely given your prayers and provided moral support for my success. It is for that faith in me that I thank you. You always said I could be anything I wanted to be and I have truly appreciated that freedom of choice. I promise that you will be the first to know when I figure out what I want to be.

A special thanks to Dr. Sophie Klein for her friendship and assistance in the preparation of this dissertation, without your help, understanding and excellent salads I never would have been able to finish.

Lastly, I cannot thank Dr. Kirk Schanze enough for his mentorship throughout this project. It was refreshing to work for and with a professional of such high caliber. Without your guidance and extreme patience, I never would have been able to complete such a demanding task.

TABLE OF CONTENTS

page

LIST OF TABLES

LIST OF FIGURES

Abstract of Dissertation Presented to the Graduate School
of the University of Florida in Partial Fulfillment of the
Requirements for the Degree of Doctor of Philosophy

DUAL MECHANISM NONLINEAR RESPONSE OF SELECTED METAL ORGANIC CHROMOPHORES

By

John D. Peak

December 2007

Chair: Kirk S. Schanze
Major: Chemistry

The goal for the research described herein is the development of a series of transition metal based metal organic chromophores that display both two-photon and excited state absorption (TPA/ESA) character. With this goal in mind, we present the preparation and photophysical characterization for a series of metal-organic chromophores containing a two photon absorbing bipyridine core combined with a transition metal component which yields a long-lived triplet excited state. The combination of these two photophysical properties represents a dual mode nonlinear optical (NLO) mechanism.

Three major areas of interest for this project are addressed here. First, to develop and instrument an in-house photophysical apparatus with the ability to evaluate and measure two photon activity as well as detect nonlinear optical responses. Second, to synthesize, characterize and evaluate an all organic chromophore system, centered on a bipyridine core, which utilizes known TPA architecture. Lastly, to synthesize, characterize and evaluate the metal organic analogs of the TPA chromophore system utilizing transition metals with high spin-orbit coupling values which help create long-lived triplet excited states leading to a possible ESA. The metal-organic analogs in turn should exhibit a dual mechanism for NLO response comprised of both TPA and ESA.

CHAPTER 1
PHOTOPHYSICAL BACKGROUND

Introduction

The major focus of this work is the synthesis and photophysical investigation of a series of transition metal based metal-organic chromophores with the potential to exhibit a dual mode nonlinear optical response mechanism. A system utilizing a dual mode nonlinear response will ideally incorporate the advantages of two separate nonlinear pathways while diminishing the drawbacks of each. A recent publication from our group presented this dual mechanism nonlinear absorption for a transition metal centered metal-organic complex and can be thought of as a proof of concept.[1] The nonlinear absorbing pathways utilized to obtain the dual mechanism nonlinear response are the same as those utilized herein, those being two photon absorption and reverse saturable absorption.

As background for the work presented in this dissertation, the following subjects are reviewed in this chapter: (1) basic photophysical properties of ruthenium polypyridine complexes; (2) the photophysical effects for substitution of bipyridine in metal-polypyridine complexes; (3) basic nonlinear optical processes; (4) structure-property relationships of nonlinear absorption as it relates to two photon absorption and reverse saturable absorption.

Basic Photophysical Properties of Ruthenium Polypyridine Complexes

Ruthenium(II) polypyridine complexes are molecules in which ruthenium is in a d^6 electron configuration and is complexed with three neutral bidentate bipyridine ligands and configured in an octahedral symmetry. The simplest and most widely studied compound of this category is the complex $Ru(bpy)_3^{2+}$ (bpy = 2,2′-bipyridine).[2-7] Discussion of the basic photophysical properties of $Ru(bpy)_3^{2+}$ is deemed beneficial in understanding other ruthenium polypyridine complexes as well as systems with similar electronic and structural configurations.

These common features can be exploited in predicting and interpreting excited-state photophysical properties across the transition metal family for the metal-polypyridine architecture. Keeping in mind the goal of exploring the nonlinear nature of a select series of metal-organic complexes, a general understanding the nature of the excited state manifold of these systems is desirable.

Electronically Excited States of $Ru(bpy)_3^{2+}$

Examination of the ground and excited states of $Ru(bpy)_3^{2+}$ primarily concerns the involvement of the π-bonding and π*-antibonding orbitals centered on the bipyridine ligands and the 4d orbitals of the ruthenium metal center. For ruthenium, the dπ (t_{2g}) and dσ (e_g) levels of the 4d orbitals are of particular interest. When in the ground state, only the bipyridine π-bonding and ruthenium dπ are filled. A representative molecular orbital diagram is shown in Figure 1-1 for a typical d^6-polypyridine complex.

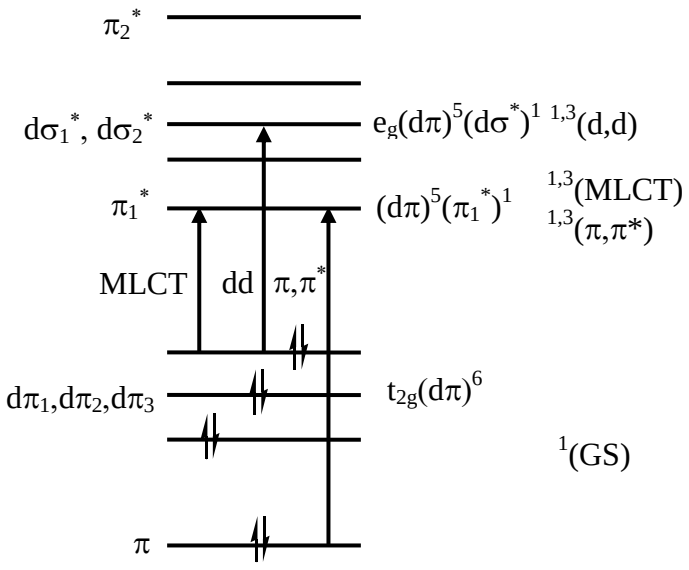

Figure 1-1. Simplified molecular orbital diagram for a d^6 metal complex of octahedral symmetry with representative energy transitions from a ground state to potential excited states.

Excited states for a system of these types may be manifested in three distinctly separate ways: (1) a metal-centered d-d ligand field transition; (2) a relatively high energy intraligand π-π* transition; and (3) a metal-to-ligand charge transfer (MLCT) configuration from a dπ to π* transition. The first type of transition, the metal-centered d-d ligand field transition, is a weak ($\varepsilon \approx 100\ M^{-1}\ cm^{-1}$) Laporte forbidden absorption. This symmetry forbidden ($t \rightarrow e$) transition would lead to a short-lived excited state that would be present in a low energy region and should not be a prominent feature to our discussion. The relatively high energy ligand centered π-π* transition is obtained through the promotion of an electron from a π orbital to a π* orbital which is localized on a single bipyridine ligand.[8] The energies of these transitions vary only slightly as the metal and its oxidation state are changed and occur around 300 nm (π-π_1*) and 240 nm (π-π_2*) with very large molar absorptivity values. The final type of excited state involves the promotion of an electron from a dπ (t_{2g}) metal orbital to a ligand centered π* antibonding orbital

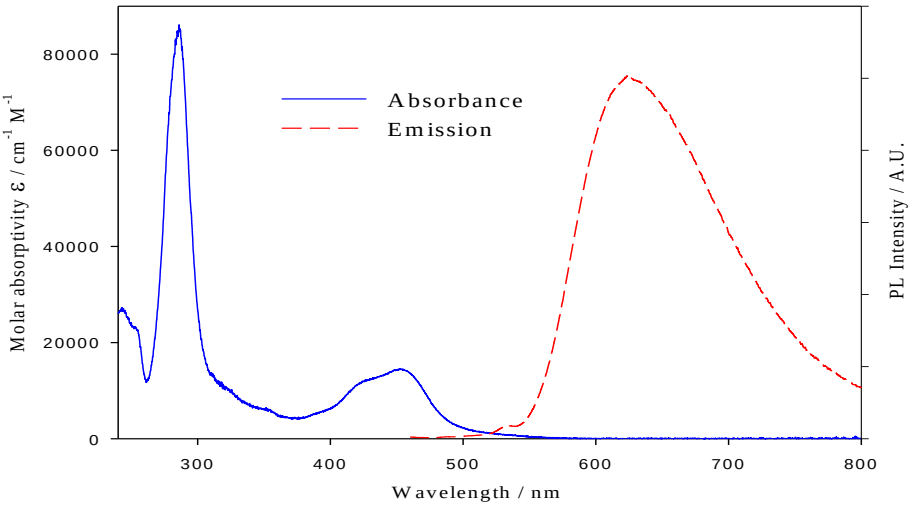

Figure 1-2. UV-visible absorption and emission spectra of tris-(2,2′-bipyridyl) ruthenium(II) in water (λ_{ex} - 450 nm).[10]

and is considered a symmetry allowed MLCT transition with moderate molar absorptivity ($\varepsilon \approx$ 15,000 M^{-1} cm^{-1}).[9]

For $Ru(bpy)_3^{2+}$, the excited states that have been shown to occur are π-π^* and MLCT in nature. In the UV-visible spectrum of $Ru(bpy)_3^{2+}$, a relatively weak absorption above 500 nm is observed as well as a broad emission centered around 600 nm. (Figure 1-2) Both features have been clearly assigned to a spin forbidden charge transfer (^{3}MLCT) excited state.[3, 11-14] ^{3}MLCT character is attributed to the interactions of the dπ (t_{2g}) orbital of the metal and the π^* orbital of the ligand. These orbital interactions combined with a large spin-orbit coupling of ruthenium lead to efficient singlet to triplet state conversion. Broadness in the emission spectrum is attributed to the emission emanating from a manifold of spin-orbit coupled triplet states rather than a single triplet state. Excitation of $Ru(bpy)_3^{2+}$ to an allowed singlet excited state is quickly followed by efficient intersystem crossing to a triplet excited state (less than 300 fs) with a lifetime of approximately 600 ns.[15] In this complex and systems like it, the intersystem crossing yields, brought about by spin-orbit coupling, are very high, often assumed to be unity.

Photophysical Effects of Substitution in Metal-Polypyridine Complexes

Photophysical investigation of metal containing polypyridine complexes as well as their non-metallated counterparts has taken place since the 1990's by groups such as Wang and Wasielewski, Yellowless *et al*., as well as the Schanze group.[8, 16, 17] Detailed studies of the photophysical effects of substitution of the bipyridine backbone as well as the effects generated from the change of the coordinating metal in these polypyridine systems have elucidated much about the complexity of their excited state manifolds. These studies have incorporated the tris-(2,2'-bipyridyl)-metal moiety into conjugated organic molecules and polymers and have yielded compounds with varied photophysical characteristics. Among the key methods in determining

the substitution effects that have been investigated are absorption and emission spectra which elucidates changes in ground state electronic nature as well as their transient absorption spectrum which are utilized to reveal the electronic nature of the excited states.

A key detail of the work that has been performed by previous group members is the determination of the nature of the interaction between π-conjugated bipyridine systems and MLCT chromophores with regard to the photophysics of substituted systems.[18, 19] The main focus of several of the studies was the equilibrium between the ^{3}MLCT generated by dπ-π* charge transfer of the metal to ligand and the ligand centered ^{3}π-π* states.

Through investigations from our group it was found that addition of electron withdrawing substituent groups to bipyridine could sufficiently influence the LUMO energies of the ligand-centered π* orbitals and provide the possibility for the reduction of MLCT excited state energy relative to the ^{3}π–π* state. The basis for this reasoning is that the excited electron would be promoted to the lowest energy electron acceptor and, if bipyridine is provided with a strong enough electron withdrawing groups, in the proper position, energy transfer would tend toward the lower energy MLCT excited state. It has also been found that the MLCT energy can be lowered by modifying the position of the substituent on the bipyridine ring [20] as well as changing the coordinated metal chromophore.[9]

A comprehensive photophysical study of substituent position on the bipyridine ligand core with regard to excited state energies has been conducted by our group which revealed a significant positional impact on both electron delocalization and MLCT excited state energy.[20] For the ruthenium(II)-bipyridine system containing identical phenyleneethynylene (PE) substituents containing electron withdrawing groups (Figure 1-1) in the 4,4′ and 5,5′ positions, several major findings were noted. First, the lowest excited state transition was definitely based

on a dπ(Ru)→π* metal-to-ligand charge transfer. Second, evidence supported the conclusion that the excited electron in the MLCT state was significantly

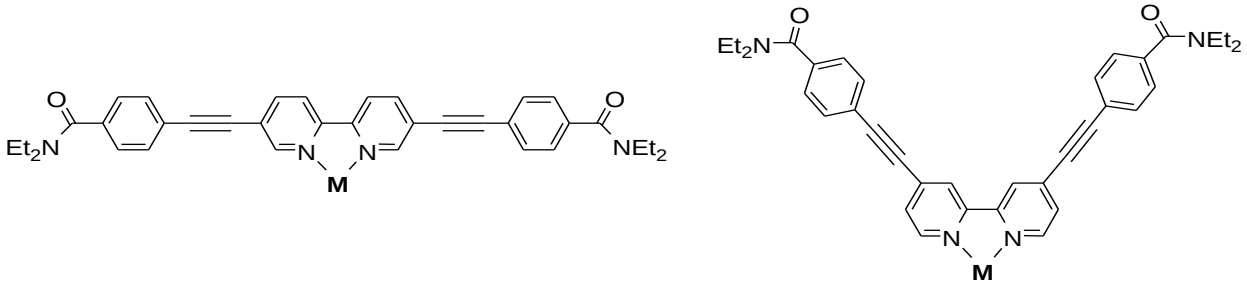

Figure 1-3. Ruthenium(II)-bipyridine complexes substituted in the 4,4′ and 5,5′ positions. **M**=$Ru(bpy)_2^{2+}$, counterion = PF_6^-.

delocalized into the PE substituent. Furthermore, data supported the counterintuitive conclusion that the extent of delocalization was greater in the 4,4′-substituted positions of the bipyridine. However, it was also found that for the 5,5′-substituted system the energy of the LUMO level was lower, which would indicate a larger intraligand delocalization. This conclusion would seem to follow the logical consequence of a conjugation enhancing para-substituted architecture. In fact, the oscillator strength of the MLCT transition in the 4,4′-substituted complex was found to be significantly stronger than that of the 5,5′-substituted and parent $Ru(bpy)_3^{2+}$ systems. This implies a larger overall transition dipole for the 4,4′-substituted system. For the 5,5′-substituted system it is important to note that the overall transition dipole is not expected to be enhanced by conjugation into the PE substituent since the axis of conjugation is perpendicular to that of the MLCT transition dipole. This perpendicular transition dipole orientation of the 5,5′-substituted system is a key factor for its choice as a potential third-order nonlinear material and will be discussed in subsequent sections. Overall, the definitive conclusion was reached by molecular orbital calculations which implied the extent of delocalization in the MLCT state was directly related to efficiency of the overlap of the low-energy π* orbital localized on the ligand and the d

orbitals of the metal. This overlap was strongly dependent on the size of the π* orbital coefficients of the nitrogen in the bipyridine which were in turn affected by the pattern of substitution of the bipyridine units.

In separate follow on studies, the influence of altering the coordinating metal center on the nature of the excited state was examined.[21, 22] Electron donating (bis)dimethoxy-substituted PE 5,5′ bipyridine ligands (Figure 1-2) were independently studied to examine the nature of the excited state manifolds utilizing a series of transition metals which included Ru, Re and Ir. It was determined the ^{3}π-π* and ^{3}MLCT levels were very close in energy and the nature of the metal center did have a slight effect on which triplet state has the lowest energy. However, in all

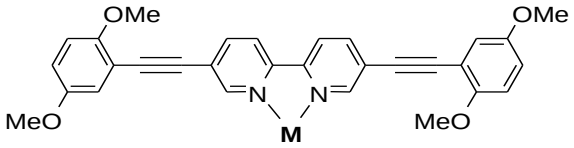

Figure 1-4. 5-5′ bipyridine complexes containing a series of transition metals. **M**=$Ru(bpy)_2^{2+}$, $ReCO_3Cl$, $Ir(ppy)_2^+$, counterion = PF_6^-(where applicable).

cases moderately increasing the conjugation length of the associated ligand served to effectively lower the ^{3}π-π* excited state energy to a level at or below the excited state energy of the ^{3}MLCT excited state. Overall, it was noted that the excited state nature was photophysically very similar regardless of whether the lowest excited state energy was ^{3}π-π* or ^{3}MLCT. Key differences, as noted in these studies, in the determination of the lowest excited state being either ^{3}π-π* or ^{3}MLCT are: (1) the presence, placement and strength of a transient absorption (TA) band in the visible region around 500-520 nm associated with ^{3}MLCT and (2) the presence and magnitude of a broad transient absorption in the near-IR in the region beyond 700 nm associated with ^{3}π-π*.

In the case of the three metal complexes of the ligand shown in Figure 1-4 a strong and relatively narrow TA band was present in the region of 500-520 nm and a significantly weaker

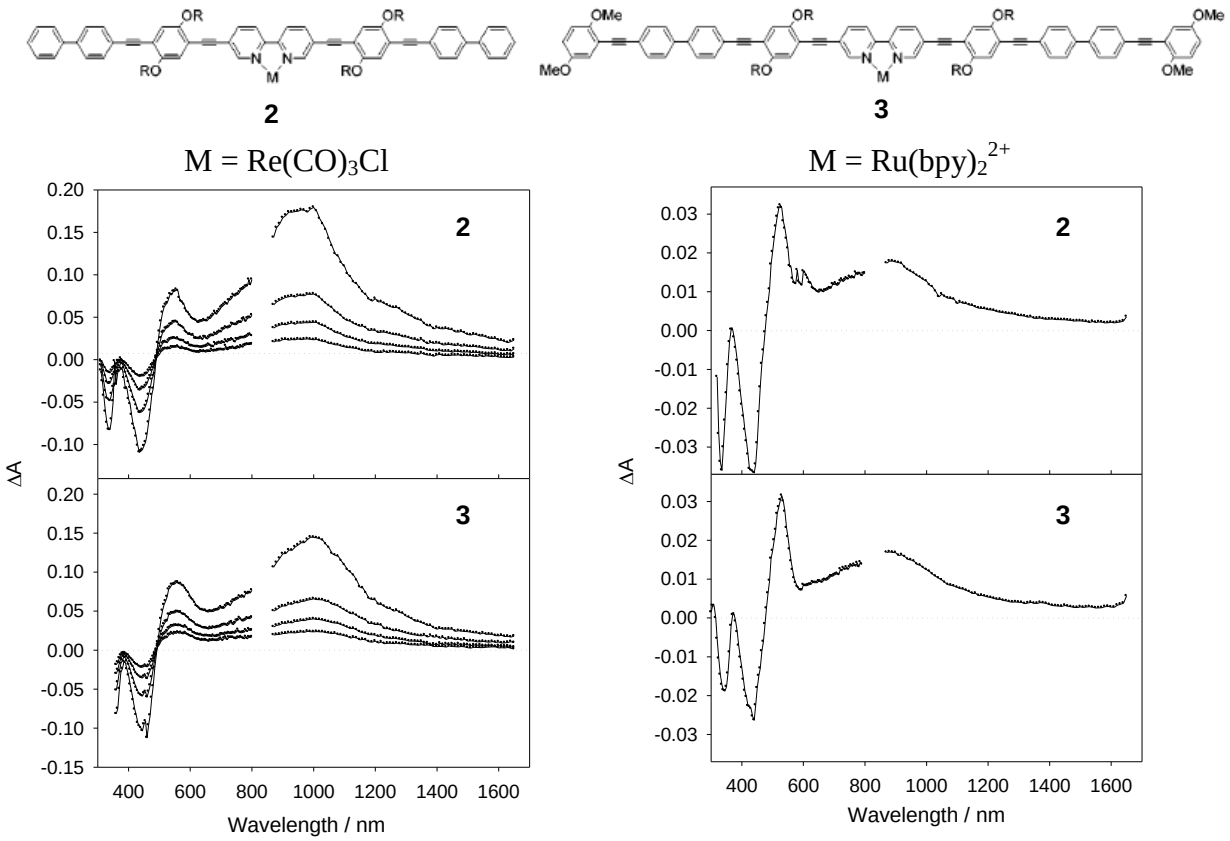

Figure 1-5. Near UV/visible/near-infrared transient absorption spectra of metal complexes of oligo(arylene ethynylene) ligands **2** and **3**. Left: metal complex is $-Re(CO)_3Cl$; right: metal complex is $Ru(bpy)_2^{2+}$.

excited state absorbance was observed beyond 700 nm in the near-IR region. In Figure 1-5, conjugation extended forms of the ligand bound to Re (left) exhibit TA spectra with prominent near-IR absorption and a less pronounced visible absorption. In contrast, for the same ligands bound to Ru (right) exhibit prominent visible absorbance which is narrower and a near-IR absorption that is blue shifted and much weaker. These complexes were selected because in previous work it has been demonstrated that when M = $-Re(CO)_3Cl$ the lowest excited state is OAE-based $^3\pi,\pi^*$, whereas when M = $-Ru(bpy)_2^{2+}$ the lowest state is MLCT.[23] These experiments show quite clearly that, at least for the family of bipyridine-substituted oligo(arylene

ethynylene)s, the $^3\pi,\pi^*$ state can be identified on the basis of the strong near-infrared transient absorption. Also in these same studies, when conjugation was extended there was a lowering in the $^3\pi$-π^* excited state energy. The energy decrease was enough to bring it on par with that of the ^{3}MLCT excited state energy. The conclusion reached was that the triplet excited state absorptions for the systems and others of similar architecture could be attributed to a triplet manifold where both $^3\pi$-π^* and ^{3}MLCT excited states are in energetic equilibrium (Figure 1-6).

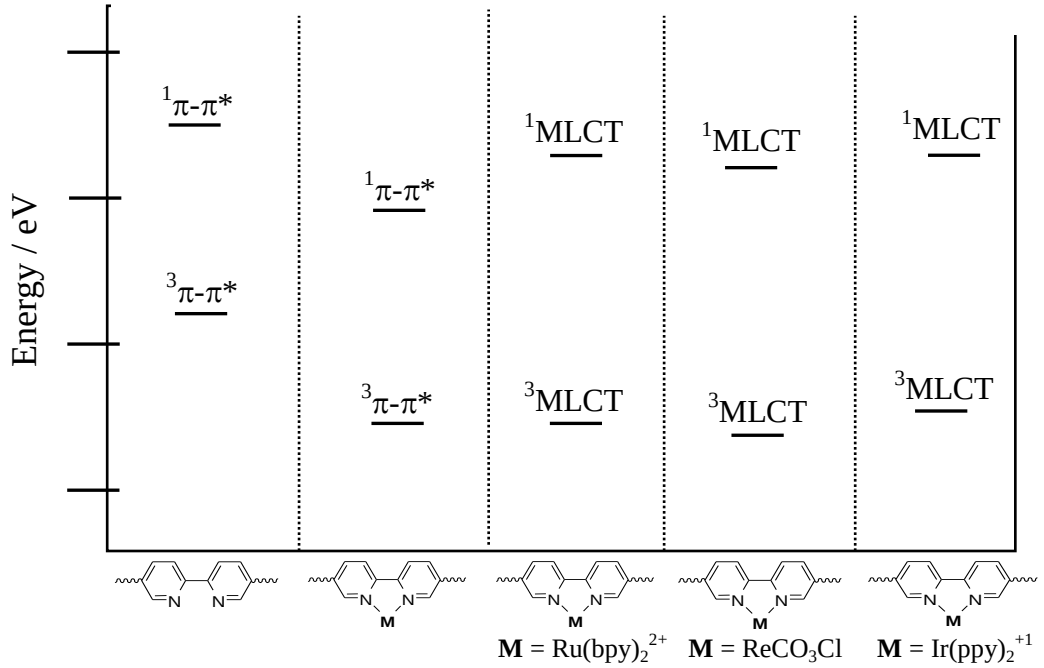

Figure 1-6. Jablonski diagram of relative energies for excited states of π-π^* in a free ligand and metallated ligand, and MLCT excited states of Re, Ru and Ir complexes.

Even though the understanding of the intricacies of this equilibrium is not critical for the success of this project, the background that has been provided has been extremely useful in understanding the basic photophysical nuances of the excited states being studied and utilized herein. Whereas in previous studies it was desirable to attempt to energetically separate the ^{3}MLCT and $^3\pi$–π^* states to allow for independent excited state manifold examination, in this

study, a combination or overlap of excited states into an equilibrated manifold is not problematic and, as will be discussed in the next chapter, can be considered a benefit.

Nonlinear Optical Mechanisms

Two Photon Absorption

Two photon absorption occurs when a molecule simultaneously absorbs two photons of lower energy whose energy sum is equivalent to the energy needed to produce an excited state equivalent to one photon absorption. (Figure 1-7a) TPA does not require the material to exhibit ground state

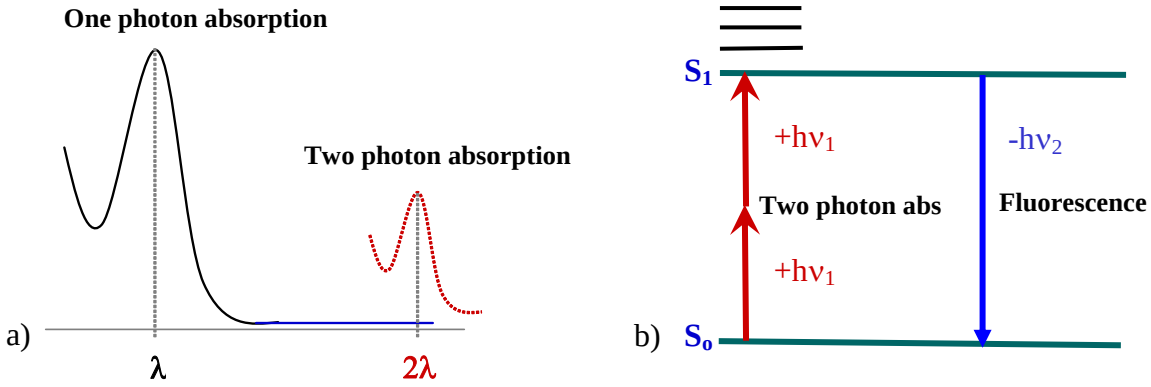

Figure 1-7. a) Illustration of two-photon absorption from a region with zero ground state absorption. b) Jablonski diagram visualizing two-photon absorption.

absorption at the two photon active wavelength, however it does require a high photon flux. (Figure 1-7b) For a material with no ground state absorption at the two photon active wavelength, it will remain optically transparent at low photon intensities. At high photon flux, however, a two photon active chromophore can access one photon excited states without being subjected to the energy absorption associated with a one photon transition, thus limiting potential damage to the material.

Considerable interest in the development of two photon absorbing (TPA) materials has grown in the past decade and significant advances in the design of these materials have been recently made, but it is thought that there is still progress that can be made.[24] Le Bozec[25] and Prasad[26] have extensively studied the enhanced TPA nonlinear optical (NLO) properties of π-conjugated transition metal-organic complexes containing 2,2′-bipyridine and 1,10-phenanthroline based chromophores. In these studies it was found the metal plays several important roles contributing to increased NLO activity. First, the metal is a template to configure ligands in a predictable octupolar arrangement. Second, the metal can induce a low-energy metal to ligand charge-transfer (MLCT) transition. Third, the Lewis acid character of the metal can induce a strong intraligand charge-transfer (ILCT) transition that is red-shifted from the free ligand. With the addition of an MLCT transition and a red-shift of the ILCT transition, enhanced two photon activity was achieved in the far-red and near-IR regions where the complexes are transparent. Several series of π-conjugated metal-organic chromophores containing similar polypyridine architectures have been synthesized by our group and have the potential to display enhanced two photon absorption.[9, 21] With a project goal for this research being the development of a series of transition metal based metal-organic chromophores that simultaneously display both two-photon and excited state absorption (TPA/ESA) in a dual mode nonlinear response; these studies provide the base model for the metal-organic chromophores to be studied.

To further enhance the TPA character of the proposed organic chromophore, recent work revealing important structure-property relationships leading to high TPA cross sections was utilized.[27-33] Chromophores containing both electron donating and electron accepting moieties, linked by a π-conjugated bridge which is polarizable, have been shown to display very large

TPA cross sections.[34] Over the past decade different arrangements of these key elements have been explored with the intention of maximizing the overall TPA cross section of the

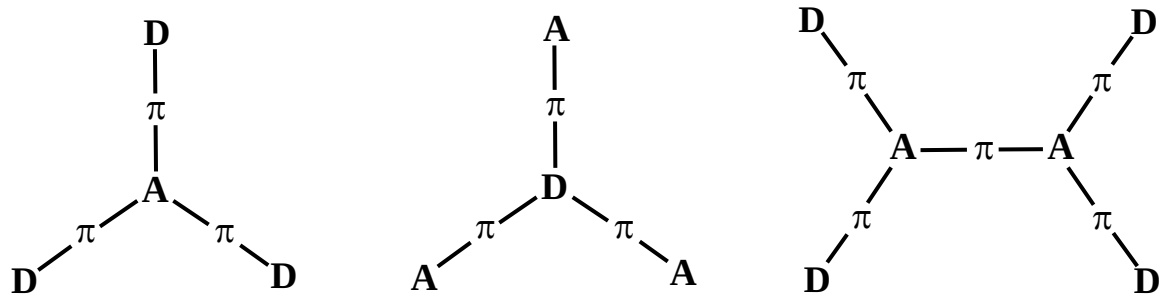

D = donor species, **A** = acceptor species, **π** = conjugated link

Figure 1-8. General chromophore structures which exhibit high TPA cross sections.

chromophore.[27-33] Essential structural elements of the architecture of these compounds, which lead to a high TPA cross section, are the presence of donor and/or acceptor units separated by a highly polarizable π-conjugated bridge. As shown in Figure 1-8, the arrangement can vary from, but not limited to, donor-π-acceptor, acceptor-π-donor and donor-π-donor.

An example of a structure which has proven to exhibit a large TPA cross section (σ) in the near-infrared and that followed this morphology is shown in Figure 1-9. It has also been suggested the branching contained in these compounds provides a cooperative interaction between the donor and acceptor units giving rise to an overall enhancement in the performance of the chromophore.[24, 35, 36]

The configuration for the organic chromophore used in this project (Figure 1-11) contains an electron donating species on the periphery linked to a central electron accepting core by a polarizable π-conjugated bridge. Using the nomenclature discussed above this would be referred to as a donor-π-acceptor-π-donor chromophore. The electronic configuration of this compound is designed to "funnel" absorbed energy to the central core of the chromophore.

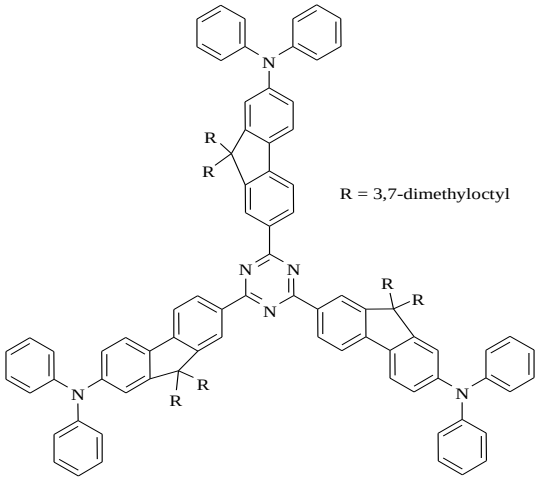

Figure 1-9. High cross section TPA chromophore AF-455.[24]

Excited State Absorption

Enhancement of nonlinear activity with the addition of excited state absorption in a multiphoton process has been effectively demonstrated in recent studies conducted by Silly,[34] Sutherland[37] and Gao.[38] By combining a large one photon excited state cross section with a large TPA cross section in the same regions of the visible or near-IR, a cumulative multiphoton nonlinear absorption is generated (Figure 1-10). This dual mode nonlinear process can achieve high transparency in at low intensities while maintaining efficient and instantaneous protection from high intensity light. For this project a further nonlinear enhancement through the incorporation of a strongly absorbing and long-lived excited state is desired. This synergistic combination of instantaneous response and long-lived nonlinear absorption is ideal for optical limiting.

Oligomers and polymers incorporating transition metals have been synthesized in an attempt to take advantage of the metal's spin-orbit coupling ability to enhance the rate of intersystem crossing to generate long-lived triplet excited states. Several of the transition metals used are ruthenium, rhenium, osmium, iridium and platinum. In these compounds the photophysical properties are dominated by a long-lived triplet excited state which are strongly

absorbing. Materials such as these, if modified to include an NLO chromophore, have the potential to display nonlinear absorption enhanced from an excited state absorption (ESA) mechanism. For ESA to be most effective at enhancing an NLO response, a strongly absorbing excited state must be rapidly and efficiently generated.

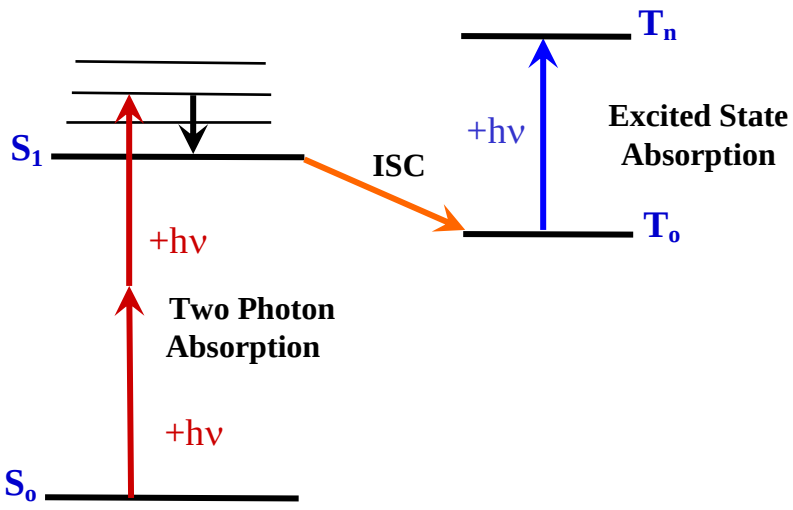

Figure 1-10. Jablonski diagram of a dual mode nonlinear absorption (TPA/ESA) mechanism.

Again, several series of π-conjugated metal-organic chromophores containing polypyridine architectures and long-lived triplet states have been synthesized by our group.[9, 21] Utilizing similar synthesis techniques, metal-organic chromophores with similar triplet character were produced which display this enhanced NLO response from ESA. It will be shown that with strong triplet absorption at the TPA active wavelength, a decrease in transmittance is observed as photon intensity increases brought about by a TPA/ESA dual mode mechanism (Figure 1-10). This characteristic therefore presents this class of metal-organic compounds as potential optical limiting materials.[30, 31, 33]

Project Objective

The goal of this research is to explore the potential for a dual mode nonlinear response in a novel series of metal-organic chromophores. The system of interest contains an all organic two photon absorbing chromophore complexed with a transition metal chromophore capable of inducing a rapid intersystem crossing of singlet excited states to long-lived triplet excited states. The desire for the inclusion of two photon absorption is two-fold. First, utilizing a two photon excitation source to produce an initial excited state limits the potential for high energy induced chromophore damage by addressing wavelengths which are optically transparent at low photon fluxes. Second, introduction of a two photon excitable chromophore incorporates a near "instantaneous" nonlinear response which operates in a time domain that is very short (femtosecond to picosecond). The inclusion of excited state absorption is desired to take advantage of available long-lived triplet states allowing for nonlinear absorption on a considerably longer time scale (nanoseconds to microseconds). Coupled together in the same system, the complementary temporal responses can be combined to generate a nonlinear response that is not only long lasting but "turn on" delay is minimized.

Central to the investigation is an organic π-conjugated chromophore (Figure 1-11) with the potential to exhibit two photon absorbing character as well as the ability to complex with a range

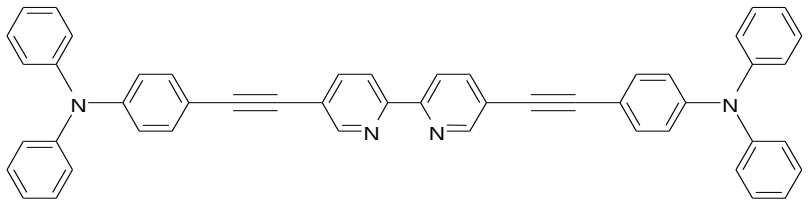

Figure 1-11. Bipyridine centered target two photon absorbing chromophore.

of transition metals that have large spin-orbit coupling potential. The functionality being integrated into the core structure of the chromophore to support metal complexation is a 5,5′-

substituted 2,2′-bipyridine unit. The desire to utilize 2,2′-bipyridine comes from its electron accepting nature as well as an ability to strongly bind to a wide variety of late transition metals. It has been shown that when coupled to transition metals such as ruthenium, rhenium and iridium, several structural, electronic and photophysical characteristics of 2,2′-bipyridine can be manipulated in tandem to enhance the spectral response of a chromophore. When combined with a transition metal, bipyridine exhibits a conjugation enhancement from a conformational change as well as an added metal to ligand charge transfer mechanism which adds absorption character to the chromophore. This ability to bind with a variety of metals yields several possible metal-organic chromophores. (Figure 1-12) Photophysical investigation of these transition metal based analogs is centered on their TPA nonlinear response and the generation of long-lived triplet excited states from both a single and a two photon excitation source.

Rapid intersystem crossing brought about by the incorporation of selected metals with large spin-orbit coupling values are utilized to efficiently generate a large population of highly absorbing triplet states. Selection of ruthenium, rhenium and iridium as the target metals is based on the previous synthetic and photophysical findings available in our group. It has been well documented that substituted bipyridine complexes of these target metals efficiently and rapidly produce triplet excited states that are highly absorptive and long-lived. The utilization of these triplet states to further absorb the excitation wavelength will enhance nonlinear absorption in this system through excited state absorption. Overall, the primary objective of this work is the two photon generation of excited states in a series of the metal-organic complexes followed by rapid intersystem crossing to a long-lived triplet excited state manifold comprised of $^{3}\pi$-π^* and/or ^{3}MLCT excited states to generate a temporally broad and wavelength significant dual mode nonlinear response

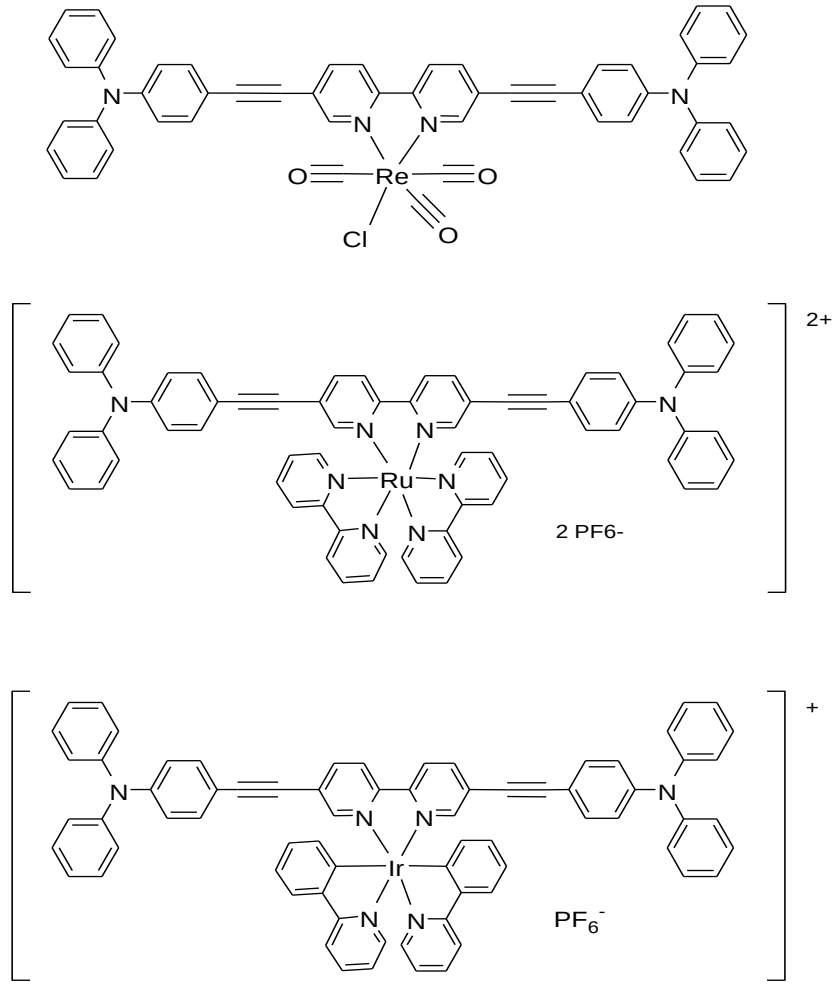

Figure 1-12. Target metal centered dual mode nonlinear absorbing chromophores.

.

CHAPTER 2
DETERMINATION OF NONLINEAR RESPONSE

Introduction

Linear Absorption

As a normal course, the absorption of light by a substance follows a process that can be easily understood and explained. Most optical interaction phenomena can be expressed as a linear relationship of the absorption of light as it travels through a medium to the amount of light entering. The most widely recognized relationship dealing with linear absorption of light is that of Beer's Law. Beer's Law is expressed in several different ways as it relates to the absorption or transmission of light through a material. In Equation 1, the linear relationships of absorbance to molar absorptivity (ε), path length (*l*), and concentration (*c*), are clearly evident. Also included is the mathematical and graphical relationship of transmittance to absorbance (Equation 2 and Figure 2-1).

$$A = \varepsilon \, l \, c \qquad (1)$$

$$A = log_{10} (1/T) \qquad (2)$$

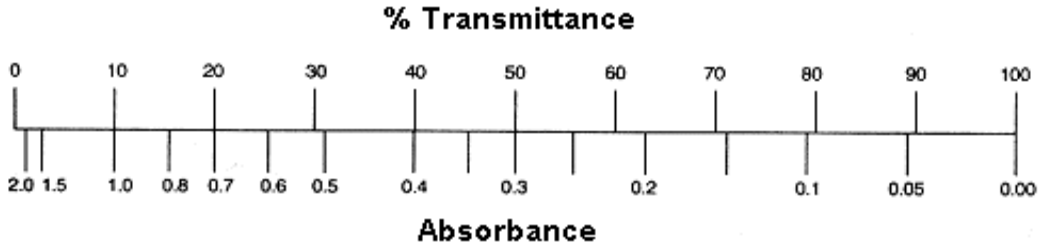

Figure 2-1. Beer's Law relationships of linear absorption.

It is important to point out that this linear relationship does not include a dependence on incident light intensity. For normal intensities of incident light energy, these linear relationships are the standard; however at very high intensities of incident light energy, materials can exhibit nonlinear optical behavior and vary their absorbance as a function of the incident light intensity.

Nonlinear Optical Behavior

To examine the photophysical ramifications of absorption which occurs in a manner that does not follow a linear "Beer's Law" relationship, understanding and explanation becomes much more difficult. With regard to the interaction of light with an organic medium, one can examine this interaction by viewing the system as a dielectric medium subject to an electric field.[39] The introduced electric field originates as the electric component of the electromagnetic field. As light is introduced to the medium an induced dipole moment is created by the applied field. In turn, an induced polarization (P_{ind}) of the medium results from this newly established dipole moment. This can be expressed as the medium's polarization susceptibility, $\chi^{(1)}$, to the applied electric field, E as shown in Equation 3. This susceptibility is related to the optical

$$P_{ind}(E) = \chi^{(1)}E \qquad (3)$$

response of a medium at a given optical frequency (ω) and is linked, in turn, to a complex refractive index (n_c). Expression of this complex refractive index exists in real (n) and

$$n_c^2(\omega) = 1+4\pi\,\chi^{(1)}(\omega) \qquad (4)$$

$$n_c = n + ik \qquad (5)$$

imaginary (k) parts corresponding to the dispersion of the refractive index and electronic absorption components, respectively.

Viewing linear absorbance utilizing this model, the medium is observed as a collection of harmonic oscillators forced by a sinusoidal optical field. For a system where the introduced field strength is of relatively low intensity and the oscillations of the medium remain harmonic and in equilibrium with small polarization/dipole displacement, the medium absorption will remain a linear process and the oscillators will exhibit sinusoidal motion with the frequency of the driving optical field. In this case, the oscillators re-emit the light but with a lag in phase. The

cumulative phase lag in the medium is due to the reduced group velocity of the light waves in the medium. In turn, the oscillators experience a damping force by the medium which is brought about by an exchange of energy between the optical field and the medium and which can be expressed classically as the wavelength difference between absorption and emission or the Stokes shift.

In the case where the electric field driving force is strong, anharmonic oscillations begin to occur in the medium. With the addition of these inharmonic oscillations to the system, the polarization expression (3) above expands to include nonlinear factors. Addition of higher order

$$P = \chi^{(1)}E + \chi^{(2)}E^{2} + \chi^{(3)}E^{3} + \ldots \qquad (6)$$

terms, such as $\chi^{(2)}$, $\chi^{(3)}$…etc, represents higher order hyperpolarizabilty factors which give rise to and are responsible for nonlinear optical effects. Nonlinear optic (NLO) phenomena are generally characterized as second-order or third-order depending on whether they are described through the $\chi^{(2)}$ or $\chi^{(3)}$ terms, though higher terms do exist.

Second-order nonlinear susceptibility, $\chi^{(2)}$ represents and is responsible for second-order effects such as second harmonic generation (SHG) and the electro-optic effect. SHG occurs when two photons of angular frequency ω combine to produce a third photon with an angular frequency of 2ω,. This doubling of frequency ($\omega + \omega \rightarrow 2\omega$) generates a photon whose wavelength is half the original. This second-order effect is the major mechanism utilized in producing frequency-doubled wavelengths in laser applications such as producing 532 nm from a 1064 nm fundamental beam of an Nd:YAG laser. The electro-optic effect is the modification of the refractive index of a medium brought about by an externally applied electric field. Two examples of this are the Pockels effect and the optical Kerr effect. The Pockels effect occurs in crystal material which is non-centrosymmetric and is referred to as the linear electro-optic effect

because the induced refractive index change is directly proportional to the external electric field strength applied. Typical crystalline materials which produce the Pockels effect, such as potassium dideutrium phosphate (KDP) and beta barium borate (BBO) are used as electro-optic modulators for Q-switching in laser applications. The optical Kerr effect is also a change in refractive index brought about by the application of an electric field however the induced refractive index change is proportional to the square of the electric field intensity. For the optical Kerr effect the electric field acting on the medium is the incident light itself, therefore the variance in the index of refraction becomes proportional to the square of the irradiance of the incident light. This nonlinear optical effect is commonly used to produce ultrashort laser pulses in the range of a few femtoseconds.

Third-order nonlinear effects are governed by the $\chi^{(3)}$ susceptibility term and represent the nonlinear factors that are of concern for this body of work. This third-order susceptibility factor is responsible for effects that include third harmonic generation (THG), and two photon absorption (TPA). THG, like that of SHG, occurs as a multiphoton event that combines three photons of angular frequency ω to generate a fourth photon with an angular frequency 3ω and a wavelength equal to one-third the fundamental. THG, however, occurs as a cascade of two second-order nonlinear events where $\omega + \omega \rightarrow 2\omega$ and $2\omega + \omega \rightarrow 3\omega$.[40] It is also noteworthy that it has been demonstrated that even-order susceptibility factors ($\chi^{(2)}$, $\chi^{(4)}$ .etc) approach zero or are nullified in molecules that contain a center of inversion. This means that in molecules containing second and third order nonlinear structural features, but also possess a center of inversion will exhibit third-order nonlinear effects almost exclusively. These factors point to the influence and importance of molecular symmetry in the preparation of model compounds for studying second and third-order nonlinear effects and will be addressed during the course of this

dissertation. Since the focus of this work is to evaluate and take advantage simultaneously of two very different nonlinear effects, a familiarity with the structure-property relationships affecting excited state absorption and the nonlinear susceptibility term that governs two photon absorption is useful

Second-order NLO processes.

The 1970's saw considerable research focused on second-order nonlinear optical effects of non-centrosymmetric molecules. Dipolar molecules like the one shown in Figure 2-2 were one of the classifications of molecules which attracted significant attention. These molecules exhibit preferential polarization with greater efficiency in one direction than the opposite direction. In such systems, Oudar and Chemla [41] expressed the origin of the first-order hyperpolarizabilty

$$\beta \propto \left(\frac{\mu_{ge}^2 \left(\mu_{ee} - \mu_{gg} \right)}{E_{ge}^2} \right) \qquad (7)$$

term, β, as a single resonance frequency, two-state model consisting of the ground and first allowed charge-transfer excited state dipole, μ, and the transition energy, E. In this model, the first-order hyperpolarizability coefficient, β, is proportional to the ratio of the dipole element's unidirectional susceptibility, $\mu_{ge}^2 \left(\mu_{ee} - \mu_{gg} \right)$ and the molecules' transition energy, E_{ge}^2. Inclusion of $\left(\mu_{ee} - \mu_{gg} \right)$ is meant to account for the preference of electron interaction with the optical field in one direction relative to the other. From this model, molecules designed for second-order NLO applications were primarily unsymmetrically endcapped, aromatic π-electron systems containing electron donating moieties at one end and electron withdrawing groups at the other. This separation of electron donating and withdrawing endcaps was designed to incorporate the desired electronic bias to the system. A typical dipolar model compound in these early studies was the NLO chromophore 4-(*N*, *N*-dimethylamino)-4′-nitrostilbene (Figure 2-2) which contains

two benzene rings linked by a double bond in a conjugated π-system to provide a polarizable bridge of electrons for the donor and acceptor groups dimethylamino and nitro to act

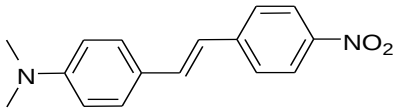

Figure 2-2. Structure of the typical dipolar model compound 4-(*N*, *N*-dimethylamino)-4′-nitrostilbene.

upon. This compound and others of similar architecture have been studied and reviewed.[39, 42]

Following the rationale of this dipolar/charge separation model, the early 1990's saw advancements in the understanding of the structure-property relationship of charge transfer in dipolar molecules and its effect on the first hyperpolarizability coefficient. Studies by Marder and Perry [29] explored how the degree of ground-state charge separation (induced polarization) was affected by chemical structure and the medium surrounding the compound. In the course of these studies, chemical structure-property variables such as structure of the conjugated π-system and the strength of the donor and acceptor substituents were examined. A positive correlation to increased hyperpolarizability was observed with the increase in bond length alternation (BLA) in polyenes having alternating double and single bonds which aided in charge transfer and charge separation. It was also shown that higher-order polarizability terms could also be correlated in a predicable manner to this charge transfer model. Initially predicted enhancements associated with increasing donor and acceptor strengths surprisingly yielded significantly lower hyperpolarizability gains than predicted. Jen, Dalton *et al*[43] determined that for molecules with large dipole moments (>10D), chromophore-chromophore interactions at high chromophore concentrations diminished polarizablity as electrostatic interactions increased. Subsequent work by Dalton and the Lockheed Martin Corporation [44] focused on highly electron deficient acceptor groups as well as minimizing chromophore interactions, Figure 2-3.

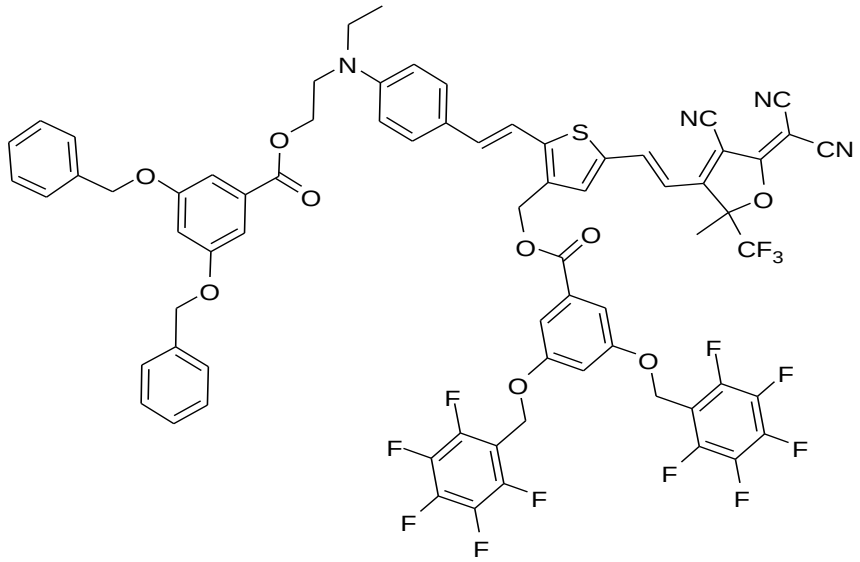

Figure 2-3. Structure of an enhanced donor-π-acceptor chromophore.

These studies also afforded considerable attention on developing a π-conjugated bridge that provided a good balance between enhancing charge transfer, preventing aggregation and promoting thermal and photochemical stability.

Third-order NLO Processes

The active presence of third-order susceptibility, $\chi^{(3)}$, in a substance leads to third-order NLO interaction and its possible uses in such applications as optical switching for optical communications or optical information processing, and optical limiting for the protection of optical sensors from damage induced by intense laser energies. Increasingly third-order nonlinear processes have proven valuable as tools for nonlinear applications as well as other technologically significant processes. The applications mentioned are among the most important and desirable uses for third-order NLO processes. Several different classes of conjugated organic molecules and polymers have been investigated to identify key structure-property relationships in the effort to develop materials with large $\chi^{(3)}$ nonlinearities for use in these applications.[45]

Considerable study into structure-property relationships influencing the third-order nonlinear processes has been performed. Early research associating chemical structure-property relationships to the strength of the second-order hyperpolarizability coefficient, γ conducted by Prasad et al [46] developed a coupled anharmonic oscillator (CAO) model based on a single resonance frequency, two-level model similar to that used to explain the first-order hyperpolarizability coefficient, β. This CAO model correctly accounted for the observed dependence of the band-gap, linear polarizability α, and second-order hyperpolarizability γ, on the number of repeat units contained in a conjugated organic molecule or polymer with structurally large repeat units. This model was found to be less accurate, however, for short-chain polyenes for which a two-level approximation model was deemed not to be valid. Further study in the early 1990's by McWilliams and Soos [47] proposed an inter-chain mechanism for third-order nonlinearity in conjugated polymers. They noted that NLO susceptibility for third harmonic generation had a contribution from inter-chain stacking and yielded a large γ component in the direction of the stacking. Continued research by Prasad [48] in this area determined that the molecular geometry of repeat units has a significant effect on $\chi^{(3)}$ values. In theoretical studies of planar geometry oligomeric diphenylbenzobisoxazole (PBO) and diphenylbenzobisthiazol (PBT) it was found they showed significantly larger γ values than similar molecules of nonplanar geometry. This increase in NLO susceptibility was attributed to

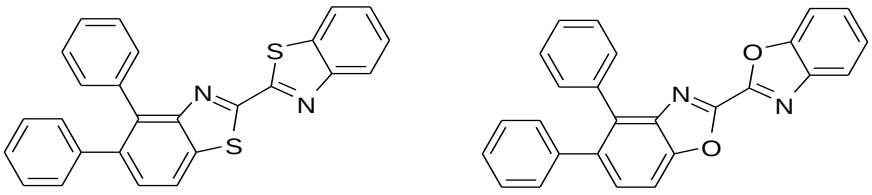

PBT PBO

Figure 2-4. Structures of diphenylbenzobisoxazole (PBO) and diphenylbenzobisthiazol (PBT).

a geometric enhancement lending to more of a free-electron structure versus a twisted-chain, which introduces a break in conjugation and restricts the free-movement of electrons. In this study it was also noted that geometrical isomerism is an important factor influencing third-order NLO effects. In general, it was found that an isomer allowing the greatest number of resonance structures and therefore better electron delocalization had a significantly higher value of γ over those having a smaller number of resonance structures.

In the area of third-order nonlinear responses, there are several mechanistic choices that are thought of as the common modes of this type of nonlinear behavior. Among them is two photon absorption (TPA), which we will examine in the course of this chapter.

Optical Limiting

Background

By definition, optical limiters are NLO materials which allow normal intensity light to be transmitted but attenuate light at high incident power (high photon flux).[49] Due to recent laser-based technological advancements of power, frequency and wavelength agility as well as improvement in efficiency, portability and operational robustness, lasers have become commonplace and incredibly important to manufacturing, medicine, entertainment and a host of other sectors including the military. The majority of the world's population is familiar with a laser's use as a tool to help level a picture, a pointer to illuminate key facts during a presentation, or the digital reading device on our home entertainment center, but concern for protection from the light energy produced by a laser is of serious concern. Damage to the retina of the eye has been shown to occur with an extraordinarily low amount of laser energy. A study conducted by the Human Effectiveness Directorate of the Air Force Research Laboratory found that for a few common wavelengths, such as 1064 and 532 nm, eye damage can occur at energies as low as 0.25 μJ at 532 nm and 5.5 μJ at 1064 nm with a 5 ns pulse duration.[50, 51] Items such as laser

pointers are designed to operate as Class 3a devices with an output of less than 1.0 mW which, according to the ANSI Z136.1-1993 American National Standards for Safe Use of Lasers, is of sufficiently low power that the blink reflex normally affords adequate eye protection. However, even for laser pointers, recent technological advances in compact diode lasers used in these devices are producing up to 5.0 mW at 533 nm which are, according to the Food and Drug Administration, capable of producing flash-blindness, glare and after-images.[52] With the threshold for safe ocular laser exposure being so low and the need to protect other sensitive mechanical devices, such as optical sensors, from high power laser exposure, the need for efficient and flexible optical limiting material is growing ever more important. The development and testing materials for optical limiting has been ongoing for as long as laser research and advances have been made, but there is still a great deal more that can be done. It is possible to protect the human eye or an optical sensor from a laser's energy using a proper filtering system as is found in a "sunglass" type device. Effectiveness of these types of systems, however, assumes the laser wavelength being utilized can be accurately anticipated. Static filtering therefore is not an adequate defense against such high energy light sources as agile wavelength pulsed lasers. To properly protect the eye or an optical sensor from such a system, the development of a series of "smart" materials capable of being transparent under ambient light levels but can rapidly "react" to high intensity light over a broad wavelength range for a sufficient period of time to allow for human (blink) or mechanical (shutter) reaction time to intervene and provide additional protection has become a necessity.

Two Photon Absorption

Two photon absorption (TPA) is a third-order nonlinear process in which a molecule has the ability to simultaneously absorb two identical photons to produce an excited state equivalent to that produced by the absorption of a single photon of equivalent energy. In the presence of

normal intensity light the probability of TPA is low even for molecules with a large two photon cross section. In the presence of intense laser pulses however, a molecule with a large two photon cross section can simultaneously absorb two identical photons with a transition probability proportional to the square of the intensity of the laser pulse. The necessity for a high intensity photon source presents an additional key feature of two photon absorption with potential for utilization in applications: spatial confinement. Spatial confinement of the TPA process arises not only due to the quadratic dependence of incident two photon resonant light but also from the quadratic decrease of the intensity of focused laser light as distance from its focal point increases. Together these factors lead to the probability of TPA occurrence decreasing by the fourth power of distance from the focus of a suitably intense laser source.

Despite considerable research in the area of two photon absorption, it wasn't until the late 1990's that detailed structure-property relationships were developed that permitted the deliberate design of new chromophores with enhanced two photon cross sections.[29, 32, 53] Several key studies by groups such as Reinhart, Perry, Marder, and Prasad have established basic design concepts which have successfully enhanced two photon absorption in different series of molecules.[29, 32]

In the late 90's, Reinhart *et al* proposed two classes of chromophores which could exhibit enhanced two photon cross sections (Figure 2-5) During their study several key structural

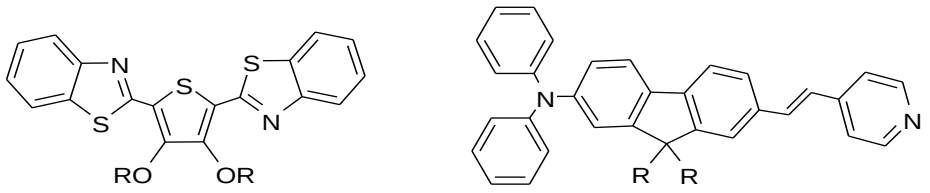

e-donor--π-bridge--e-donor e-donor--π-bridge--e-acceptor

Figure 2-5. Chromophore structures for enhanced two photon absorption (Reinhart).

features became apparent as key design parameters for enhancing a chromophore's two photon cross section: (1) conjugation length, (2) nature of the polarizable π-conjugated bridge (3) π-donor strength, (4) number of polarizable double bonds, and (5) the increase of planarity in the chromophore.

Along similar lines Perry and Marder, working with Jean-Luc Bredas[29], found a positive correlation between large two photon cross section values and a π-conjugated chromophore's ability to undergo a large change in quadupole moment upon excitation. Successful enhancements of two photon cross sections where achieved in chromophores utilizing these architectures which promoted the ability to induce large quadupole moment changes with structural motifs containing acceptor-donor-acceptor (A-D-A), donor-acceptor-donor (D-A-D), and donor-π-donor (D-π-D) moieties (Figure 2-6, left).

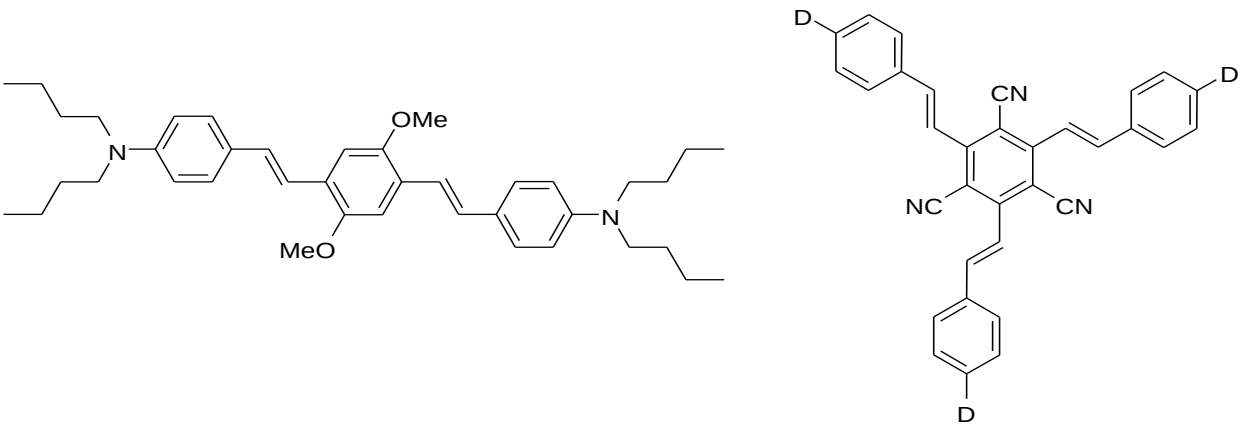

Figure 2-6. Structures of quadupolar (left) and octupolar chromophores (right) found to have large two photon absorption cross sections. D represents electron donating group.

This strategy was further expanded to octupolar chromophores by Cho et al [54] (Figure 2-6, right) with considerable success. This structure-property strategy to enhance two photon absorption has persisted and was a primary consideration in the design of the organic two photon absorbing chromophore in the work described herein.

In optical limiting applications TPA is a desirable quality due to its high linear transparency at low light intensities as well as its fast temporal response. Utilization of TPA as a complementing NLO mechanism to RSA in a dual mode optical limiter allows for an ultra-short "turn-on" with response times that are sub-picosecond in nature and lasting for several nanoseconds. Therefore by implementing TPA as the ground state excitation pathway with its inherent nonlinear absorption, though short in duration, covers the gap between exposure and excited state absorption which can be in the order of a nanosecond.

Excited State Absorption and Dual Mode Limiting

When excited state absorption (ESA) is combined with another NLO mechanism it acts as a cumulative nonlinear absorption effect. As an optical field interacts in a nonlinear manner with a medium or material to produce an excited state, a subsequent absorption by the excited state leads to further reduction of transmission. This additional absorption pathway leads to an enhancement of the initial NLO response. In this project a combined TPA/ESA process was utilized to further enhance the nonlinear character of the target TPA chromophore. A five level energy diagram, shown in Figure 2-7, was used to model the process. Two photon induced ESA is a three photon process, but the photons are not all absorbed simultaneously. Initiation of

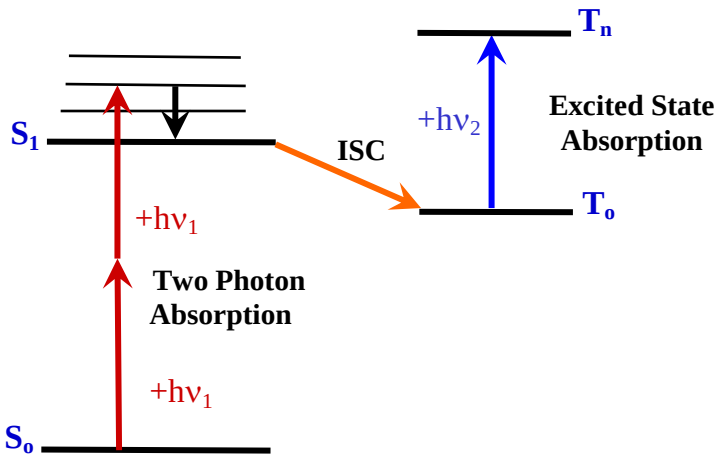

Figure 2-7. Five level energy diagram for two photon induced excited state absorption model.

the process is the simultaneous absorption of two photons from a TPA mechanism to generate a singlet excited state. Rapid intersystem crossing subsequently populates the lowest triplet state. A third photon is then absorbed by the triplet state. Though the possibility exists that the singlet excited state may be absorptive, its lifetime is significantly shorter than the nanosecond laser pulse due to rapid intersystem crossing (~300 fs)[15] and its effects can be considered negligible. As the efficiency of TPA increases, light transmittance at low input intensities remains high whereas light transmittance at high input intensities decreases. Chromophores exhibiting highly efficient TPA/ESA absorption are considered excellent candidates for use as optical limiters. In addition to high linear transmission at low intensities, other key factors in favor of the utilization of the TPA/ESA mechanism to achieve power attenuation include source absorption, temporal duration, and spectral range. For a limiting system utilizing this dual mode mechanism, optical energy is absorbed and converted to heat as opposed to being redirected as is the case in nonlinear scattering or reflective materials. This facilitates a response which is reliable, more predictable, and limits unwanted exposure to the surrounding area. In addition, a dual mode TPA/ESA chromophore with an efficient and rapid intersystem crossing mechanism producing a long-lived triplet excited state is ideal for power attenuation for laser pulse widths ranging from sub nanosecond to several microseconds. Lastly, chemical modification of metal-organic-based TPA/ESA chromophores has the potential to produce systematic structural manipulations to attain the desired triplet absorption properties directly related to the enhancement of optical limiting responses favorable to the protection of a system of interest.

Recent studies by Sutherland[37] and Li[55] have modeled and experimentally verified the intensity dependence of the TPA/ESA mechanism. A qualitative comparison of the

enhancement from ESA was noted. In a modification of their model, the attenuation of intensity *I* as light passes through a sample can be described by Equation 8 where N_{S_0} and N_{T_0} represent

$$\frac{\delta I}{\delta z} = -\sigma_2 N_{S_0} I^2 - \sigma_T N_{T_0} I \qquad (8)$$

the molecular densities of molecules in the S_0 and T_0 states and σ_2 and σ_T represent the two photon and triplet absorption cross sections respectively. Describing the TPA/ESA mechanism in this fashion illustrates the cubic dependence on incident light intensity of this dual mode process. These studies also noted this cubic dependence can be used to differentiate TPA/ESA from other NLO processes such as TPA or reverse saturable absorption (RSA). An example where TPA alone was clearly differentiated by its quadratic relationship between attenuated intensity and incident light intensity versus a cubic dependence for TPA/ESA is shown in Figure 2-8.

Assessing the magnitude of the NLO enhancement gained through ESA in AF-455 shown in Figure 2-8 was also compared versus the excited state absorption cross sections.[34] The excited state absorption cross sections were reported as follows: (1) two photon cross section (σ_2), 0.51 x 10^{-20} cm^4/GW, (2) singlet state (σ_S), 1.68 x 10^{-17} cm^2 and (3) triplet state (σ_2), 17.1 x 10^{-17} cm^2. Initial studies of the excited states of AF-455 identified the triplet state as a potential source of enhanced nanosecond nonlinear absorption because of its large triplet-triplet absorption cross section. Subsequent determination of a modest triplet quantum yields (<10%) led to singlet state absorption being identified as the dominant ESA pathway but with a significant contribution from triplet-triplet absorption (due to its large absorption cross section). Figure 2-9 represent the comparison of experimental data versus a numerical model based on Equation 8 and the absorption cross sections reported above. A second theoretical curve was added using a different

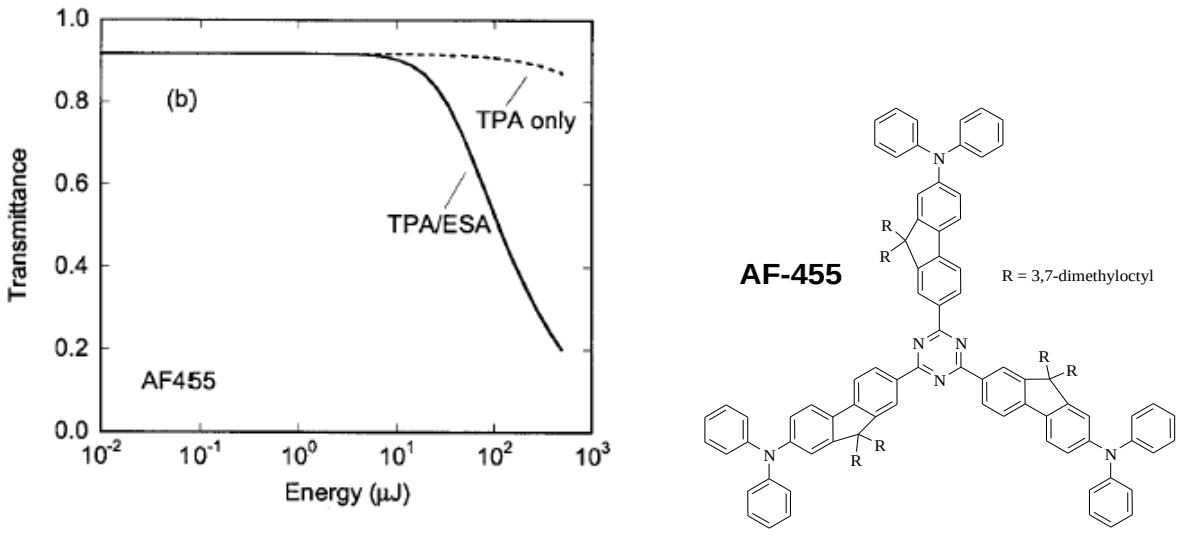

Figure 2-8. Illustration of the difference in transmission loss by TPA alone and by TPA/ESA in AF-455.[37]

two photon cross section of AF-455 reflecting an alternate experimental method (σ_2 = 1.7 x 10^{-20} cm^4/GW). It was concluded that the three photon absorption model provides a reasonably accurate estimate (± 10%) of the nanosecond nonlinear transmittance in this system. It was noted that the largest source of error in making the estimations was the variation in experimental measurements of the two photon cross sections. Also noteed was that excited state absorption is

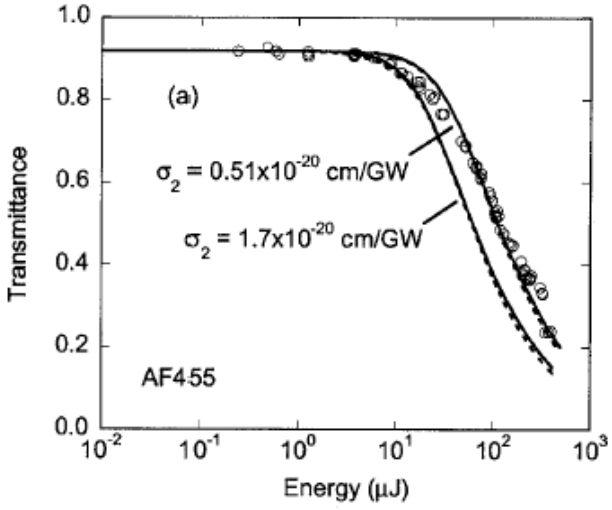

Figure 2-9. Comparison of theoretical (curves) versus experimental (circles) nanosecond nonlinear transmittance as a function of laser pulse energy for AF-455 at 800 nm.[37]

the dominant contribution to nonlinear transmission in AF-455 for the TPA/ESA mechanism on a nanosecond time scale. It was concluded that two photon absorption did not contribute significantly to overall transmission loss despite a reasonably large two photon absorption cross section, but was an essential process for producing the excited states.

Experimental Determination of Nonlinear Response

Z-scan

Many experimental techniques have been developed to measure third-order nonlinearity over the past two decades. Among the most popular is Z-scan which was developed in 1989 by Van Stryland.[56] The experimental methodology is based on the observation of beam distortion generated by nonlinear refraction in conjunction with the overall change of transmitted intensity due to nonlinear absorption. Researchers utilizing this technique have described it as a useful spectroscopic tool due to its simplicity and high sensitivity. A typical Z-scan experimental setup used to investigate third-order nonlinear refraction and absorption is presented in Figure 2-10.

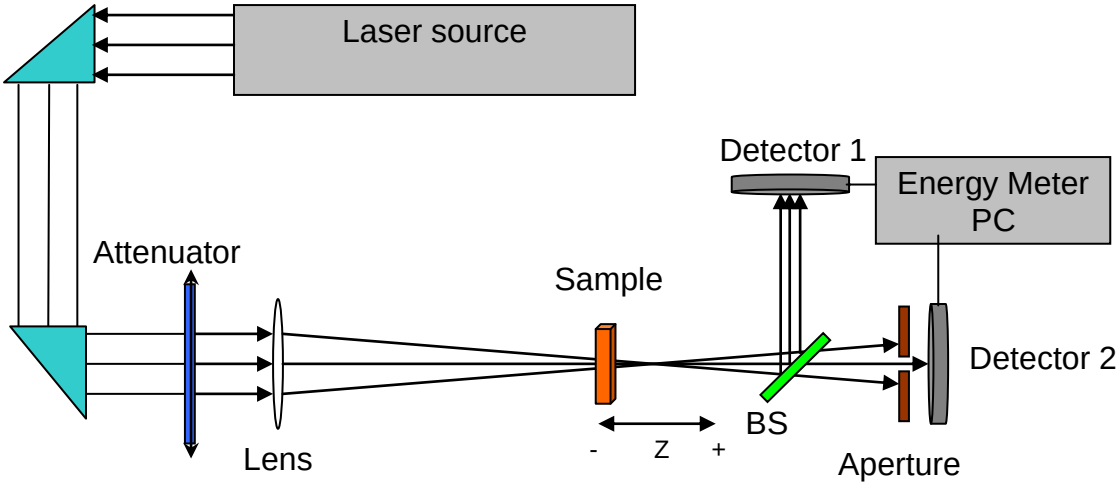

Figure 2-10. Generalized illustration of a Z-scan experimental setup.

In general the Z-scan setup contains a single laser beam passing through a focusing lens and is utilized as the incident light source. The beam can be attenuated prior to the focus to achieve the desired input energy and is kept constant throughout the experiment. The sample is

placed in a sample holder mounted on a single axis translation stage positioned at the focus of the laser source with the axis of movement parallel to the laser source. Calibration of position with regard to the focus and precision of movement is of primary importance to obtain accurate results and is why the translation stage is ideally controlled by a computer. With the incident energy kept constant, the sample is moved from a point along the optical axis of source light prior to the focus (-Z) through the focus (Z = 0) to a position beyond the focus (+Z). The extremes of positive and negative Z are positions relative to the focal point where only linear absorbance is present. Data collection involves recording the resulting change in transmitted energy by detectors 1 and 2 and correlated versus change in the Z-position. Plotting normalized transmission versus Z-position produces the typical open aperture Z-scan curve (Figure 2-11b) which graphically depicts the nonlinear absorption character of the sample. A variation of this technique, known as closed-aperture Z-scan, places an aperture in front of transmission detector 2. Utilizing an aperture prior to detector 2 allows for the determination of the sign and magnitude of third-order nonlinear refraction. Nonlinear refraction occurs in the presence of self-focusing and is detected as the sample is translated through the focus.

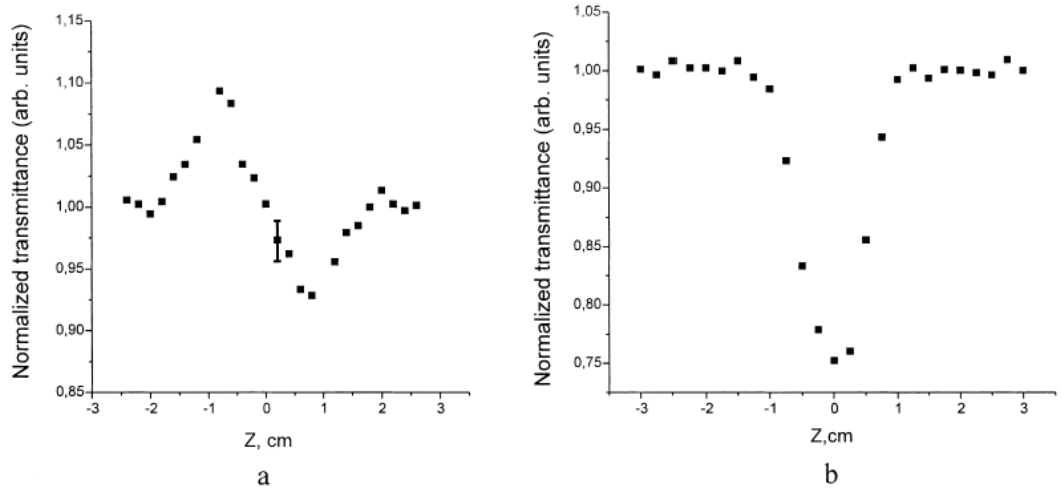

Figure 2-11. Z-scan curves of C60 in toluene (0.5% wt) at an excitation wavelength of 1064 nm. a) closed aperture b) open aperture.[57]

For molecules presenting negative nonlinear refraction values, as shown below for C_{60}, self-focusing occurs prior to the point of focus and is detected as an apparent increase of transmittance above the normalized value of 1.0. As the sample passes the focus, transmission drops off to values less than 1.0 due to defocusing by the same mechanism (Figure 2-11a).

Nonlinear Transmission

Another common and often used nonlinear absorption determination technique is nonlinear transmission (NLT). NLT is an experimental methodology conceptually similar to that described above for Z-scan. The nonlinear transmission method, sometimes referred to as an "optical limiting measurement," is the technique chosen for nonlinear response detection for this project due to its ease of setup, relatively minimal equipment requirements and low startup cost. A

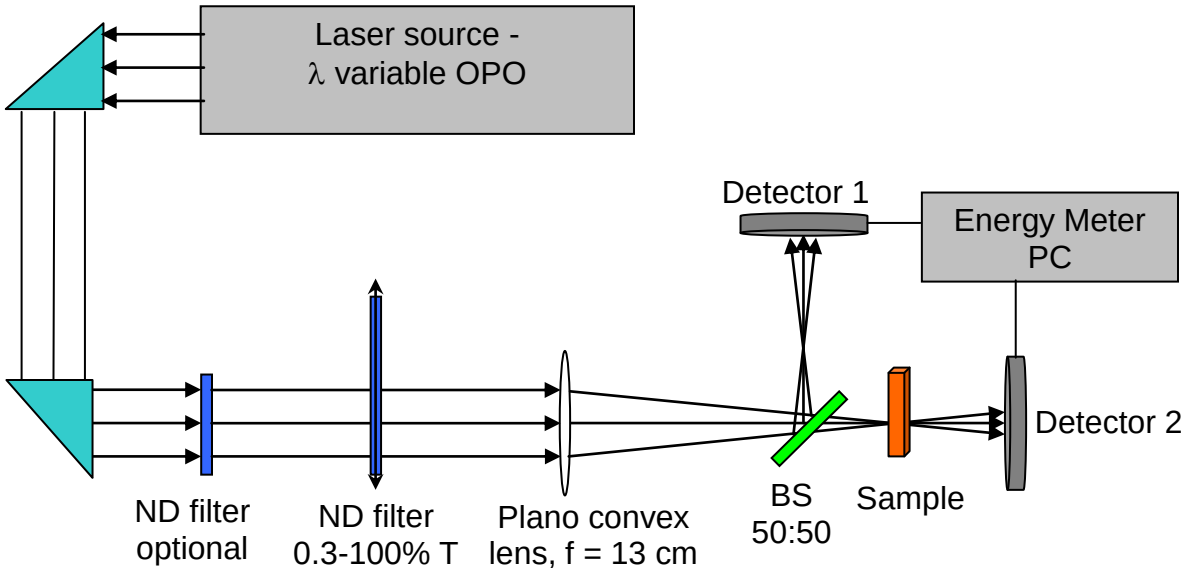

Figure 2-12. Schematic illustration of the nonlinear transmission (NLT) experimental setup.

schematic illustration of the NLT experimental setup developed for this project is depicted in Figure 2-12. Important differences in this experimental setup versus a Z-scan apparatus are as follows. First, the sample remains stationary with respect to the spot of laser focus. Second, the beam energy is sampled prior to the sample and compared to the energy after passing through the

sample. This arrangement allows for the determination of absolute energy input to the sample by a simple differential determination in the presence of a sample cell containing solvent only. Lastly, utilization of the ratio of transmitted and incident energies in this manner eliminates the influence of any inherent laser radiation instability which has the potential to vary results between experiments.

Two different representations of the information gathered by an experimental nonlinear transmission setup are easily depicted. First, directly plotting input energy versus output energy yields a graphical representation visualizing any nonlinearity of the obtained signals. In

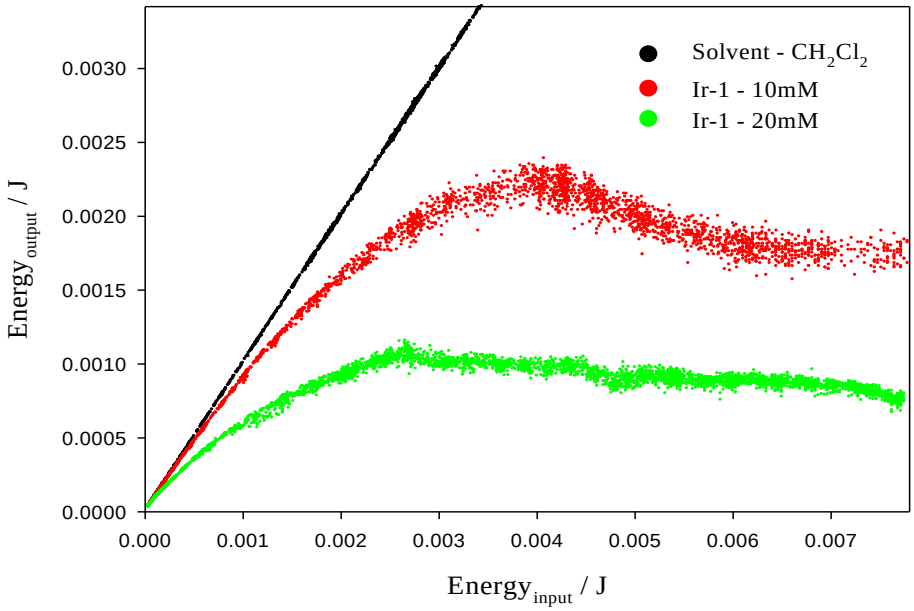

Figure 2-13. Example NLT curve plot of input energy versus output energy and depicting a clamping state energy in the sample.

addition, this method clearly represents the limited output energy (clamping energy) of the system if one is present (Figure 2-13). For the low energy region in this presentation style, it is difficult to distinguish nonlinear absorption from low initial transmission. For this reason a second representation is utilized to better highlight the low energy region of NLT data. It is also

noted that there is a spreading out of data as light intensity increases. As the material transitions into regions of increased nonlinear absorption the transmission error in the system also increases with a quadratic and cubic dependence and generates data that is more dispersed. In the second representation of NLT data (Figure 2-14), input energy (plotted on a common logarithmic scale) is plotted versus energy transmission through the sample (output energy divided by input energy). This representation clearly indicates transmittance at low light intensities as well as the nonlinear threshold energy. For this data presentation linear absorption is depicted as a data set of zero slope and any nonlinearity is represented as a data set with a nonzero slope.

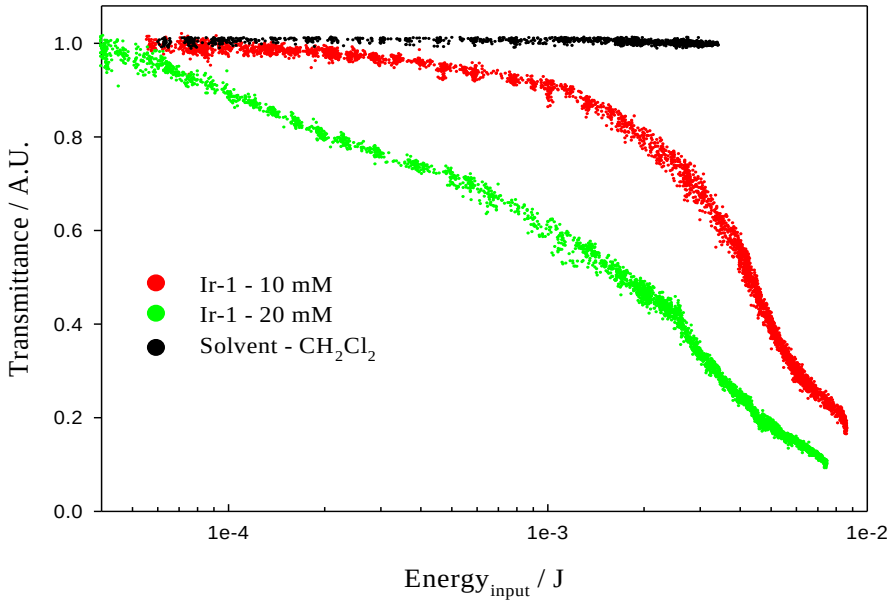

Figure 2-14. Example NLT curve plot depicting input energy versus transmittance.

Nonlinear Transmission Test Case

Test Objective

In order to verify the experimental capabilities of the newly designed and built nonlinear transmission (NLT) apparatus, it was determined a survey study should be conducted. The survey's aim was threefold: (1) establish that the apparatus was capable of detecting a nonlinear

response in a consistent and repeatable manner, (2) establish an experimental method for apparatus setup, data acquisition and data presentation, and (3) determine the capability of the apparatus to acquire data from a nonlinear chromophore of known nonlinear character and compare the findings to a similar chromophore series in a semi-quantitative manner. The last criterion is considered the most important because the apparatus was not designed nor intended to measure an absolute value associated with a nonlinear response, such as absorptive cross section or nonlinear coefficients. The desired capabilities of the NLT apparatus were to detect the presence and judge the relative strength of a nonlinear response in an NLO active system. Therefore, the capability to gather consistent and repeatable data from multiple samples under a standard set of experimental conditions was considered a key objective.

Apparatus Setup

Nonlinear transmission (NLT) experiments were performed on an in-house built setup similar to that described in a previous section. A detailed user's manual is included in Appendix B to aid in the setup and operation of the NLT apparatus that is described below. A photo rendered schematic is presented in Figure 2-15. The NLT apparatus used for the test consisted of a variable wavelength laser source provided by a Continuum Surelite II-10 Nd:YAG laser (355 nm, third harmonic of the 1064 nm fundamental) augmented with a Surelite OPO Plus (wavelength range: 420-570 and 590-1200 nm). A single laser beam passing through a focusing lens was utilized as the incident focused light source. This beam could be attenuated prior to the focus (if desired) to achieve the desired beam energy and stability. Upon achieving the adequate beam stability and maximum laser energy desired for the experiment, beam attenuation for power dependent measurements is achieved with the addition of a continuously variable neutral density (ND) filter placed prior to the focusing lens. Nominal laser energy requirements for the experiments ranged from sample input energies of 50 μJ to approximately 5.0 mJ. These were

achieved utilizing an ND filter capable of attenuations ranging from 0.1 to 100% transmittance. A 50.8 mm plano convex lens with a focal length of 10 cm was positioned in the incident

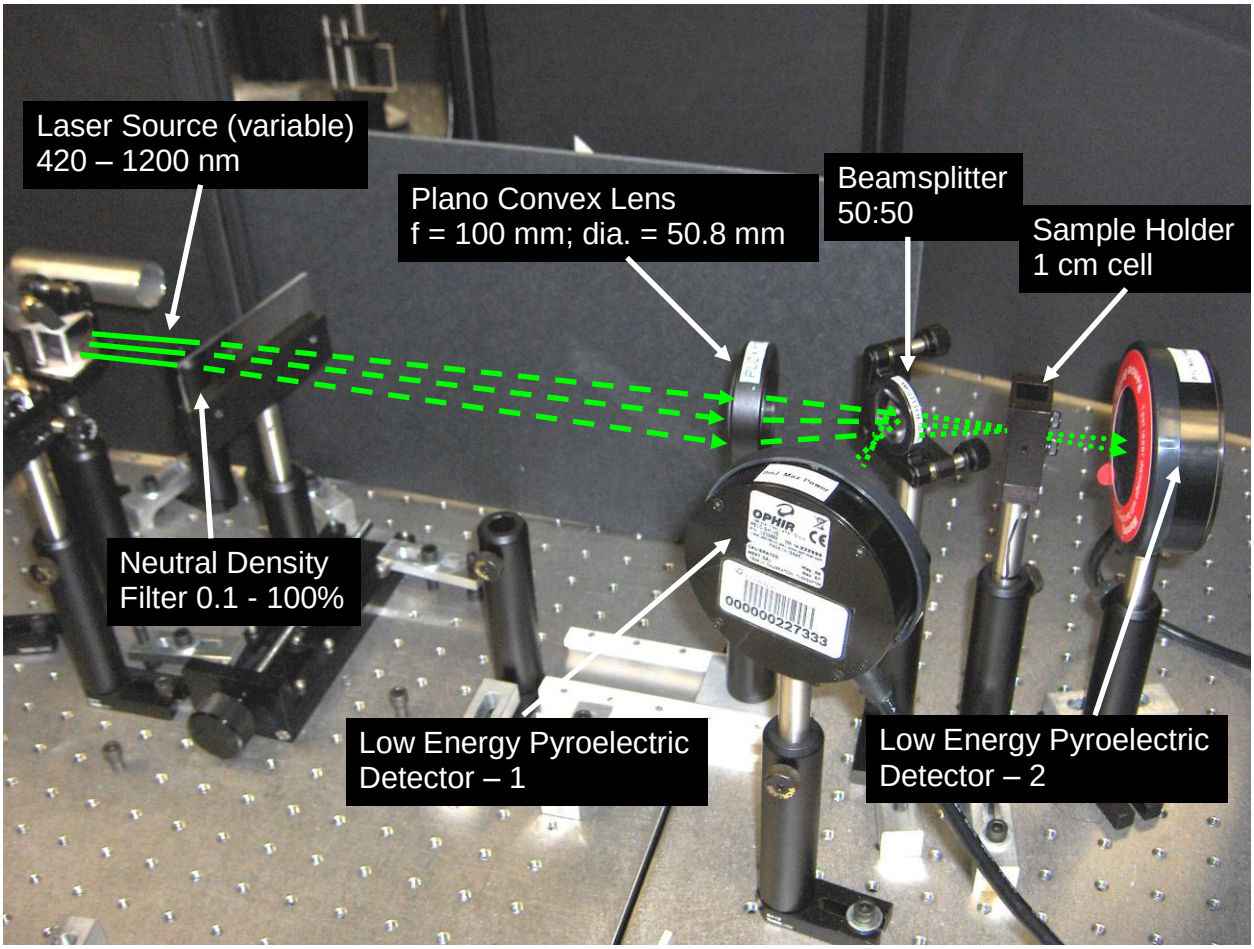

Figure 2-15. Photo schematic of OPO-based nonlinear transmission apparatus.

laser pathway. The beam diameter at the lens was 14 mm. Utilizing Equation 9[58], a calculated

$$\omega = \frac{\lambda f}{\pi \omega_0} \qquad (9)$$

beam waist of 63 μm was attained assuming a Gaussian beam shape with an energy density range of 0.01 - 1.10 J/cm^2. λ, f, and ω represent the wavelength, lens focal length and half the Gaussian beam diameter at the lens respectively. The focusing lens was positioned so the tightly focused beam falls within the confines of the sample holder. Adjustment of the focus to the

exact center of the sample holder is facilitated by placing the focusing lens on single axis translation stage. A 50:50 beamsplitter is placed prior to the focus and directed towards detector 1. Detector 2 is placed at an equivalent distance from the beamsplitter behind the sample holder. Both detectors are positioned so that the entire beam occupied no more than one half the detector's available area, thus insuring no light energy emitting from the sample misses the detector. It is important to note that the exact linear distance from the 50:50 beamsplitter to each detector was maintained to insure an identical spot size on each of the matched detectors.

SAFETY NOTE: Special attention must be given to safety during the course of the experiment due to, as depicted in Figure 2-12, the generation of an additional spot of focused laser energy between the 50:50 beamsplitter and detector 1. This area must be avoided at all times during the course of the experiment as the potential for serious equipment damage or personal injury due to the presence of high energy density laser light.

NLO Chromophore Test Series

The investigation of a series of platinum-acetylide dimers containing large two photon cross section chromophores linked to a variety of arylene core units of differing electron donating abilities which can provide different triplet excited state energies was undertaken to determine the presence of enhanced nonlinear absorption. The combination of two photon excitation and platinum induced intersystem crossing to afford triplet excited states which are strongly absorptive was proposed to have a dual mode (TPA/ESA) nonlinear mechanism for enhanced nonlinear absorption. The platinum-acetylide dimers presented here were synthesized by Dr Kye-Young Kim and she also assisted in the collection of data for this study. The series of platinum-acetylide dimers, **Pt2-Ar**, containing different triplet chromophores are shown in Figure 2-16 along with the parent model chromophore **E1-DPAF** which has been shown to have

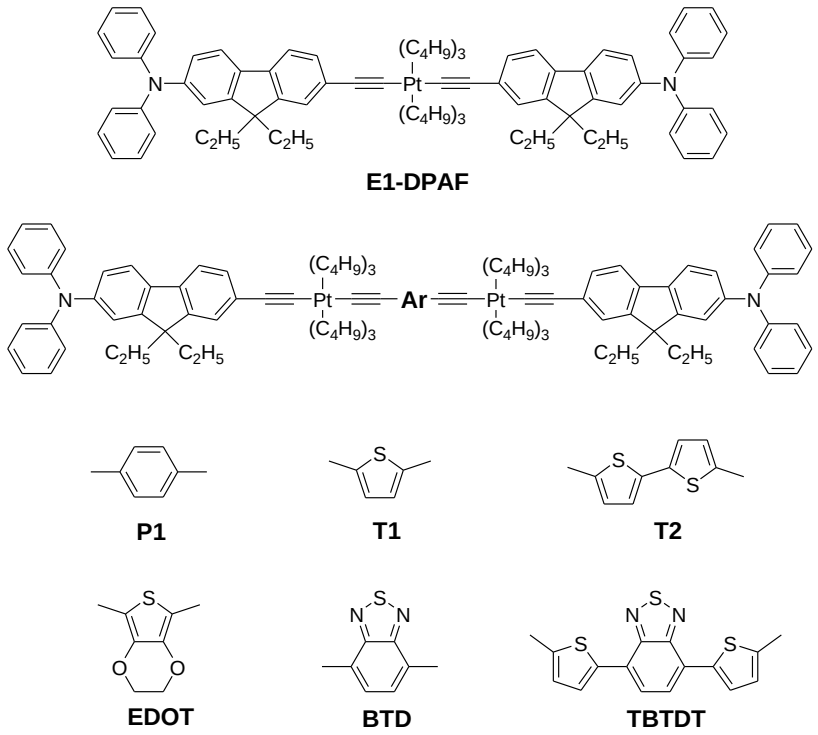

Figure 2-16. Platinum-acetylide dimers, **Pt2-Ar**, utilized for the NLT test study.

significant nonlinear character.[59] These platinum-acetylide dimers were the subject of a test study for the newly constructed nonlinear transmission apparatus examining for the evidence of nonlinear activity. **E1-DPAF** was utilized as a control due to its documented large TPA cross section and efficient intersystem crossing to afford strongly absorbing long lifetime triplet states.[59] Because of these factors, **E1-DPAF** has the potential to exhibit a dual mode (TPA/ESA) nonlinear mechanism. These factors make **E1-DPAF** a suitable model to judge the relative strength of the nonlinear response in the **Pt2-Ar** series and to verify the relative effectiveness of the detection capability of the experimental setup.

The reason for conducting the test study was two-fold. The primary goal was the desire to evaluate the nonlinear detection capability of the newly designed and constructed NLT apparatus and evaluate its ease of use, quality of data obtained and its flexibility of use with a variable wavelength source. Central to this goal was the ability to integrate the NLT apparatus with our

group's newly acquired optical parametric oscillator (OPO) which is the source of the variable wavelength laser energy. Second was the desire to evaluate the nonlinear response of the **Pt2-Ar** series for evidence of optical limiting character.

Photophysical Properties

A comprehensive photophysical study of the **Pt2-Ar** series was accomplished by Dr Kye-Young Kim but only the key photophysical features affecting the experimental parameters of the nonlinear determination will be presented here.

Ground State Absorption

Ground state absorption spectra were obtained for the **Pt2-Ar** series in optically dilute THF solution and are shown in Figure 2-17. The main absorption feature of the **Pt2-Ar** series is a strong ligand-based $\pi-\pi^*$ transition which varied only slightly from 382 nm to 387 nm. Additional absorption bands present as the arylene core units are varied and appear red-shifted to the main absorption feature. As the arylene core units are varied, the red-shift of these absorption bands indicates the energy change of the lowest excited state. Therefore the lowest excited energy state of the series can be ordered as: **P1** > **T1** > **EDOT** > **T2** > **BTD** > **TBTDT**. In general, as the energy of the core unit decreases so does the energy of the lowest excited state. In addition, for BTD and TBTDT it was determined the addition of an ^{1}MLCT component to the $\pi-\pi^*$ transition attributes to the dramatic red-shift in these compounds.

Transient Absorption

Nanosecond transient absorption measurements of the **Pt2-Ar** series were conducted in deoxygenated THF solution and are shown in Figure 2-18. For the series each chromophore displays strong triplet-triplet absorption in the visible and near-IR regions. The general excited state absorption characteristics of **P1**, **T1**, **T2** and **EDOT** are quite similar with only minor

differences while **BTD** and **TBTDT** present transient absorption spectra which are significantly different in shape.

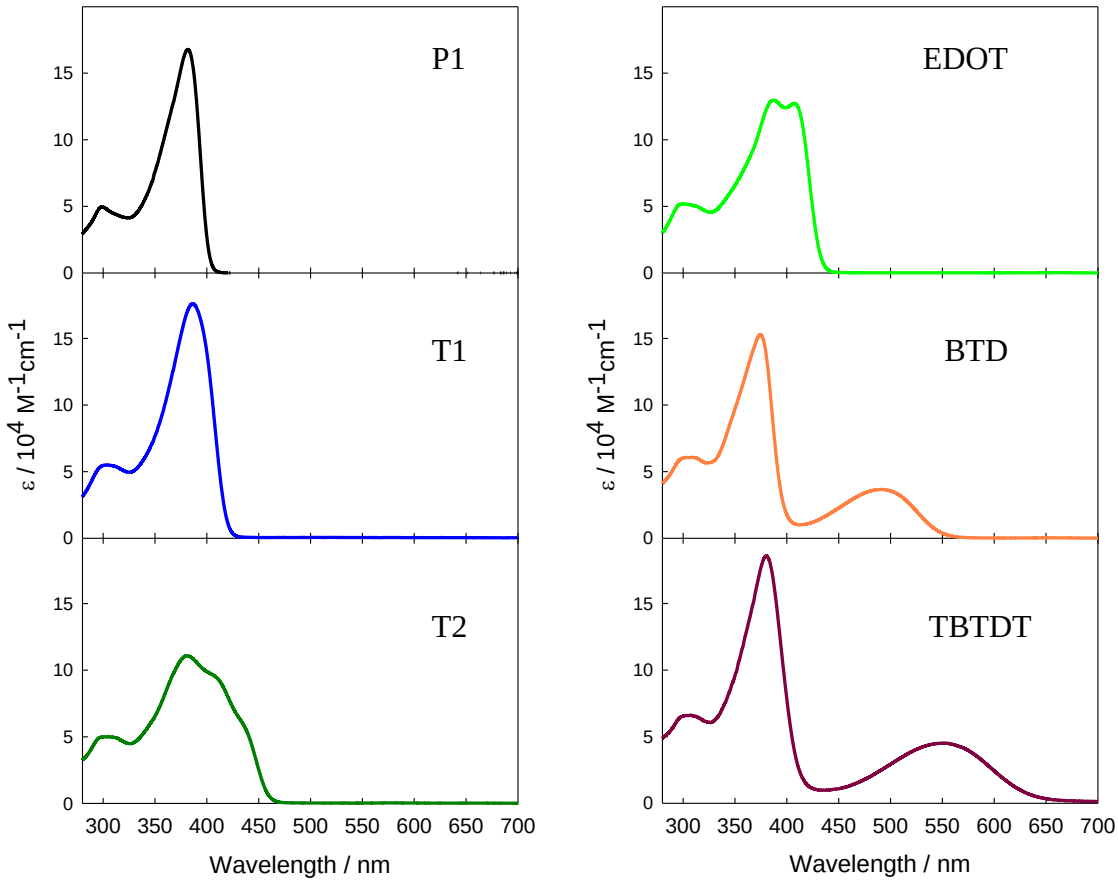

Figure 2-17. UV-visible ground state absorption spectra of **PT2-Ar** series in THF solutions.

P1 exhibits a broad transient absorption ranging from 400 to 900 nm with the longest transient lifetime of 17 μs. **T1** also presents a broad transient absorption which is only slightly narrower and weaker than that of **P1** with a range of 420 to 750 nm and lifetime of 8.4 μs. The transient absorption range of **EDOT** is identical to that of **T1** but is slightly stronger with a lifetime 3.6 μs. **T2** exhibits a narrower transient absorption with a range of 450 to 720 nm but has the strongest triplet-triplet absorption.

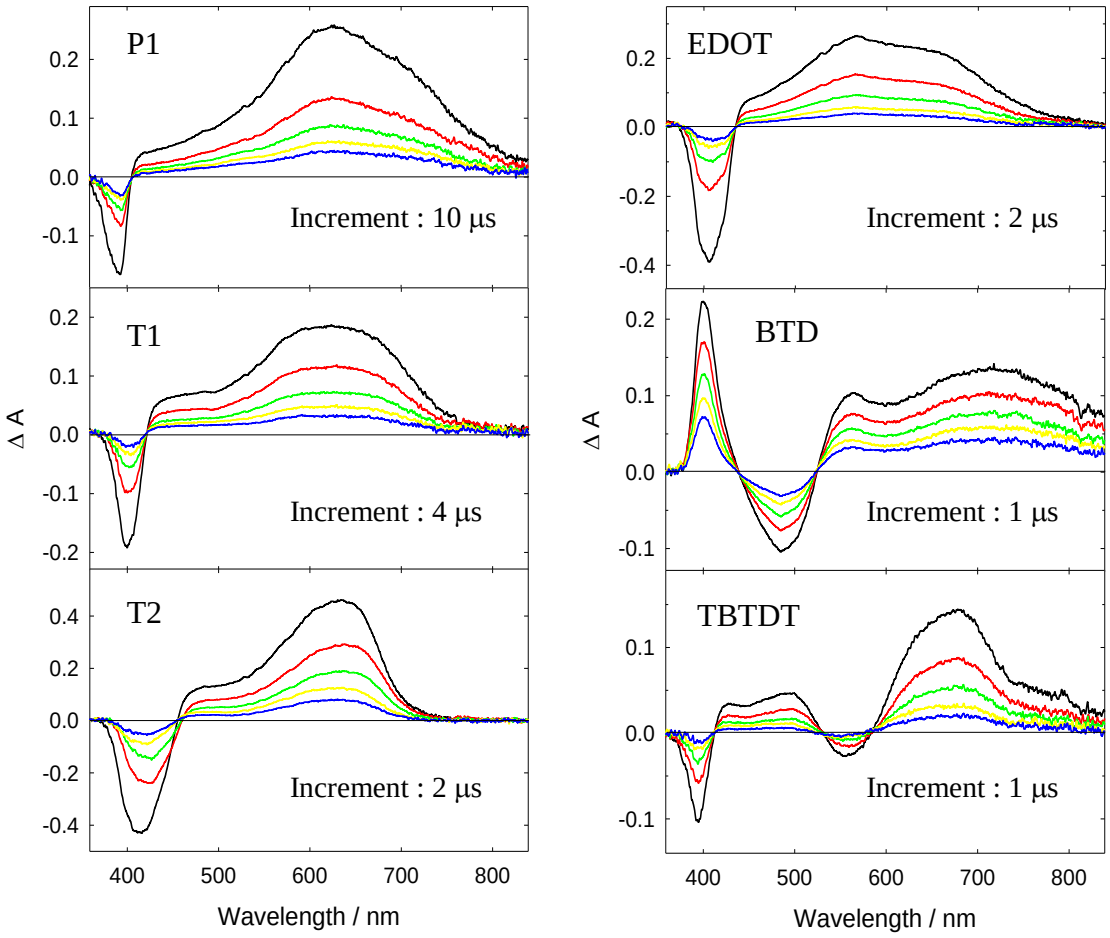

Figure 2-18. Transient absorption spectra of **Pt2-Ar** series in deoxygenated THF solution.

BTD and **TBTDT** transient absorption shapes are significantly different than those of **P1**, **T1**, **T2** and **EDOT**. **BTD** exhibits a bimodal shape with a strong transient absorption from 375-450 nm and weaker absorption which begins at 520 nm and extends well into the near-IR. **TBTDT** also exhibits a bimodal shape with a relatively weak transient absorption band in the visible region with a range of 420-530 nm and a modest transient absorption from 600 to the near-IR region. It was noted the transient absorption decay lifetimes mirrored the phosphorescence lifetimes, indicating excited state absorption for the **Pt2-Ar** series originates primarily from the lowest energy excited states and its absorption character is determined by the arylene contained at its core. Due to the fact that the **Pt2-Ar** series utilizes the same TPA

chromophore and should show similar excited state absorption cross sections it become evident the differences in the triplet-triplet absorption manifest from the differences in the arylene units.

Nonlinear Absorbance Determination

To detect the nature and strength of a dual mode nonlinear response comprised of two photon excitation followed by excited state absorption from a highly absorbing excited state, it was necessary to first determine the appropriate wavelengths and conditions to obtain the desired response. The first consideration was the determination of range of excitation wavelengths which could potentially elicit a two photon induced excitation of the chromophore to a singlet excited state. For this information the ground state absorption data were used to choose a potentially suitable wavelength range. For the series a generous range of strong ground state absorption exists for all the complexes from 250 nm to at least 400 nm. This equates to a potential two photon active range for the TPA chromophore of 500-800 nm. This correlated well with the reported two photon absorption maximum wavelength of 612 nm for **E1-DPAF** which contains the same TPA chromophores as the **Pt2-Ar** series.[59] The effort to optimize the TPA excitation conditions was deemed essential to generate a sufficient singlet excited state population which could in turn be converted through intersystem crossing to triplet excited states. A systematic survey of wavelengths and chromophore concentrations was carried out to determine the optimum conditions with which to proceed.

For the survey, a variety of concentrations were explored from 60 mM to 20 mM to establish a viable concentration range. It was determined that for concentrations of 40 mM and higher, initial energies needed to transmit enough energy to be detected were above the nonlinear thershold or the sample was undergoing optical scattering due to the high solute concentration. As shown in Figure 2-19 for concentrations of 60 mM, 800 nm excitation seemingly did not produce a two photon excitation of the **Pt2-Ar** series. Also at 60 mM concentrations, it can be

noted nonlinear response was evident at both 600 and 625 nm. For both sets of data near saturation clamping of the output energy was discovered. Given these results, a systematic reduction in concentration was performed. As the concentration of chromophore was reduced, the input energy necessary to detect output energy was greatly reduced and positive evidence of a nonlinear response was seen. Upon reaching concentrations of 20 mM, sufficient transmission of lower intensity light was noted and it was determined a region of near linear transmission was present. For the same samples it was noted that as the input energy increased the ratio of input energy to output energy began to change and thus the absorption was becoming nonlinear. Since it was deemed desirable to observe the region where transmission of light changed from linear to nonlinear the concentration of 20 mM was chosen as optimum. The determination of wavelength was decided in much the same manner. At both 600 and 625 nm a region of linear absorption was evident, however it was noted that departure from linear absorption occurred at slightly lower energies for 600 nm than for 625 nm. In addition, the OPO was able to produce more power at 600 nm than at 625 nm and the availability of output energy from the OPO would mean the ability to sample a much wider energy range.

Final determination of the nature of the nonlinear response for the **Pt2-Ar** series was conducted at the two photon excitation wavelength of 600 nm and 20 mM in a solution of benzene (Figure 2-21). Benzene was used as the final solvent as it was determined to be the best for complex solubility and had the overall effect of raising the initial light transmission through the sample. To effectively evaluate the relative strength of the nonlinear response in the **Pt2-Ar** series the model complex **E1-DPAF**, for which the two photon and excited state absorption properties are known,[59] was also measured at 20 mM in benzene. In Figure 2-21 a plot of input energy versus transmittance yields the nonlinear transmission results for the **Pt2-Ar** series.

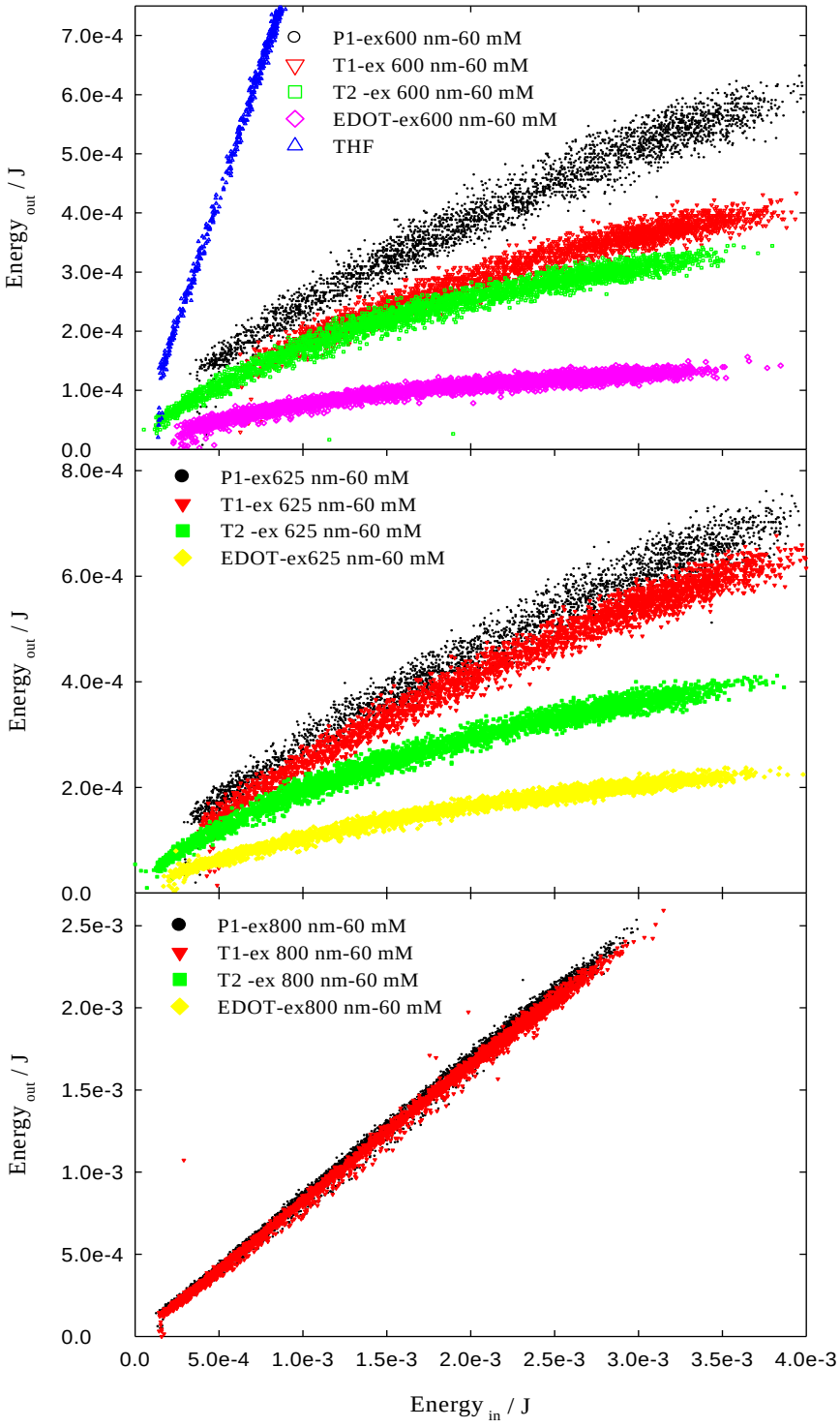

Figure 2-19. Nonlinear determination results of **Pt2-Ar** series in 60 mM THF solutions at two photon excitation wavelengths of: 600 nm (top), 625 nm (center), and 800 nm (bottom).

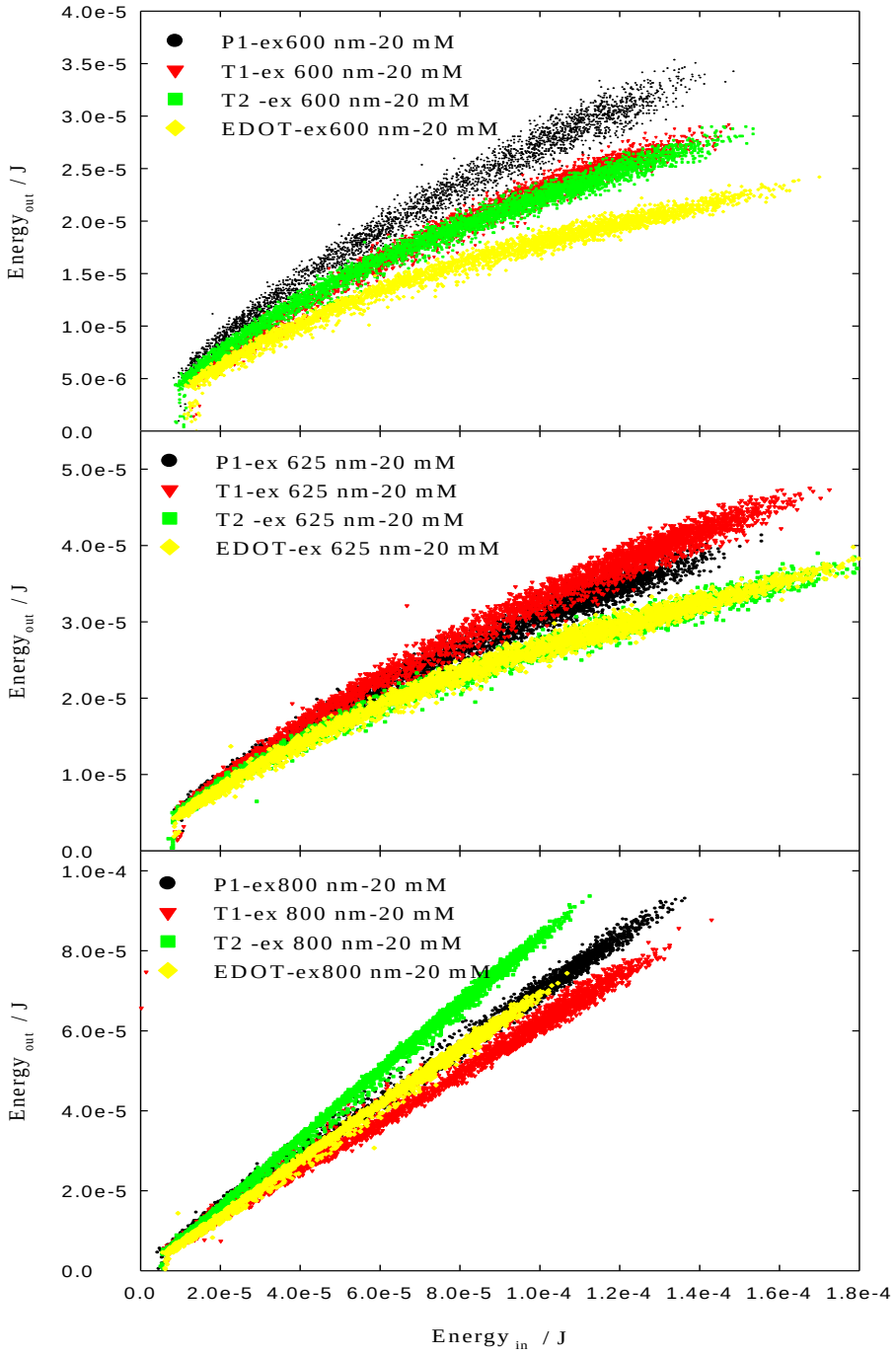

Figure 2-20. Nonlinear determination results of **Pt2-Ar** series in 20 mM THF solutions at two photon excitation wavelengths of: 600 nm (top), 625 nm (center), and 800 nm (bottom).

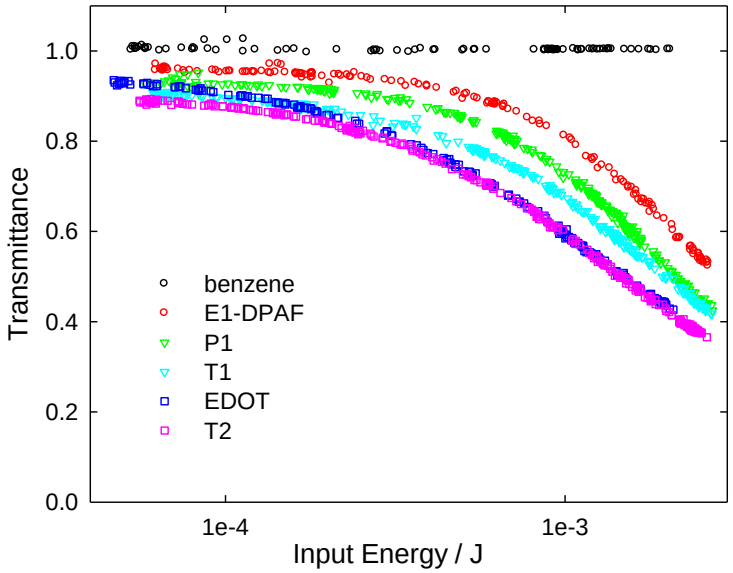

Figure 2-21. Nonlinear transmission curve of the **Pt2-Ar** series in 20 mM benzene under two photon excitation condition at 600 nm.

Test Results

The nonlinear transmission apparatus was designed, tested and built in-house for determining the presence and relative strength of a nonlinear response and optical limiting. The NLT setup was able to detect and render data to depict the desired nonlinear responses of interest. In the current configuration the NLT apparatus is capable of a repeatable semi-quantitative representation of nonlinear response. Ease of setup and data collection presents this NLT technique as an experiment that can be utilized with only a minimum of prior training and orientation. The quality of data gathered is excellent and very easy to compile into useable nonlinear absorption and optical limiting curves. Complete details on data collection and presentation are contained in the user manual found in Appendix B.

A key goal in this test study was the ability to measure the relative strength of a detected NLO response. This goal was considered only a marginal success. Despite detailed two photon cross section data and excited state absorption data being available for **E1-DPAF**[59] the lack of NLT or other nonlinear absorption data such as Z-scan makes direct NLT comparison difficult.

Future use of this setup in conjunction with experiments capable of determining nonlinear absorptive cross sections will allow for direct quantitative comparisons of nonlinear data results with those from other studies with little need for exhaustive model compound synthesis or standard sample preparations.

A positive result from the testing and utilization of the nonlinear transmission setup was the successful collection of nonlinear data for the **Pt2-Ar** series of platinum-acetylide dimers as well as the confirmation of an enhanced dual mode nonlinear response. Successful two photon excitation of the TPA followed by excited stated absorption was also confirmed and verified. Excitation at the TPA wavelengths of 600 and 625 nm was successfully accomplished in a wavelength region where no ground state absorption is present, eliminating the possibility of contribution from a one photon absorption process. Evidence of further enhancement from an ESA mechanism was also determined to be present. As noted previously, TPA alone affords a quadratic dependence on incident light intensity where as a TPA/ESA system affords a cubic dependence. For **E1-DPAF**, the cubic nature of the data is fairly pronounced. Interestingly as the series progresses in the rank order of the observed strength of triplet-triplet absorption as found by transient absorption spectra reported in a previous section, the cubic nature lessens to a nearly quadratic dependence for **Pt2-EDOT** and **Pt2-T2**. This trend would seem to contradict the previous conclusion and indicate a decreased contribution from an ESA mechanism, possibly due to smaller absorption cross sections, and a more dominate nonlinear contribution from TPA.

Despite this inconsistency the **Pt2-Ar** series appears to display an overall enhanced NLT response when compared to the model **E1-DPAF** chromophore. A reason for this difference in nonlinear response can be attributed to the variation in the core arylene units. This is logical since the TPA chromophore is identical for each complex in the series. With the TPA nonlinear

excitation pathway identical for each compound the differences seen are deemed to originate from the ESA active portion of the chromophore. Preliminary analysis of the data found here point to the strength of triplet-triplet absorption as the main variable that correlates to the strengthening found in the nonlinear response in the **Pt2-Ar** series.

Instrumentation

Nonlinear transmission determination experiments were performed on an in-house built optical limiting setup which was described in a previous section. A variable wavelength laser source was provided by a Continuum Surelite II-10 Nd:YAG laser (355 nm, third harmonic of the 1064 nm fundamental) augmented with a Surelite OPO Plus (wavelength range: 420-570 and 590-1200 nm). Dual one inch uncoated BK7 glass prisms from Thor Labs were utilized to position the laser source at the entry of the optical limiting setup. A variable neutral density filter capable of transmission values ranging from 0.3% to 100% obtained from Thor Labs was utilized to attenuate the laser source to obtain a variable power profile. An uncoated plano convex lens obtained from Thor Labs with a nominal focal length of 130 mm and a 50.8 mm diameter was used to achieve a tightly focused beam at the sample. Prior to the focus, an economy, laser stable 50:50 beamsplitter from Thor Labs was used to redirect a portion of the incident laser source toward detector 1 and to permit the remaining energy to continue through the sample to detector 2. Change in transmittance as a function of laser power was monitored directly utilizing an Ophir Laserstar dual channel power meter configured with a pair of matching Ophir OPH PE10-SH V2 pyroelectric detectors (detectors 1 and 2) having a sensitivity range of 10 μJ to 10 mJ.

CHAPTER 3
SYNTHESIS AND PHOTOPHYSICS OF NLO CHROMOPHORES

Introduction

The main focus of this project was the synthesis and photophysical investigation of a selected series of metal-organic chromophores with the potential to exhibit an enhanced dual mode nonlinear response. The dual mode mechanism utilized is a combination of two photon excitation followed by an NLO enhancing excited state absorption. The characteristics of this mechanism have been explained in detail in previous chapters. The experimental method employed to detect and identify this dual mode NLO response utilized the nonlinear transmission apparatus developed in Chapter 2.

To achieve the desired enhanced TPA/ESA mechanism a series of metal-organic chromophores were developed utilizing established large cross section TPA architecture in concert with moieties known to afford long-lived triplet excited states with strong excited state absorptions. It was found that the metal-organic complexes produced exhibited an enhanced TPA/ESA nonlinear response consistent with the models presented previously and in the literature. Also in this chapter, modifications to the NLT apparatus along with an excitation source modification on an emissions instrument to allow for detection of two photon induced emissions will be presented.

Synthesis

Organic Chromophore Synthesis

The synthesis of the two photon absorbing chromophore ligand, 4,4'-(2,2'-bipyridine-5,5'-diylbis(ethyne-2,1-diyl))bis(N,N-diphenylaniline), **TPA-1**, is shown in Figures 3-1 through 3-3. A general synthesis for the metallated complexes of the **TPA-1** chromophore is shown in Figure 3-4. Initial attempts to synthesize **TPA-1** focused on a "core-out" approach which was similar to

the approach used in previous work done in our group on similar compounds. [1, 9, 17, 20-22, 60, 61] However this methodology proved to be inefficient due to synthetic limitations of material purification necessary for the final coupling step. The initially proposed final step involved a Sonogashira coupling of 5,5'-diethynyl-2,2'-bipyridine and 4-bromo-*N*,*N*-diphenylaniline to produce **TPA-1** (not shown). Under Sonogashira conditions this coupling was only effective in producing pure **TPA-1** in good yield if the mono-brominated triphenylamine starting material was very pure. Specifically, the reaction of triphenylamine with *N*-bromosuccinimide (NBS) in $MeCl_2$ at 0 °C (Figure 3-2, step i)

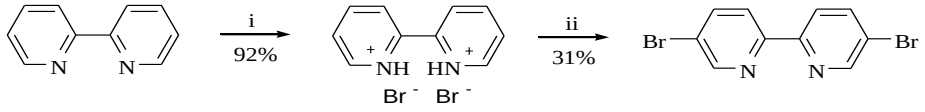

i. Acetyl bromide, MeOH; ii. Br_2, 180 °C, 4 days.

Figure 3-1. Synthesis of **TPA-1** chromophore ligand central core.

resulted in a majority product of 4-bromo-*N*,*N*-diphenylaniline but also returned starting material and the dibromo analog. Lack of chromatographic resolution in nonpolar hexane ($\Delta R_f < 0.10$) of these products required multiple elutions on silica gel to retrieve a product pure enough to proceed. The drawbacks initially lead to a disappointing 18% yield of the mono-brominated triphenylamine. An improved route to the synthesis of 4-ethynyl-*N*,*N*-diphenylaniline **5** was synthetically explored which, in turn, lead to the exploration of a more convergent approach (Figure 3-2 and 3-3) to synthesizing **TPA-1**.

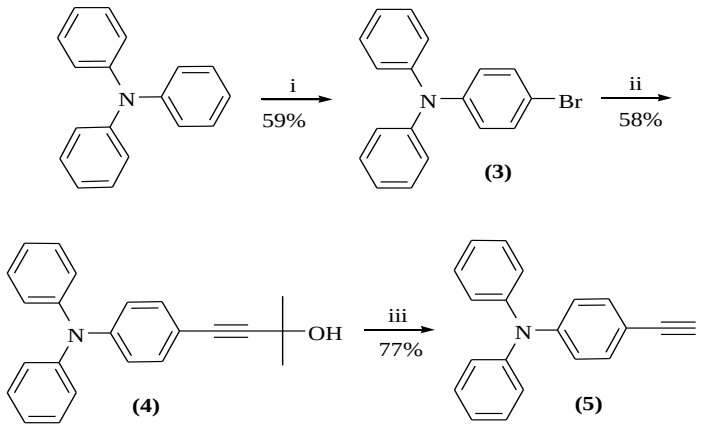

i. *N*-bromosuccinimide, $MeCl_2$, 0 °C, 6hrs; ii. 2-methyl-3-butyn-2-ol, Et_3N, Pd/CuI (cat.) 70 °C, 6 hrs; iii. KOH, toluene, reflux, 6 hrs.

Figure 3-2. Synthesis of chromophore ligand end caps.

The Sonogashira coupling of mono-brominated triphenylamine with 2-methyl-3-butyn-2-ol (Figure 3-3) incorporates a highly polar protecting group (along with the desired ethynyl moiety) onto the triphenylamine framework. This greatly simplifies the chromatographic separation and purification of the alcohol protected ethynyl product and eliminates the need for multiple purification steps of mono-bromo triphenylamine prior to a subsequent reaction. Following the coupling reaction, **4** can easily be separated from the starting material and its dibromo analog via flash chromatography on silica gel utilizing 2:1 hexane/Et_2O with ΔR_f values > 0.50. Deprotection of **4** with KOH in toluene at reflux produces **5** in a 77% yield. Overall, the revised synthetic route was successful in producing **5** in three steps with an overall yield of approximately 26%. The final synthetic step in the generation of **TPA-1** (Figure 3-3) involves the coupling of **2** and **5** under Sonogashira conditions and proceeds with a 50% yield. This final step was again a marked improvement over the previously attempted "core out" route which yielded only 29% upon the Sonogashira coupling of 5,5'-diethynyl-2,2'-bipyridine and 4-

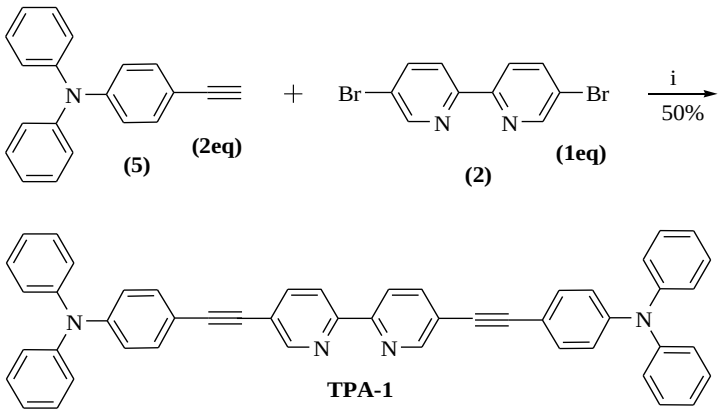

i. Et_3N, Pd/CuI (cat.) 70°C.

Figure 3-3. Synthesis of TPA chromophore.

bromo-*N*,*N*-diphenylaniline (not shown). Overall, the synthesis of **TPA-1** could be completed in six steps with a combined yield approaching 13%.

Metal-organic complex synthesis

Metallation of **TPA-1** with a slight excess of $Ru(bpy)_2Cl_2$ in refluxing THF/MeOH affords Ru(**TPA-1**)$(bpy)_2^{2+}2\cdot Cl^-$. A saturated solution of NH_4PF_6 was added drop wise to afford the PF_6^- analog **Ru-1**. Flash chromatography on silica gel, yielded pure **Ru-1** as a dark red powder. Metallation of **TPA-1** with a slight excess of $Re(CO)_5Cl$ in refluxing toluene affords Re(**TPA-1**)$(CO)_3Cl$. Solvent evaporation and repeated rising with acetone yields pure **Re-1** as a bright red powder. Metallation of **TPA-1** with $Ir_2(ppy)_4Cl_2$ (ppy = phenylpyridine) was accomplished in refluxing 2-methoxyethanol under an argon atmosphere. Upon cooling, a saturated solution of NH_4PF_6 was added drop wise to generate the PF_6^- analog **Ir-1**. Flash chromatography on neutral alumina, yielded pure **Ir-1** as a dark yellow powder. The synthetic scheme is depicted in Figure 3-4.

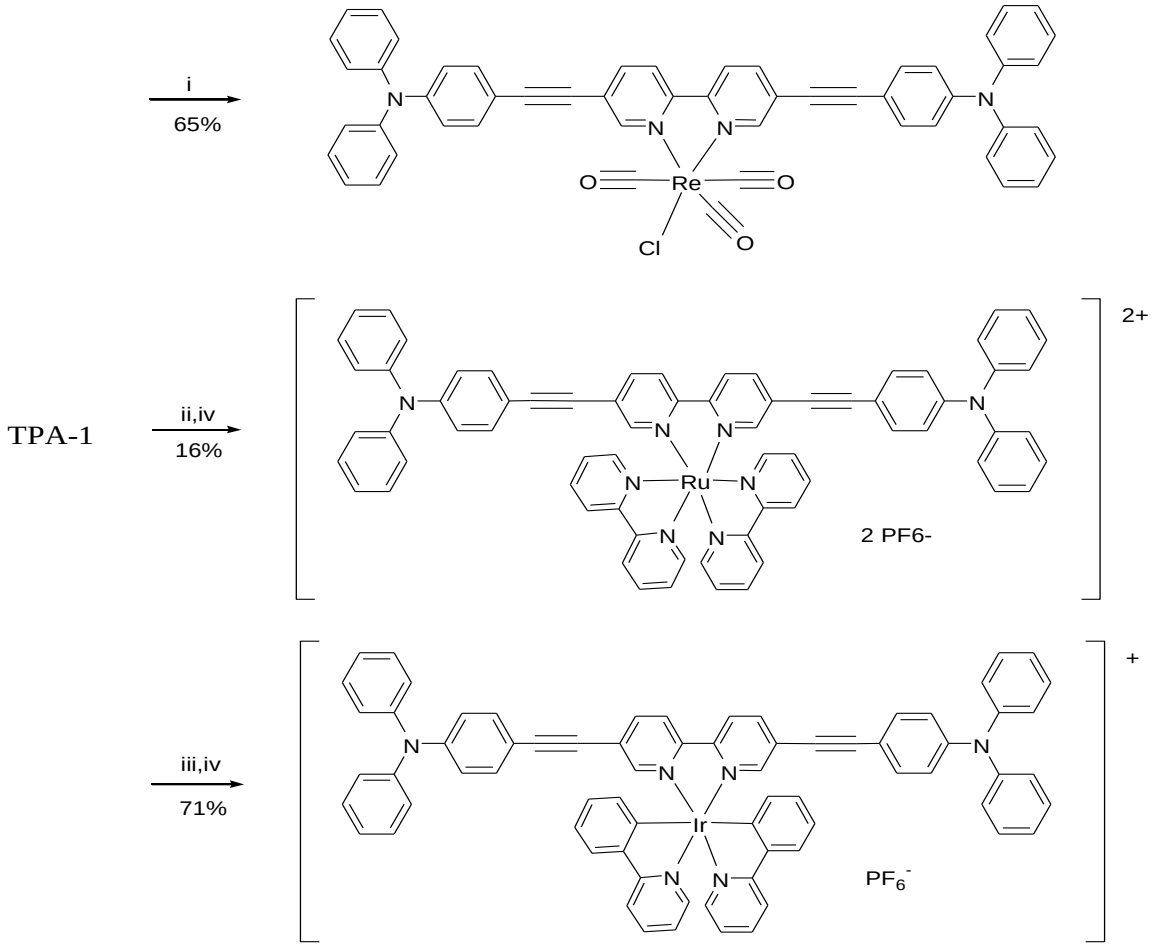

i. $Re(CO)_5Cl$, toluene, reflux, 45 min. ii. *cis*–$Ru(bpy)_2Cl_2$, MeOH/THF (4:1), reflux, 18 hrs. iii. $Ir_2(ppy)_4Cl_2$, 2-methoxyethanol, reflux, 26 hrs. iv. Sat. aq. NH_4PF_6.

Figure 3-4. Metallation of TPA chromophore.

Results and Discussion

Photophysical Properties

UV-Visible Absorption Spectroscopy

Absorption spectra of each compound were obtained utilizing optically dilute CH_2Cl_2 or THF solutions (OD ~ 0.1). The absorption spectra for the series are presented in Figure 3-5. Table 3-1 presents the list of absorption maxima, extinction coefficients / molar absorptivity values and absorption band assignments. Molar absorptivity values (ε) were calculated based on

$$\text{Absorbance (A)} = \varepsilon\, b\, c \qquad (1)$$

Equation 3.1 where (A) equates to the absorbance of the sample, b is the cell path length (1 cm), and c is the sample concentration (M).

The free ligand (**TPA-1**) absorption is dominated by high energy short-axis polarized π-π* transitions of the bipyridine core at 301 nm as well as a long-axis polarized π-π* transition feature incorporating both the bipyridine core and the triphenylamine end caps that appear at 399 nm. It should be noted that in the free ligand the bipyridine unit is not in a coplanar configuration. When unbound, 2,2′-bipyridine is free to rotate about the 2,2′ bond and prefers a twisted confirmation in its unbound low energy state. As seen below, this has an impact on the energy of the π-π* transitions.

The absorption of each of the metal complexes is very similar relative to the free ligand. In the condition where the ligand is complexed with a metal, however, the geometric constraints of the coordinated metal dictate the bipyridine central core of the ligand are directed into a coplanar configuration relative the central axis of the ligand. With this planarity as a core platform, the ligand generates a longer effective conjugation length and one would expect an absorption red shift of the main features of the parent ligand. There is in fact a red shift of the 301 nm absorption bands to 334 nm for the bipyridine core in both **Re-1** and **Ru-1** and a shift to 336 nm in **Ir-1**. The red shift of the absorption associated with the long axis transition of the ligand moves from 399 nm to 460 nm for **Re-1** and **Ru-1** and 471 nm for **Ir-1**. This band, in addition to red shifting, becomes broader than in the free ligand π–π* system. The extinction coefficient values are consistent with those of other similarly metallated complexes.[17,20-22-] Despite their

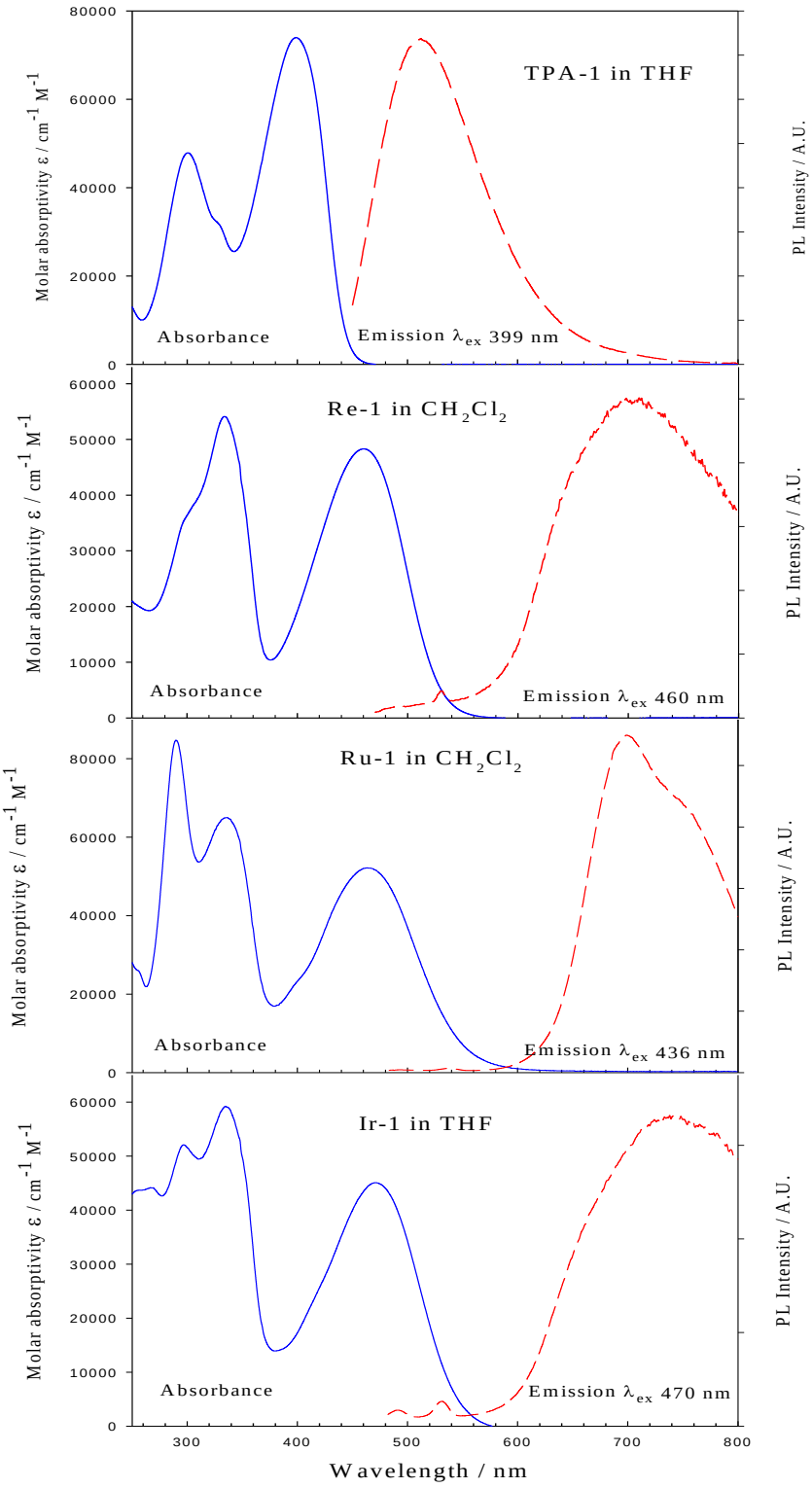

Figure 3-5. UV-visible absorption and emissions spectra. OD - 0.1, solvent– noted above (deoxygenated for emission). λ_{ex}: **TPA-1** - 399 nm, **Re-1** - 460 nm, **Ru-1** -463 nm, and **Ir-1** - 470 nm.

Table 3-1: Near UV-visible absorption bands of target ligand and metal-organic complexes.

Complex	λ_{max} / nm (ε_{max} / $M^{-1}cm^{-1}$)	Assignment
TPA-1 [b]	301 (48,200) 399 (73,900)	π–π* - bpy (short axis) π–π* - ligand (long axis)
Re-1 [a]	334 (55,000) 460 (49,300)	π–π* - **TPA-1** (short axis) π–π* - ligand (long axis) & MLCT
Ru-1 [a]	290 (74,300) 334 (57,600) 462 (46,500)	π–π* - bpy π–π* - **TPA-1** (short axis) π–π* - ligand (long axis) & MLCT
Ir-1 [b]	297 (52,600) 336 (59,500) 470 (45,600)	π–π* - ppy π–π* - **TPA-1** (short axis) π–π* - ligand (long axis) & MLCT

a Measurements were collected with optically dilute (OD~0.1) CH2Cl2 a or THF b solutions at 25 °C.

absolute values being lower than the 74,000 cm^{-1} M^{-1} extinction coefficient value for the π–π* band in the free **TPA-1** ligand it appears overall oscillator strength is maintained. As the electronic nature of these bands change, variations of the individual values of the extinction coefficients should be expected.

Addition of the metals Re, Ru, and Ir to the ligand affords an electronic transition pathway between the metal and the ligand with the potential to transfer charge density from the metal to the ligand. This metal to ligand charge transfer (MLCT) represents an added energy transition which, as previously discussed, is similar in energy to the π–π* transition and therefore should manifest its presence by introducing absorption in the general vicinity of the π–π* transitions. The MLCT absorption arises as a result of the transfer of an electron from the dπ orbital of the

metal to the π* orbital of the ligand. If the absorption bands centered at 460 nm (471 nm for **Ir-1**) are assigned as pure spin-allowed MLCT bands, the extinction coefficients would be expected to be much smaller and in the range of 5,000 for typical (diimine)$Re^{I}(CO)_3Cl$ [62, 63] and 15,000 for polypyridine Ru^{II} compounds,[9] therefore some of the absorption presented for the metal complexes are considered to contain both π–π* and MLCT character. As an example, in the absorption band of **Ru-1** centered around 460 nm, a hint of a shoulder exists at 405 nm which could be evidence of MLCT absorption obscured beneath the main π-π* absorption band of stronger overall oscillator strength.

This implies the overall nature of these absorption bands is made up of the combination of red-shifted π–π* intraligand charge transfer (ILCT) character rising from the conjugation enhancement of the bipyridine rings at the core of the **TPA-1** ligand and MLCT character of the dπ to π* transitions from the coordinated metals.

Emission Spectra

The mission spectrum of each compound was obtained at room temperature utilizing an optically dilute, deoxygenated THF solution. Lifetimes were obtained with time-correlated single photon counting utilizing 375 and 450 nm excitation sources. Emission quantum yields were measured by relative actinometry with 9,10-diphenylanthracene in cyclohexane (Φ_{em} = 0.90) [64] and $Ru(bpy)_3$ in water (Φ_{em} = 0.037) [1, 65] as the actinometers for **TPA-1** and the metal complexes respectively. The emission spectra for the series are presented in Figure 3-5. Table 3-2 presents the list of emission maxima, quantum yields, and lifetimes. Excitation of **TPA-1** at 301 and 399 nm yielded identical results and presented a very intense, short-lived, broad emission at 512 nm with a quantum yield of unity (ϕ_{fl} = 1.0). Lifetimes of both aerated and deoxygenated solutions are both less than 5 ns.

Each metallated complex, in contrast, displayed very weak emissions and long lifetimes. Emission spectra for **Re-1** and **Ir-1** afforded broad and featureless emissions while **Ru-1** afforded a narrower emission band with a hint of structure. **Re-1** emission was observed at

Table 3-2: Photophysical properties of target ligand and metal-organic complexes.[a]

Complex	λ_{em} nm	τ_{em}[b] ns	ϕ_{em}	$10^3 k_r$[c] s^{-1}	$10^6 k_{nr}$[c] s^{-1}	τ_{TA}[d] ns
TPA-1[2]	512	2.3	1.0	-	-	-
Re-1[1]	696	3300	0.0051	1.5	0.3	441
Ru-1[1]	700	796	0.0018	2.3	1.3	431
Ir-1[2]	742	1600	0.0009	0.5	0.6	428

[a] Measurements were conducted on Ar deoxygenated CH_2Cl_2[1] or THF[2] solution at 298 K. [b] Lifetimes were calculated with a single exponential decay fit. [c] $k_r = \phi_{em}/\tau_{em}$; $k_{nr} = 1/\tau_{em}(1- \phi_{em})$. [d] Triplet lifetimes were calculated transient absorption spectra with a single exponential decay fit.

excitation wavelengths of 334 and 460 nm. Upon excitation at 334 nm, **Re-1** generated two broad and weak emission bands at 520 and 696 nm (ϕ_{fl} = 0.0051), presenting at relatively the same intensity. When observed at an excitation wavelength of 460 nm, emission at 520 nm was negligible and the broad emission at 700 nm was the sole emission feature. The lifetime of the 520 nm emission is very short, less than 5 ns, and can be assigned as fluorescence generated from the π-π* state of the ligand. The short lifetime and low quantum yield of this fluorescence is due to quenching brought about by rapid intramolecular energy transfer to the MLCT manifold and intersystem crossing resulting in energy states residing at lower energies. It has been noted in previous studies, that even though π-π* fluorescence attributed to a ligand complexed with a transition metal is not typically observed, a ligand with a large radiative decay rate allows fluorescence to "leak out" even though the π-π* state is short lived.[60] The broad emission of **Re-1** centered at 696 nm have the lifetimes of 590 ns for an aerated solution and 3.3 μs for a solution which has been deoxygenated with Ar for 30 minutes. Long emission lifetimes that are prolonged with the removal of oxygen strongly suggests that it can be assigned to emission originating from a triplet manifold comprised of ^{3}π-π* and ^{3}MLCT excited states.

Ru-1 emission was observed with excitation at wavelengths of 336 and 463 nm. Upon excitation at 336 nm, **Ru-1** also generated two broad and weak emission bands at 520 and 700 nm (ϕ_{fl} = 0.0018), however relative intensity of the two emissions differed significantly. The intensity of the 700 nm emission was on the order of six times larger than that of the 520 nm emission indicating less fluorescence "leaking" from the ruthenium complex. Upon excitation at 463 nm only emission at 700 nm was observed with an overall shape identical to that of the 334 nm excitation. As before the lifetime of the 520 nm emission was less than 5 ns and the emission can be attributed to fluorescence generated from the π-π* state of the **TPA-1** ligand, and the broad emission centered on 700 nm, $\tau_{aerated}$ = 370 ns and τ_{deoxy} = 796 ns, again suggesting assignment as ^{3}π-π* and ^{3}MLCT emission. **Ru-1** was the only complex to exhibit emission with a ^{3}MLCT feature. The overall emission shape was broad but a narrow prominence at 700 nm was observed. This narrow feature is assigned as a ^{3}MLCT emission superimposed on the much broader and weaker ^{3}π-π* emission suggesting **Ru-1** may exhibit more ^{3}MLCT character than either **Re-1** or **Ir-1**.

Ir-1 emission was observed at excitation wavelengths of 335 and 470 nm. **Ir-1**, similar to the other two complexes, yielded very weak emission. The quantum yield (ϕ_{fl} = 0.0009) was the lowest of the three complexes, and unlike **Re-1** and **Ru-1**, only a broad emission centered at 742 nm dominated the spectrum with no indication of fluorescence from the ligand. This suggests a more efficient energy transfer or a faster intersystem crossing brought about by iridium. Lifetimes of the 742 nm emission are: $\tau_{aerated}$ = 440 ns and τ_{deoxy} = 1.6 μs and are also assigned to a mixed ^{3}π-π* / ^{3}MLCT manifold.

Transient Absorption

Transient absorption spectroscopy was performed for all compounds in an effort to provide further information on the electronic nature of their excited states. Deoxygenated CH_2Cl_2 or THF solutions with optical densities of approximately 0.8 at the excitation wavelength of 355 nm were used for this study. Transient absorption spectra following 5 ns pulsed laser excitation at 355 nm are presented in Figure 3-6. Excited state absorption was monitored in both the visible (350 nm to 800 nm) and near-IR (800 nm to 1600 nm) regions utilizing two separate detection sources. Data from the two sources were interlaced, without modification, to present a continuous spectrum.

A transient absorption spectrum of **TPA-1** was attempted but insufficient triplet population was generated to record triplet-triplet absorption. The transient absorption spectra for the metal-organic complexes feature ground-state bleaching at 360 and 440 nm. These correlated well with the short and long-axis π-π^* ground state absorption of each complex. Each complex presents moderately broad excited-state absorption in the visible region as well as a very broad and strong excited-state absorbance in the near-IR (Figure 3-6). The excited-state absorption bands in the visible and near-IR present moderately long lifetimes of just under 0.5 μs in duration. (Table 3-2)

Similar to the emission spectra, the transient absorption spectra for **Re-1** and **Ir-1** were similar and **Ru-1** was much different. In the TA spectrum, the relationship of relative ΔAbsorbance difference between the excited-state absorbance in the visible region versus that of

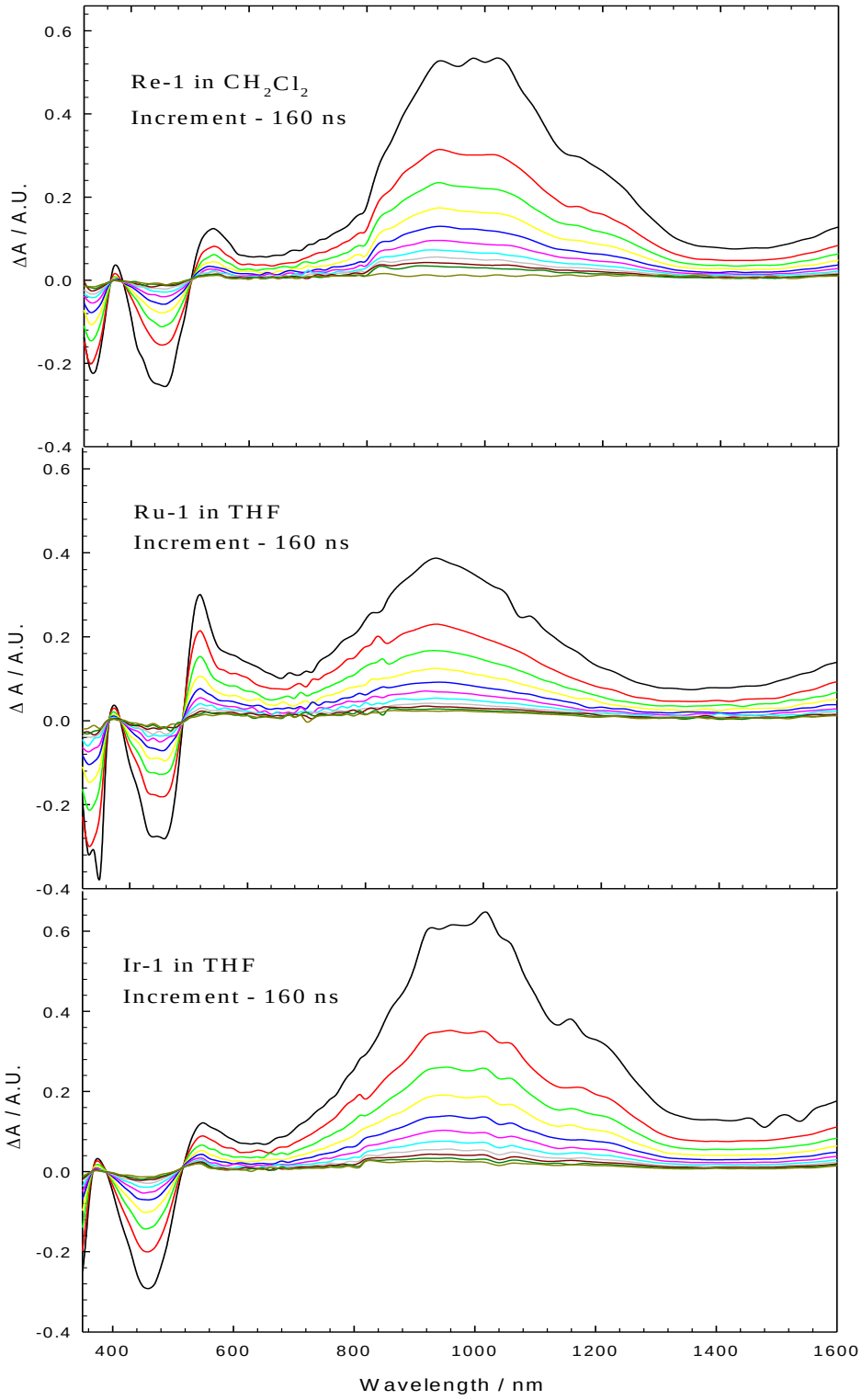

Figure 3-6. Transient absorption spectra of metal-organic complexes. Solvent (deoxygenated) – THF (**TPA-1**, **Ru-1**, **Ir-1**) and CH_2Cl_2 (**Re-1**), OD - 0.8, laser excitation – 355 nm, 5 ns pulse.

the excited state absorbance in the near-IR region provided information on the triplet character of the excited states. As described in Chapter 1, a prominent narrow visible excited state absorption equal to or exceeding the strength of a broader near-IR excited state absorption (Figure 1-5a) is indicative of an excited state of mostly ^{3}MLCT character. The TA spectra for **Ru-1** presents this type of relationship and is therefore afforded a triplet-triplet absorption assignment that is mostly ^{3}MLCT in nature. In contrast, the transient absorption spectra of **Re-1** and **Ir-1** are identical in character. Both exhibit relatively weak visible excited state absorption and strong near-IR excited state absorption which is an indication of an excited state of mostly $^3\pi$-π^* character (Figure 1-5b).

Further correlation of these assignments is based on the comparison of emission and excited state lifetimes. In systems whose excited states are mainly ^{3}MLCT, triplet excited state lifetimes are roughly equivalent to the emission lifetime. This is the case for **Ru-1**. In the case of **Re-1** and **Ir-1** their triplet excited state lifetimes are mush different than their respective emission lifetimes. This is an indication that the excited state is dominated by $^3\pi$-π^* character.

Despite the difference in excited state character, it is interesting to note that all three complexes afford nearly identical excited state lifetimes and decay profiles. This similarity is likely due to the mixed $^3\pi$-π^* / ^{3}MLCT triplet manifold proposed earlier for in these types of systems. In the excited state decay profiles in Figure 3-7 each complex displays a fast decay component which is constant and reproducible. Due its extremely fast decay and the timescale limitations of the instrument further investigation into its origin was not possible. However a logical explanation for this behavior would be a preferential population of a higher energy triplet excited state of either $^3\pi$-π^* or ^{3}MLCT character and a subsequent relaxation of the excited state into the lower lying manifold of mixed $^3\pi$-π^* or ^{3}MLCT character. To address the equivalent

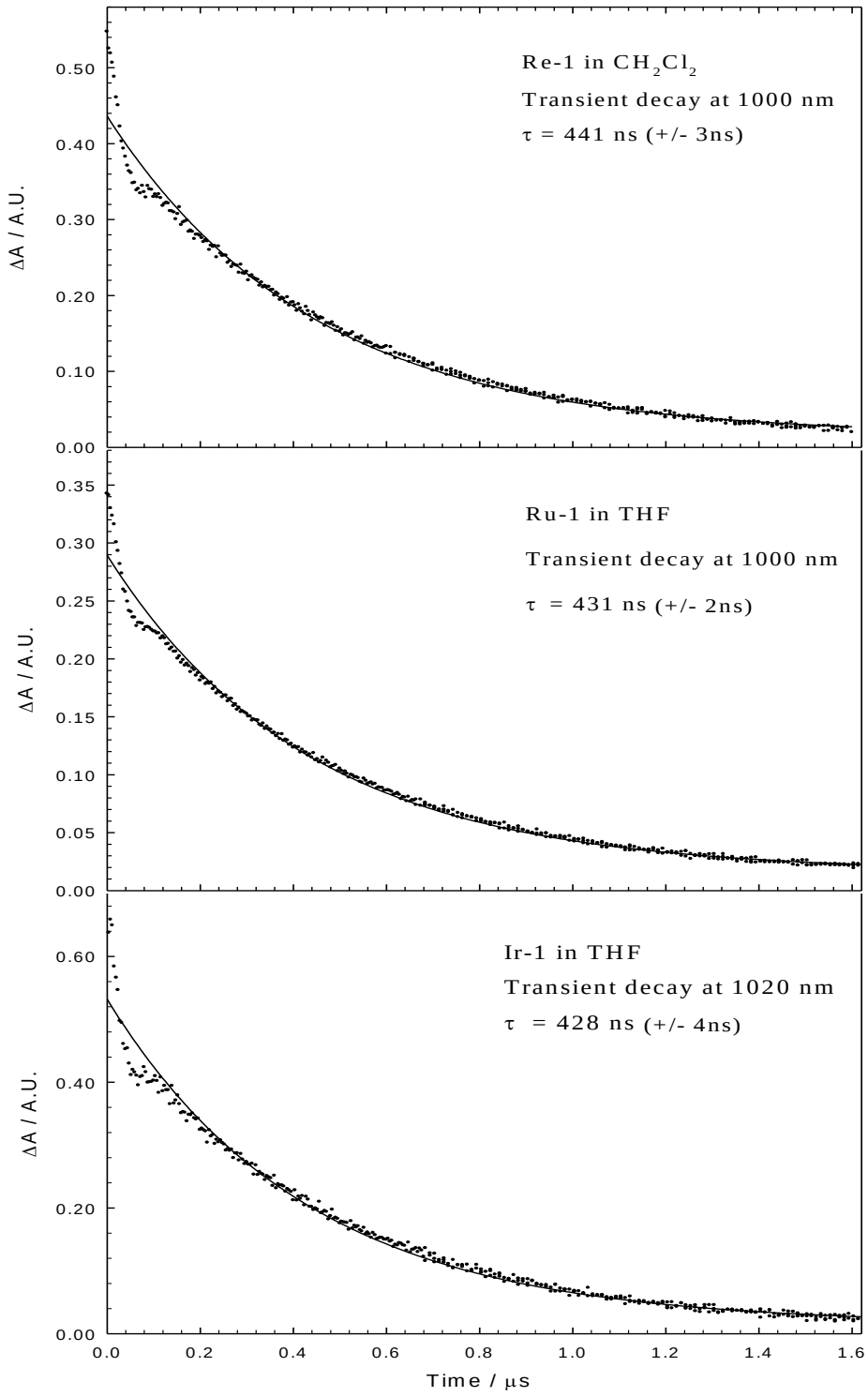

Figure 3-7. Excited state lifetimes of metal-organic complexes. Solvent (deoxygenated) – THF (**TPA-1**, **Ru-1**, **Ir-1**) and CH_2Cl_2 (**Re-1**), OD - 0.8, laser excitation – 355 nm, 5 ns pulse. Spectra fit with single exponential decay fit.

triplet excited state lifetimes, the model of an equilibrated $^3\pi$-π^* / ^{3}MLCT manifold combined with a common decay pathway is also logical. Even when either the $^3\pi$-π^* or ^{3}MLCT excited state is dominant, if a relative excited state energy equilibrium is present, the most efficient decay pathway would be preferred and equivalent excited state lifetime would be afforded.

Nonlinear Absorption Determination

Two Photon Emission

Two photon excited emission spectra of each compound were obtained at room temperature utilizing aerated solutions at solution concentrations of 10 mM for all compounds except **Re-1** which was 2.0 mM. A comparison of the one and two photon emission spectra are presented in Figures 3-9 and 3-10.

Two photon excitation was accomplished utilizing only minor modifications of the time-resolved emission instrumentation setup currently in use. Directing of the optical path and the addition of focusing optics were the major modifications that allowed the current instrumentation setup to be utilized for two photon excited emission detection. Two factors became immediately apparent as key to the success of this instrument being able to detect the presence of emission of a two photon excited species. These two factors were a tightly focused beam and sufficient laser energy. First, the need to focus the incident laser pulse to provide the needed excitation intensity to produce two photon excitation was vital since the probability of two photon excitation is proportional to the square of the intensity of the incident photon flux. In order to provide the necessary intensity of photon flux, a plano-convex lens with a nominal focal length of 9.5 cm was placed on single-axis translation stage in an appropriate position in the beam path. Beam diameter at the lens was measured at 28 mm. A calculated beam waist of 30 μm was attained assuming a Gaussian beam shape and energy densities of approximately 1.5 J/cm^2 at 5.0 mJ were

generated. The translation stage was included to insure the tightly focused beam was centered (front to back) in the 1 cm sample cell and to aid in focusing of the input beam. As the excitation wavelength was changed the translation stage was adjusted to compensate for minute changes in the final focus of the excitation beam, Figure 3-8.

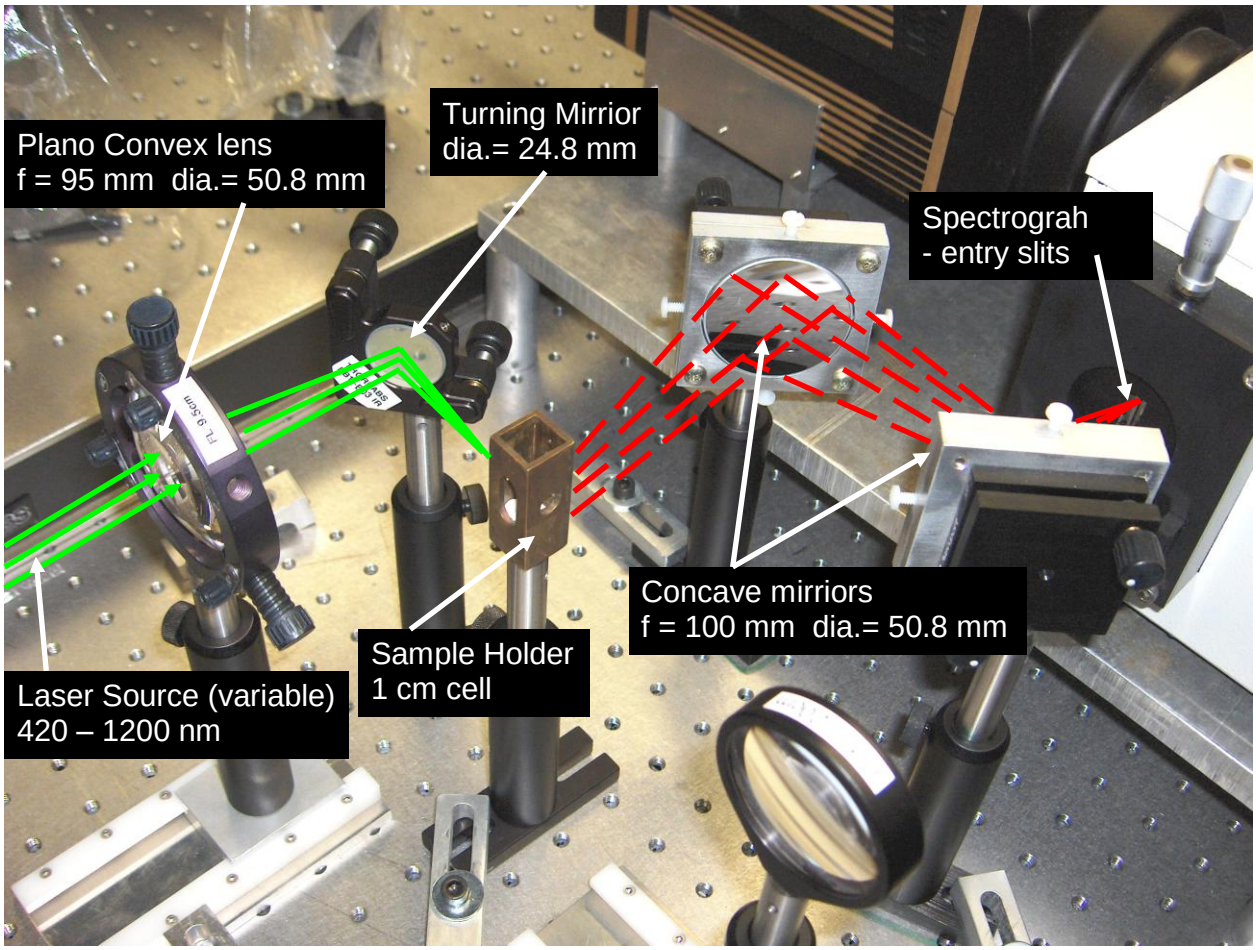

Figure 3-8. Two photon emission instrument modification showing focusing optics, sample holder, emission collecting mirrors and spectrograph entrance slits.

Tunable-wavelength laser energy was provided by an optical parametric oscillator (OPO) pumped by the third harmonic of a 1064 nm Nd:YAG laser which provides an available wavelength range of 420 - 570 nm and 590-1200 nm. Despite the continuum of wavelengths available from the OPO equipped laser source, it is noted that available laser power at any given

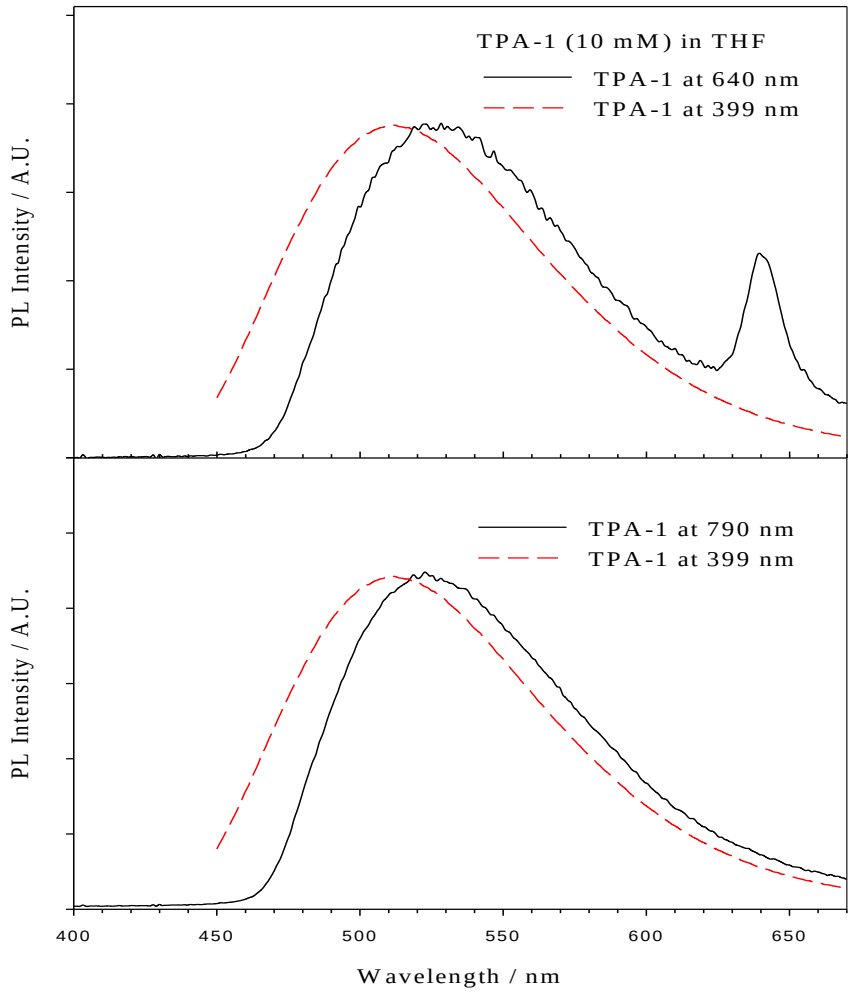

Figure 3-9. Two Photon Emission Spectra of **TPA-1** (10 mM in aerated THF, 1 cm cell) following focused laser excitation at 790 nm, 6 mJ / 5 ns pulse (top) and 640 nm, 5 mJ / 5 ns pulse (bottom). The comparative one photon excited steady-state emission spectra is the same as presented in Figure 3-5.

wavelength is highly variable. This is especially true near the limits of the wavelength ranges, where the available power drops off dramatically. Careful consideration of available wavelengths with sufficient energy led to the choice of utilizing the wavelengths 640, 790, 940

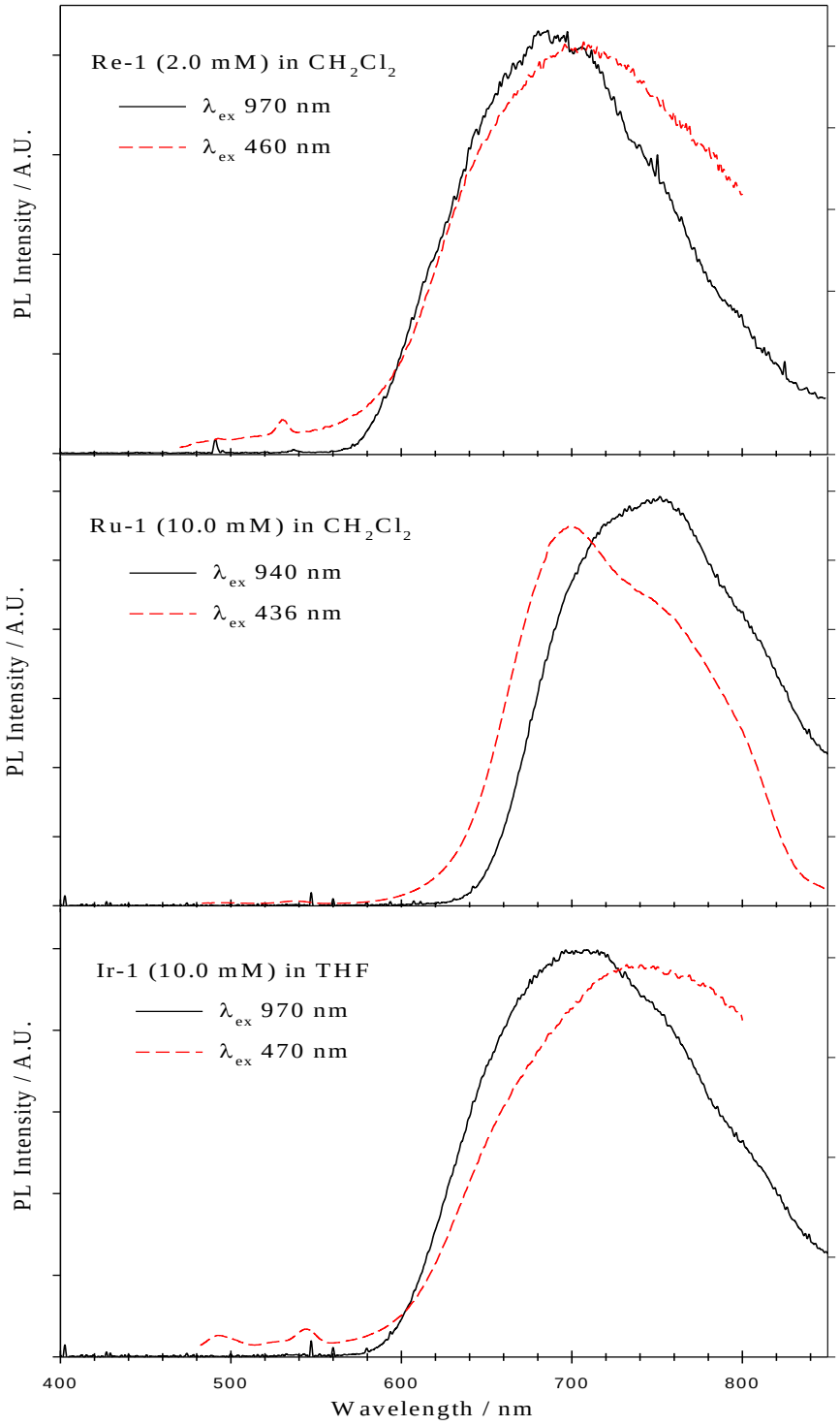

Figure 3-10. Two photon emission spectra of metal complexes (concentrations noted) in deoxygenated solvent, 1 cm cell) following focused laser excitation at 970 nm, 5 mJ / 5 ns pulse. The comparative one photon steady-state emission spectra are the same as Figure 3-5.

and 970 nm for the excitation wavelengths for this experiment. For the excitation wavelengths of 640 and 790 nm, a 5 ns delay of the CCD detector was utilized to avoid detector saturation.

It has been well documented that the peak of two photon absorption occurs at wavelengths considerably shorter (more red) than simply two times the one photon maximum.[66] This, coupled with moderately broad and reasonably intense absorption bands of the ligand and metal-organic complexes, allowed for utilization of wavelengths 20 nm more blue and greater than 40 nm more red than the calculated desired wavelength of twice the one photon absorption maximum.

Successful two photon excitation of **TPA-1** was conducted at the projected two photon wavelengths associated with the major absorption bands of 301 nm and 399 nm. Despite the extremely short lifetime of the fluorescence from **TPA-1** and the needed gating of the detector to avoid saturation, sufficient emission signal was captured due to the intense emission generated by the molecule's high quantum yield. The resulting emissions presented a spectral shape and lifetime similar to those found upon one photon excitation. One photon emission spectra were acquired on a different corrected instrument (PTI Felix 32I fluorometer), therefore the spectral shift of the uncorrected two photon data is difficult to directly compare. However, it was noted the emission afforded by two photon excitation did not shift in wavelength with a change in excitation wavelength.

Two photon excitations of **Re-1**, **Ru-1** and **Ir-1** were also found to produce detectable, albeit weak, emission. Despite the longer emission lifetime of the complexes compared to the free ligand **TPA-1**, insufficient emission intensity was present in all complexes to accomplish a time resolved emission determination of lifetime. Because of the weak emission intensity, all two photon excitation emissions were collected with an extended CCD gate time of 100 ns. The

resulting emissions again presented a spectral shape similar to those found upon one photon excitation. Since the one photon emission spectra were acquired on a different instrument (PTI Felix 32I fluorometer) which is corrected, the spectral shift is again unresolved. Emission wavelength afforded by two photon excitation was again not altered with a change in excitation wavelength, identical to the behavior found in the free ligand.

Nonlinear Absorption of C_{60}

C_{60} has been considered among the best of all materials for optical limiting of laser radiation at 532 nm since the mid-1990's.[67] More recently, experimental evidence of C_{60}'s ability to present a nonlinear response at 1064 nm has again focused attention on this molecule as viable optical limiter.[57] The nonlinear absorption and optical limiting potential of C_{60} in a toluene solution was first reported by Tutt and Kost in 1992[68] utilizing a nanosecond pulsed Nd:YAG laser at 532 nm. Since that time, extensive investigation of the optical limiting potential of [60]fullerene and [60]fullerene derivatives has been pursued. Initial investigations into the origin of the NLO response of C_{60} at 532 nm focused on reverse saturable absorption (RSA) as the primary nonlinear mechanism responsible for its NLO activity. Recent NLO evaluations of C_{60} at 1064 nm focused on two photon absorption as the mechanism responsible for its NLO activity. For these reasons and due to its commercial availability, C_{60}, was examined in the present study as a benchmark compound for the newly developed nonlinear transmission apparatus, and to establish the potential utility of C_{60} as an optical limiting standard for use to judge the strength of optical limiting in the series of dual mechanism limiting metal-organic chromophores discussed here.

Utilizing room temperature solutions of C_{60} in toluene, McLean et al [69] used a five-level modeling of RSA to correlate the optical limiting responses with ground and excited-state absorption cross sections in C_{60}. Excellent correlation of experimental optical limiting results

towards nanosecond pulsed 532 nm were obtained utilizing light fluences up to ~ 1 J / cm^2 and their data were subsequently supported by study findings of other researchers.[70] Despite these strong correlations provided by a five-state model supporting RSA-based limiting due to strong triplet-triplet absorption, the overall mechanistic details on the optical limiting properties of fullerenes remains a subject of debated. Subsequent studies have suggested additional NLO mechanisms provide contributions to the overall efficiency of C_{60} as an optical limiter.[71-73] These studies point to experimental evidence that optical limiting performance of C_{60} is different in a solid matrix when compared to that of a solution. The differences in performance was determined not to be attributed to a change in nonlinear absorption behavior since it was shown ground-state and triplet-triplet absorptions of both a solid matrix and solutions remained relatively unchanged. This presents the possibility that contributions from other nonlinear processes, such as optical scattering, may play an important role in the optical limiting response in C_{60}.

Table 3-3: Optical limiting properties of C6067.

Transmittance	Limiting threshold[a] (J/cm^2)	I_{out} at saturation (J/cm^2)
55%	0.18	0.05
65%	0.20	0.06
70%	0.31	0.10
82%	0.45	0.18

[a] The optical limiting threshold is defined as the input fluence at which output fluence is 50% of that predicted by linear transmittance.

In a comparison study accomplished by Sun and Riggs [67] baseline C_{60} optical limiting data was presented and is shown in Table 3-3. For the study, an Nd:YAG laser generating the second harmonic, 532 nm, was used. The input beam diameter was reported as 6 mm and output ranged from 5-160 mJ with yielded corresponding energy densities of 0.02-0.60 J/cm^2.

In addition to RSA based optical limiting of C_{60} at 532 nm, studies have also shown C_{60} has the capability of two photon absorption at 1064 nm. Investigations of the nonlinear refractive indices of C_{60} and C_{70} in toluene were performed by Usmanov et al[57] utilizing Z-scan and the resultant data for C_{60} was presented in Figure 2-11. In addition, optical limiting experiments utilizing similar apparatus methodology as was used herein discovered only the toluene solution of C_{60} presented two photon nonlinear absorption (Figure 3-11).[57]

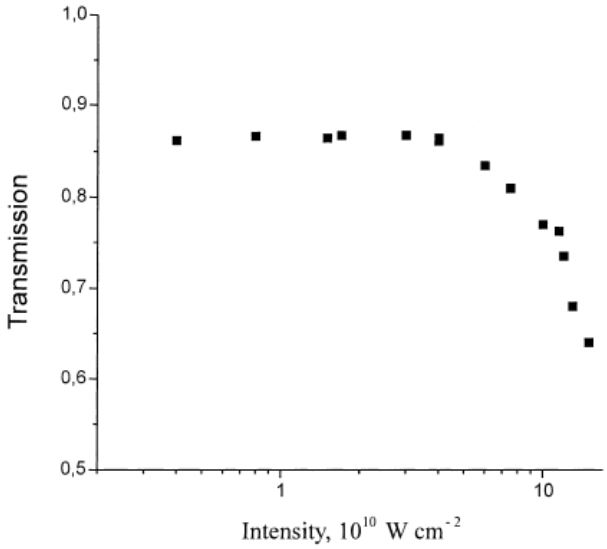

Figure 3-11. Power dependence, two photon generated optical limiting determination of 0.5% wt C_{60} in toluene at 1064 nm.[57]

It has been observed during the course of our investigations while using C_{60} as a benchmark, extreme diligence must be taken to ensure C_{60} has been completely dissolved into solution. Incomplete solubility, even at concentrations of less than 1.0 mM, was found to lead to linear transmissions well below the values stated in the literature as well as evidence of optical scattering leading to extreme variations in the transmitted energy through the sample. Additionally, comparison of C_{60} NLO data was, at times, difficult given the relatively low initial transmittance of C_{60} solutions. A decision to use a concentration which matched the initial transmittance value shown in Figure 3-11 was made based on previous experimental techniques

used by other groups at different wavelengths (Table 3-3). The concentration that yielded initial transmittances most representative to the previous 1064 nm data was 3.0 mM in toluene. This concentration is one-half the concentration used by Usmanov's group but afforded similar or better NLT responses. Despite these potential drawbacks, utilization of C_{60} as a benchmark for comparison of compounds without suitable model compounds of known nonlinear optical character was deemed a valid choice due to its well documented nonlinear optical properties at wavelengths utilized in this project.

Nonlinear Absorbance Determination

Following positive confirmation of the ability to two photon excite **TPA-1** and each of the metal-organic complexes during the two photon excited emission experiment, examination of the optical limiting character of this series was able to proceed. With the goal of detecting the nature and strength of a dual mode nonlinear response comprised of two photon excitation followed by excited state absorption from a strongly absorbing excited state it was deemed necessary to determine the appropriate wavelengths and concentration conditions which would exhibit the clearest evidence of the desired NLO responses.

Initial efforts were focused on the determination of the nonlinear response and optical limiting potential of the free ligand **TPA-1**. The experimental determination of nonlinear response utilized the setup as previously described in Chapter 2 and visually represented in Figure 2-15. For this portion of the study it was noted that only the TPA mechanism would present as the nonlinear absorption mechanism. Isolating and separately viewing the nature and

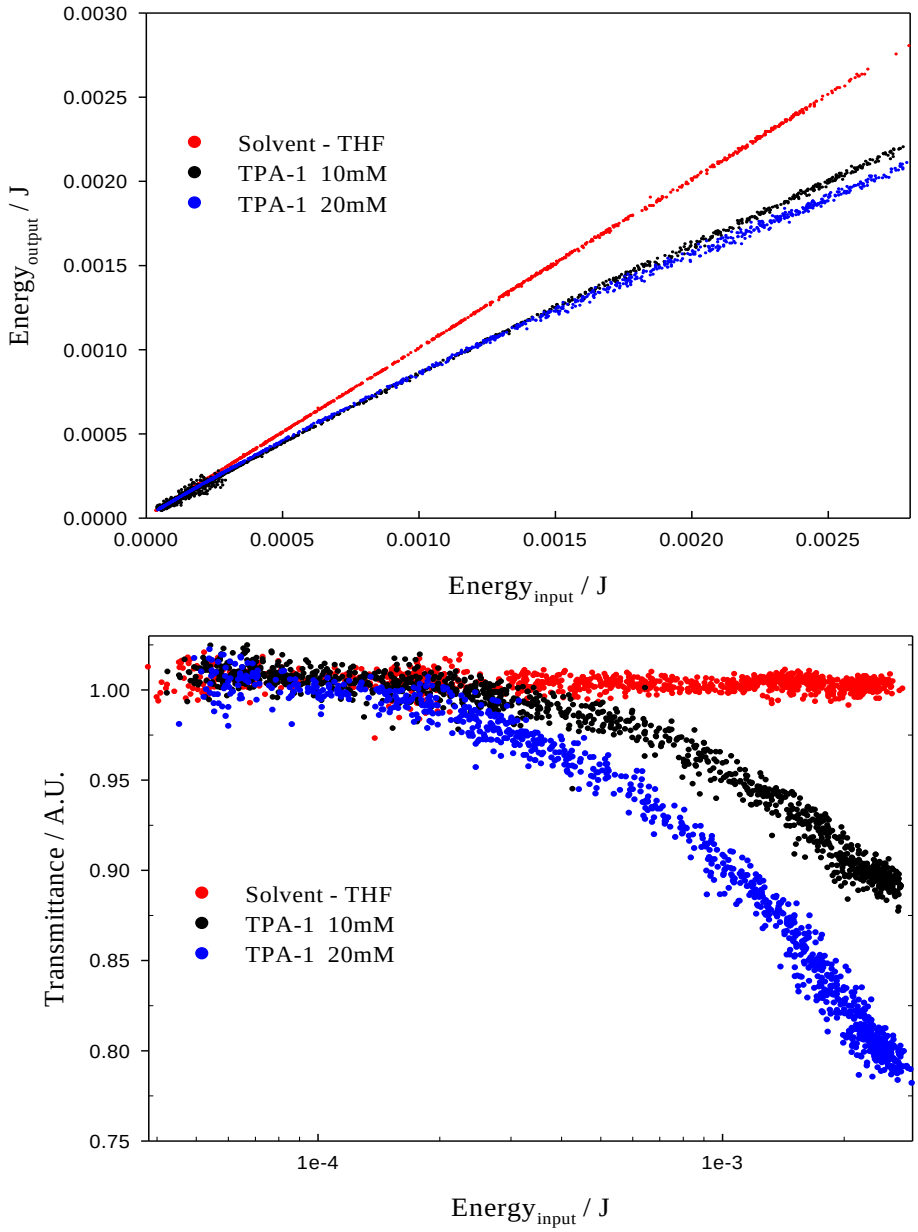

Figure 3-12. Nonlinear determination of **TPA-1** at 645 nm (top) and nonlinear transmission curve of **TPA-1** at 645 nm (bottom).

strength of the TPA response for the free ligand was a deliberate attempt to obtain two photon-only NLO data with which to judge the magnitude of enhanced NLT response gained by the addition of the ESA capable metal-based chromophore. Nonlinear response determinations for **TPA-1** were accomplished at 645 nm (Figure 3-12) and 970 nm (not shown) for concentrations

of 10 mM and 20 mM. Despite acquiring effective two photon excited emissions at both 645 and 970 nm, only 645 nm elicited a nonlinear response detectable in the energy ranges utilized for these experiments. At 645 nm, **TPA-1** exhibited a moderate departure from linear absorption which correlates to an observed 12% and 23% reduction in transmittance for 10 and 20 mM respectively. At 970 nm, however, no departure from linear absorbance was noted for sample input energies up to approximately 5.0 mJ. A possible explanation of this apparent inconsistency in findings is that 970 nm is near the far-red extreme of the two photon excitation envelope of **TPA-1**. Most likely, two photon excited emission was observed due to the high quantum efficiency of the free ligand despite having a relatively low two photon cross section at this wavelength. Additionally, it was confirmed that **TPA-1** presented as optically transparent at both 645 and 970 nm even for concentrations as high as 20 mM. Concentrations higher than 20 mM are possible but were not attempted since concentrations utilized for the metal complexes that this data is meant to be compared with were limited to this concentration or less and will be discussed later in this section. Referring to the quadratic and cubic dependence NLT models presented in Chapter 2, it is clear that **TPA-1** follows a quadratic relationship between attenuated intensity and incident light intensity for both 10 and 20 mM, fitting the TPA only model profile.

Once nonlinear data from two photon only excitation of the free ligand **TPA-1** was successfully obtained tests were performed to determine the range of excitation wavelengths which could elicit a two photon induced excitation of the metal-organic chromophores **Re-1**, **Ru-1** and **Ir-1** to the appropriate singlet excited state. Information from ground state absorption data was used to choose a potentially suitable wavelength range. For the series, a generous range of strong ground state absorption exists for all the complexes from 250 nm to 550 nm. This equates

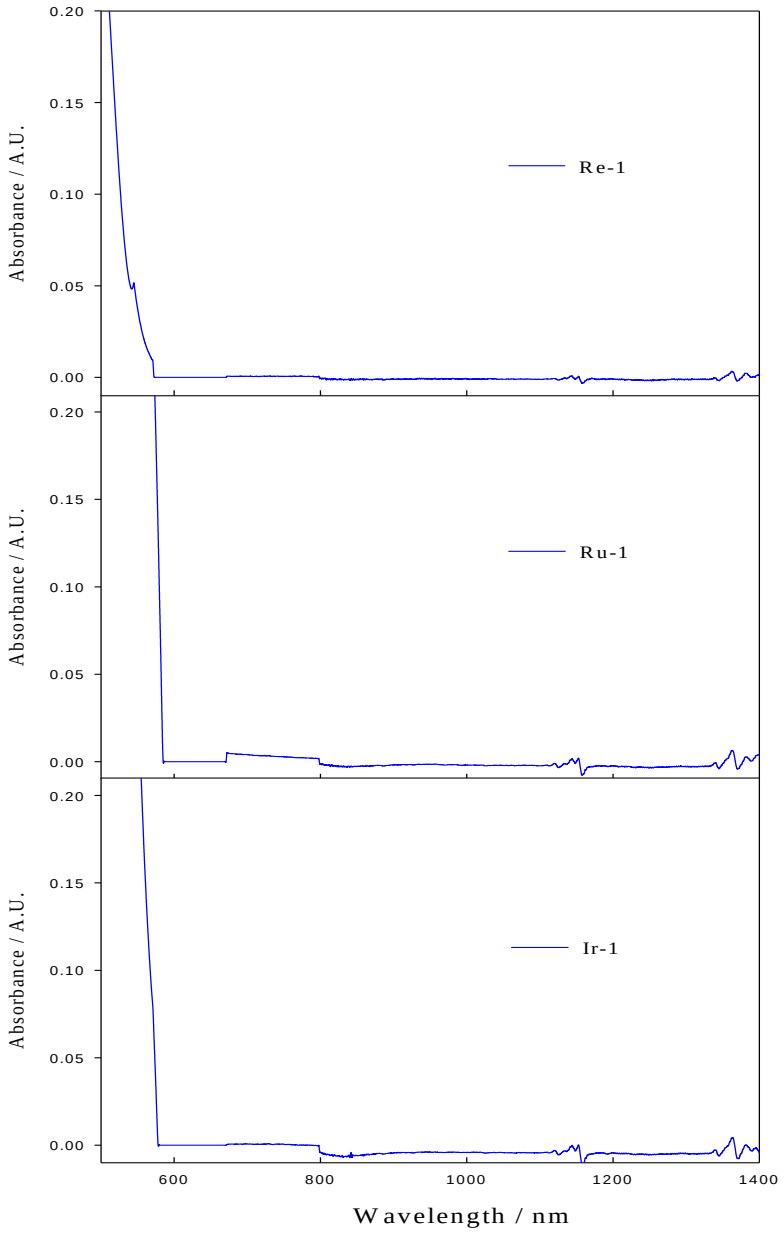

Figure 3-13. Ground state absorption spectra for the near-IR of 2.0 mM metal-organic complex solutions in CH_2Cl_2.

to a potential two photon active range for the TPA chromophore of 500-1100 nm. Optimization of TPA excitation conditions was deemed essential due to the need for a sufficient singlet excited state population which could in turn be converted through intersystem crossing to triplet excited states available for enhanced nonlinear absorbance through an ESA mechanism. In addition to

the ground state absorption data, a great deal of consideration was given to the two photon excited emission data discussed in a pervious section in choosing an effective wavelength to utilize. A systematic survey of wavelengths and chromophore concentrations was carried out to determine the optimum conditions with which to proceed. The wavelength range examined was 800 to 970 nm. Preliminary test results of the surveyed wavelengths revealed positive nonlinear results for the wavelength range. During this conditions survey, acute solubility limitations for the series became a significant factor. As concentrations were increased each metal complex exhibited very different solubility and optical transparency characteristics. For **Re-1**, it was noted that solution saturation occurred at chromophore concentrations of just over 3.0 mM in CH_2Cl_2. In THF, benzene, toluene, and DMSO were tested for evidence of higher solubility but it was determined none would support higher concentrations than that of methylene chloride. Despite the low solubility of **Re-1**, it was noted that optical transparency remained high even at near saturated solution concentrations. For **Ru-1**, solubility initially seemed less critical and solution concentrations of up to 10 mM were obtainable. Optical transparency however dropped off very rapidly as concentrations increased. Even at a concentration of 3.0 mM, initial transmission values of 80% were observed (not shown) .To eliminate ground state absorption as the reason for this lack of transparency; absorption spectra were obtained in the near-IR region out to a wavelength of 1400 nm. Ground state absorption data obtained at concentrations of 2.0 mM for all three complexes showed no absorbance for wavelengths ranging from 550 nm through 1400 nm as shown in Figure 3-13. The reason for this lack of optical transparency at higher concentrations of **Ru-1** is presumed to be due optical scattering. Previous NLO studies, where low optical transparencies were experienced, such as C_{60}, the reason given is optical scattering. For this reason it is suspected that incomplete solubility at higher concentrations of

Ru-1 may indeed be a factor. In stark contrast to **Re-1** and **Ru-1**, **Ir-1** exhibited very high solubility in conjunction with high optical transparency for solution concentration up to 20 mM. The test survey at 970 nm concluded with concentrations of 10.0 mM for **Ir-1,** 7.5 mM for **Ru-1** and 2.0 mM for **Re-1** showing the most consistent and greatest magnitude NLT responses. The results of the nonlinear determination at 970 nm are shown in Figure 3-14. Assembled in Figure 3-15 are the nonlinear transmission plots for the series at 970 nm at the same concentrations. Noteworthy is that despite a variation of chromophore concentration the energy of nonlinear onset appears to remain at 100 μJ for each complex. This is the energy that was observed for the onset of limiting for the free ligand **TPA-1** (Figure 3-12). This correlation of onset energies

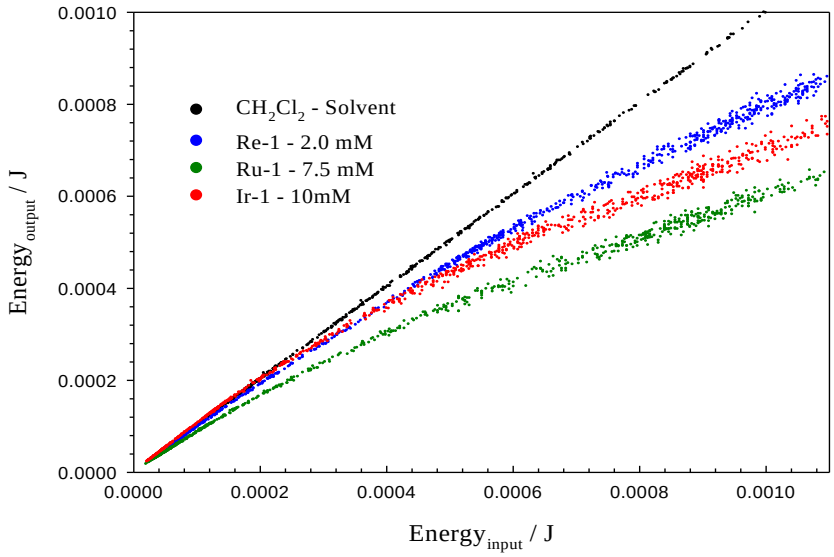

Figure 3-14. Nonlinear determination results of metal-organic chromophores; **Re-1**, **Ru-1** and **Ir-1** at 970 nm in CH_2Cl_2 solutions (concentrations noted).

suggests the nonlinear threshold is controlled more by the nature of the TPA ligand and less by the character of the ESA chromophore. As expected overall limiting response was greater in **Ir-1** which had the highest chromophore concentration and achieved the greatest reduction in

transmission (100% to 62 %). **Ir-1** also remained completely transparent until the point of limiting onset. **Ru-1** displayed an overall limited transmittance of 60% at 2 mJ but had an initial

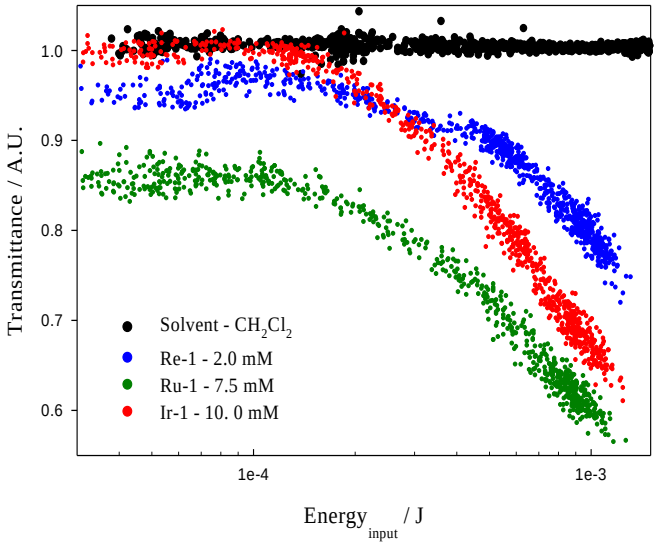

Figure 3-15. Nonlinear transmission results of metal-organic chromophores; **Re-1**, **Ru-1** and **Ir-1** at 970 nm in CH_2Cl_2 solutions (concentrations noted).

transmission of 87% in the low energy linear region. **Re-1** which had the lowest concentration and was near solution saturation retained a transmittance of 97% and still managed to attenuate the transmittance to 75% at 2 mJ.

A second experimental study of the metal-organic series was undertaken at 1064 nm. From results gathered in the NLT test series in Chapter 2 where a cubic relationship between attenuated intensity and incident light intensity can be used to confirm the presence of a dual mode TPA/ESA mechanism, it was determined a study of limiting characteristics at higher incident energies may provide more insight into the overall character of the complex's limiting mechanism. Each of the complexes present strong excited state absorption around 1064 nm as seen in Figure 3-6 and since this wavelength is available as the fundamental output from the Nd:YAG laser it was decided to modify the nonlinear determination apparatus to accept higher

flux 1064 nm laser energy. Figure 3-16 shows a photo rendered schematic of the modified nonlinear transmittance setup for 1064 nm. A key modifications to the apparatus involved the attenuation of the high energy fundamental beam emanating from the Nd:YAG laser. Laser outputs greater than 15 mJ at 1064 nm were necessary to achieve a stable beam profile which is well beyond the damage threshold of the sample cells and the energy detectors being utilized. Figure 3.17 depicts the schematic of the system and clearly shows the addition of a 3:97 beamsplitter placed in the pathway of the main source beam. With the addition of this beamsplitter only 3% of the main beam is diverted to the main NLT apparatus. Additionally a static 30% transmission filter was placed prior to the continuously variable neutral density filter for further protection and control of the incident beam at higher incident powers. The focusing optic was also replaced by a 50.8 mm plano-convex lens with a nominal focal length of 13 cm. The beam diameter at the lens was 10mm. Again utilizing Equation 9 from Chapter 2, a calculated beam waist of 130 μm was attained assuming a Gaussian beam shape with an energy density range of 0.005 - 0.90 J/cm^2.

The final determination of the nature of the response for the series **Re-1**, **Ru-1** and **Ir-1** was conducted at the two photon excitation wavelength of 1064 nm. Concentrations of 1.0, 3.0 and 5.0 mM in CH_2Cl_2 for **Ru-1** and **Ir-1** and 1.0, 2.0 and 3.0mM in CH_2Cl_2 for **Re-1** were prepared and examined in an effort to compare overall optical limiting character for common chromophore densities. In Figure 3-18 the NLT results are presented for each complex at

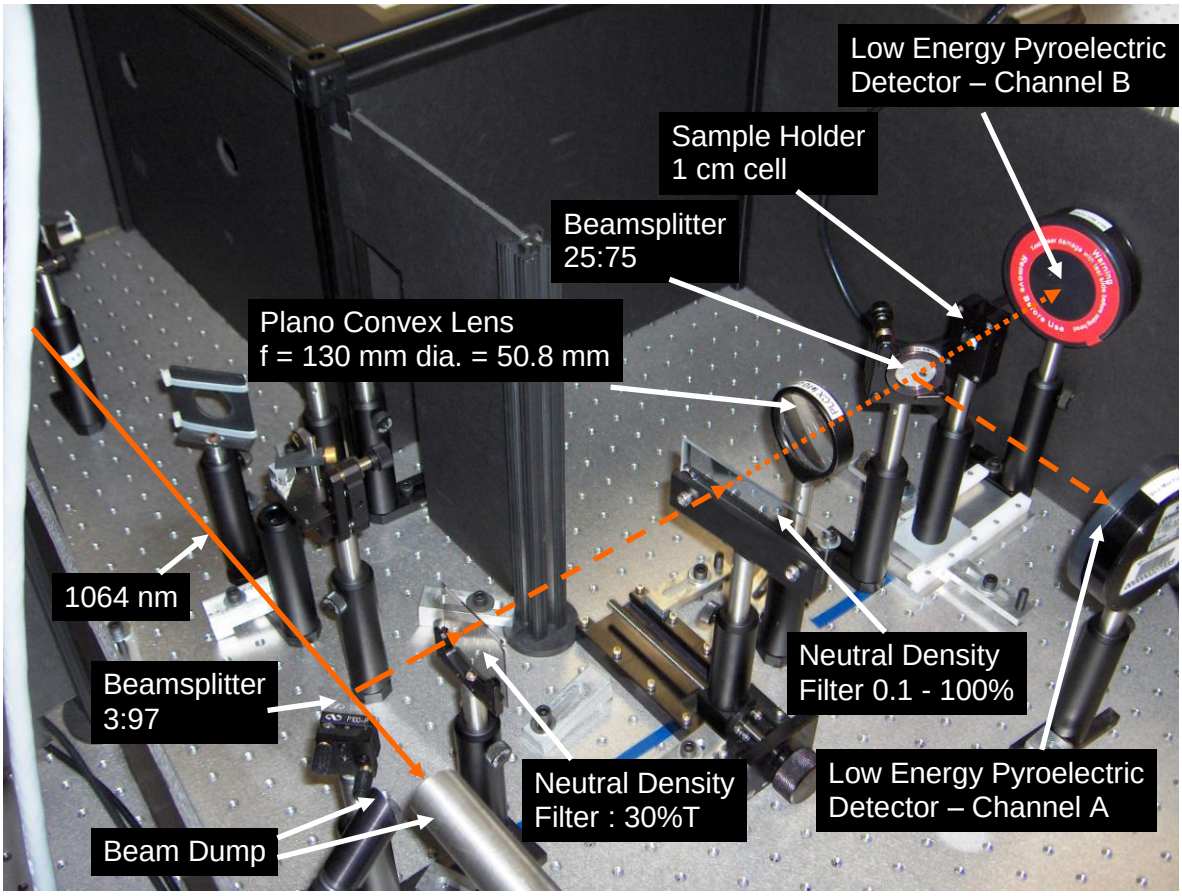

Figure 3-16. Photo schematic of modified nonlinear transmission setup.

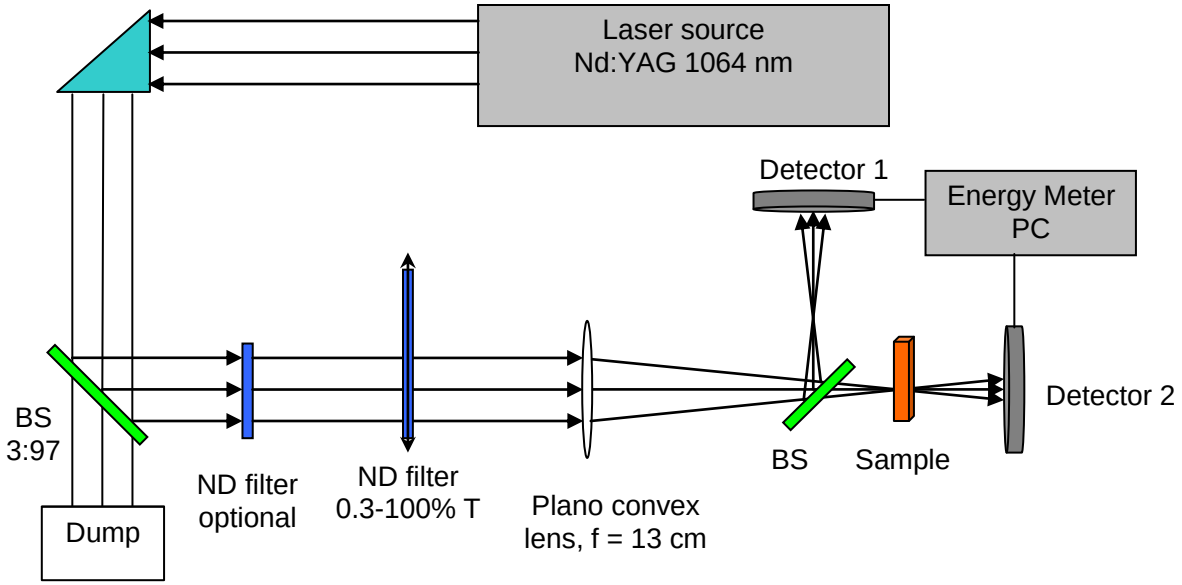

Figure 3-17. Schematic drawing of the modified nonlinear transmission setup.

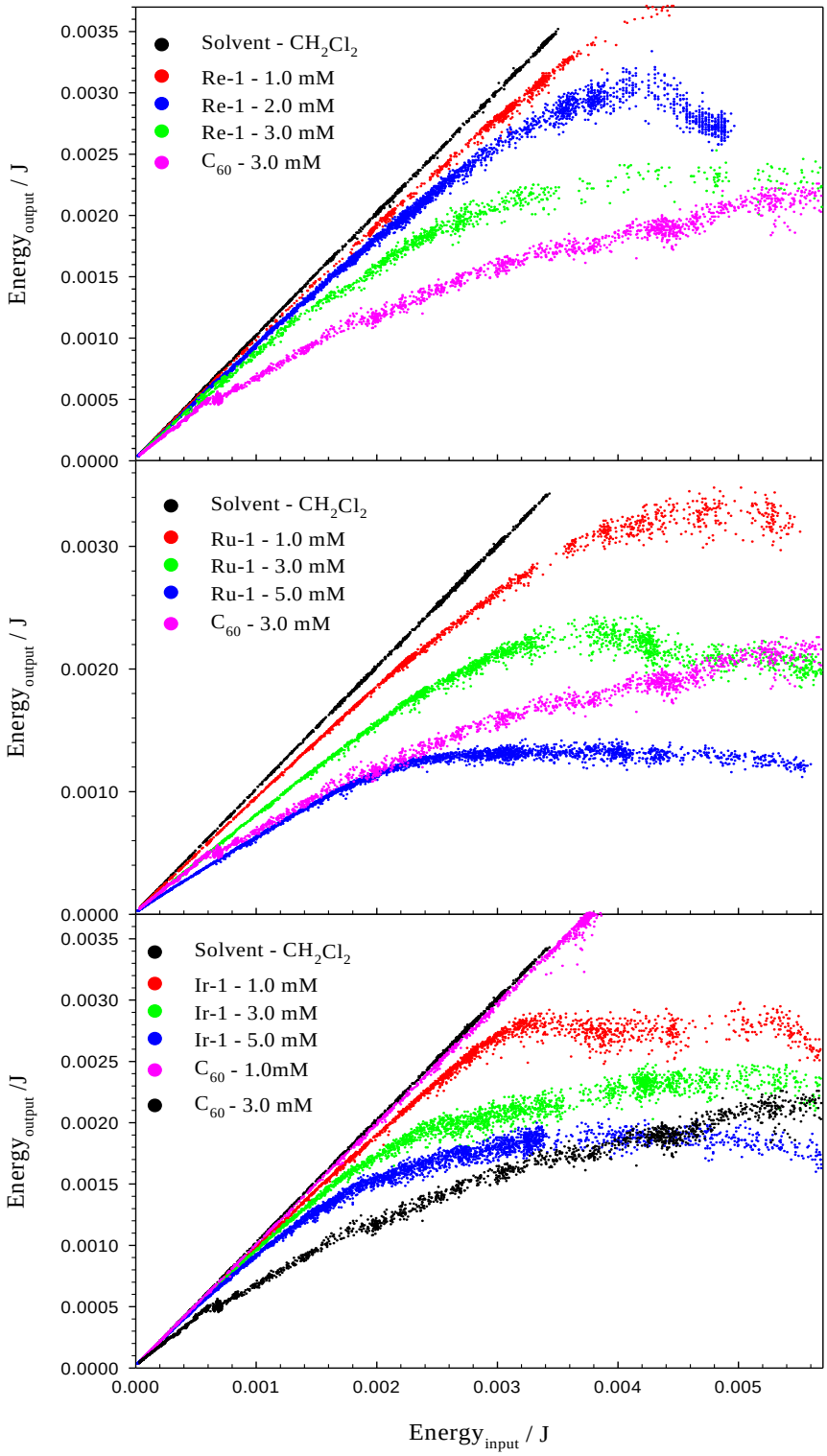

Figure 3-18. Nonlinear determination results for **Re-1** in 1, 2, 3 mM, **Ru-1** and **Ir-1** in 1, 3, and 5 mM CH_2Cl_2 solutions at the two photon excitation wavelength of 1064 nm.

varying concentrations. Along with the complex data, a comparative plot of the nonlinear response for a 3.0 mM solution of C_{60} in toluene complied under identical experimental conditions is included. Also included with the nonlinear determination plot of **Ir-1** is an additional comparative plot for a 1.0 mM solution of C_{60} in toluene and presents overlaid on the solvent plot. It of interest to note that for C_{60}, no detectable nonlinear response is obtained at a 1.0 mM concentration at 1064 nm under these experimental conditions with the energy densities approaching 1 J/cm^2. For the 3.0 mM solution of C_{60}, a larger magnitude NLO response compared to the literature, was noted (Figure 3-11). Despite beginning at near equal transmittances (~85%), a final transmittance of 25% was attained at 9 mJ versus 65-70% for the previously sited study.

For each complex excellent nonlinear response was noted at all concentrations and with the exception of **Re-1** at 1.0 mM all exhibited an output energy saturation level referred to as energy clamping or limiting saturation. Compared to the free ligand **TPA-1** with only two photon absorbing abilities where no clamping was noted for the energy range examined, a significant enhancement in NLO response brought about by the addition of the ESA active chromophore is evident.

The limiting response is seen more clearly in the optical limiting plots of the same data. Figure 3-19 presents the dramatic NLT character of this series even at relatively low chromophore concentrations. Once again the data obtained for the 3.0 mM C_{60} solution is shown as a relative comparison of optical limiting strength. For all the complexes, the highest energy limiting data for 3.0 mM concentration shows equivalent or better limiting and is trending to far surpass the C_{60} limiting response for energies just beyond those sampled in these experiments.

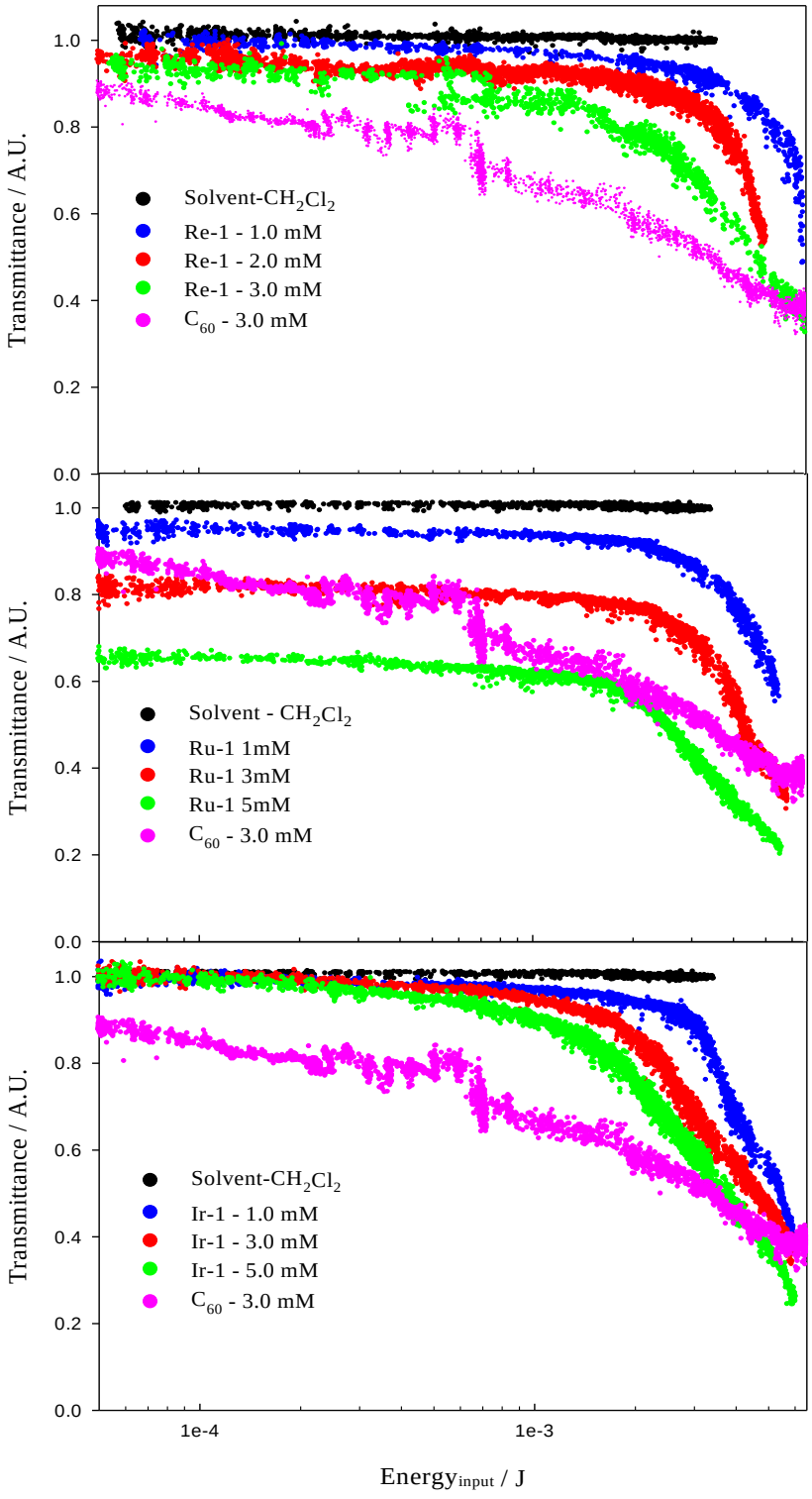

Figure 3-19. Nonlinear transmission of **Re-1**, **Ru-1** and **Ir-1** CH_2Cl_2 solutions at various concentrations at 1064 nm. 3.0 mM C_{60} in toluene data is included as a relative standard.

Also evident from the NLT plots in Figure 3-19, is the stark difference in relationship between attenuated intensity and incident light intensity. Clearly the C_{60} model exhibits a quadratic dependence which is what would be expected for the proposed TPA nonlinear absorption mechanism for this molecule. In contrast, each metal-organic complex exhibits a definitive cubic dependence between attenuated intensity and incident light intensity. This result is considered benchmark evidence of an enhanced dual mode TPA/ESA mechanism present in the metal-organic chromophore series.

Even more dramatic is the comparison of higher concentrations of **Ir-1** versus C_{60} with regards to overall optical limiting. Compared to the relatively low solubility of **Re-1** and the low optical transparency of **Ru-1**, the high solubility and high transparency of **Ir-1** proved to be a great advantage for the further enhancement of the optical limiting ability of this complex. As seen in Figure 3-20, even at concentrations of 20 mM **Ir-1** remains optically transparent at low laser powers for 1064 nm. In stark contrast, 3.0 mM C_{60} at best transmits 85% at low laser energies at a 3.0 mM concentration for 1064 nm. In addition, both 10 and 20 mM solutions of **Ir-1** surpassed the optical limiting capabilities of C_{60} at high energies. The 10 mM sample of **Ir-1** out performs C_{60} at input energies approaching 5 mJ and 40% transmittance where as the 20 mM surpassed the limiting capabilities of C_{60} at only 175 μJ at a 80% transmittance. A definitive cubic dependence between the attenuated intensity and incident light intensity is present in the 10 mM solution of **Ir-1**. For the 20 mM **Ir-1** solution NLT data, the cubic dependence seemingly breaks down. This inconsistency is likely due to the onset of an additional NLO mechanism or effect. Several times during the course of this NLT study it was noted that an unexpected and inconsistent decrease of transmittance would present at higher energy densities. Examples of this can be seen in Figures 3-18 for **Re-1** at 2.0 mM and **Ru-1** at

3.0 mM as well as in Figure 3-21 for **Ir-1** at 10 mM. Occasionally these reductions in transmission were accompanied by an audible popping noise. The source of the noise was confirmed not to be from material degradation of the sample cell, but the possibility of solution heating in the vicinity of the beam focus can not be ruled out. If this is the case, the apparent

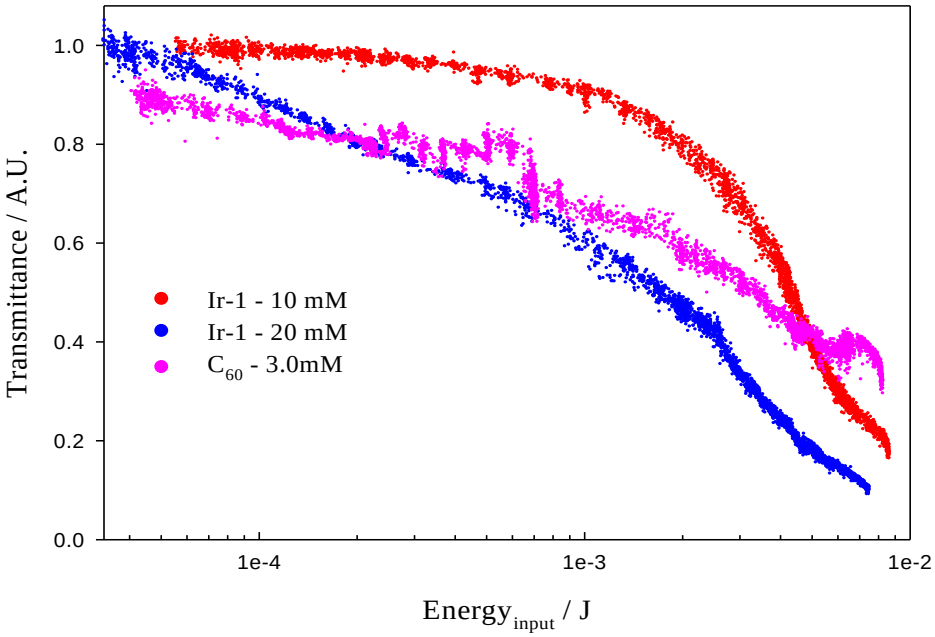

Figure 3-20. Nonlinear transmission for 10 and 20 mM, CH_2Cl_2 solutions of **Ir-1** at 1064 nm. 3.0 mM C_{60} in toluene data is included as a relative standard.

transmission reduction could be due to a thermal lensing effect as opposed to an intrinsic NLO mechanism of the complexes. Despite these occasional anomalies the 10 and 20 mM solutions consistently limit incident energies of up to 9 mJ to less than 200 and 100 μJ respectively by means of an enhanced dual mode NLO mechanism.

Discussion

The desired goal of developing a novel series of metal-organic chromophores that exhibit an enhanced dual mode nonlinear response utilizing both two photon excitation and excited state absorption was successfully realized. Also realized was the ability to detect and semi-

quantitatively characterize the nature and relative strength of an NLT active chromophore utilizing an in-house developed nonlinear transmission apparatus.

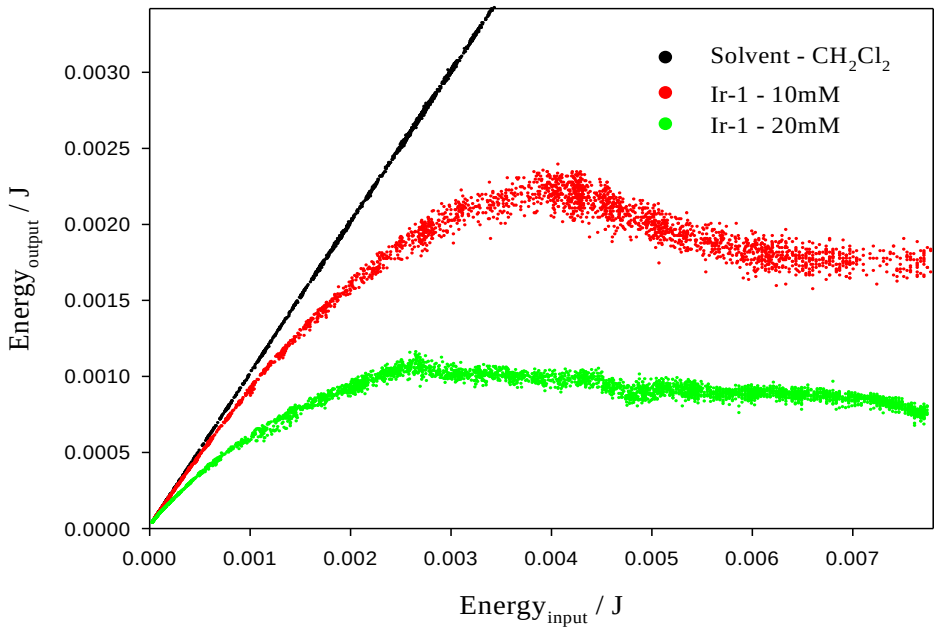

Figure 3-21. Nonlinear determination results for **Ir-1** in 10 and 20 mM CH_2CL_2 solutions at a two photon excitation wavelength of 1064 nm.

The highly soluble TPA chromophore **TPA-1** was confirmed to elicit a robust two photon response capable of optical limiting by a two photon mechanism at 645 nm. Complexation of **TPA-1** with $Re(CO)_3Cl$, $Ru(bpy)_2^{2+}$, and $Ir(ppy)_2^{+}$ yielded the metal-organic complexes **Re-1**, **Ru-1** and **Ir-1** which were shown to enhance the nonlinear capabilities of **TPA-1** with the addition of strong triplet-triplet absorptions leading to the establishment of an NLO enhancing excited state absorption mechanism. A systematic study of the presence and relative strengths of enhanced dual mode nonlinear absorption in the target metal-organic series was successfully compared to a solution of C_{60} for which the nonlinear characteristics and mechanisms are known. This study was accomplished utilizing the NLT apparatus for detecting: the presence of

nonlinear absorption, the determination of the relative strength of optical limiting, and the differentiation of a single verse dual mode optical limiting mechanism,

During the photophysical investigation of the target compounds; ground state absorption, emission and transient absorption (TA) spectra were used to identify the triplet excited character of the metal-organic chromophores. The triplet excited state of **Ru-1** was identified as having mostly ^{3}MLCT character based on the overall structure of its TA spectrum. **Ru-1** affords a strong and relatively narrow visible excited state absorption as well as a broad near-IR excited state absorption of equal intensity. This general TA profile along with typical MLCT features such as structured excited state emission and evidence of a shoulder on the lowest energy ground state absorption spectra, all point to a definitive classification of the excited state of **Ru-1** having mostly ^{3}MLCT character. Similar characterization methodology was used to identify the triplet excited states of **Re-1** and **Ir-1** as having mainly $^3\pi-\pi^*$ character. Both complexes exhibited broad and featureless excited state emission and absorption spectra. Additionally, their TA spectra clearly exhibited features previously shown to be characteristic of a triplet excited state having mostly $^3\pi-\pi^*$ character. These features are a broad and weakly absorbing visible excited state absorption and a very strong near-IR excited state absorption.

During the course of the NLT investigations, validation of the detection capability and establishment of experimental reliability of the NLT apparatus was accomplished. Additionally, it was shown that the NLT apparatus could be used to distinguish the difference between a system having a TPA or RSA only NLO mechanism and an enhanced dual mode TPA/RSA mechanism. Utilizing a published model meant to characterize NLO mechanisms in conjunction with data obtained in the course of these investigations, the differentiation of a single NLO process from a dual mode mechanism was accomplished successfully. For a single NLO

process, such as TPA or RSA, a quadratic dependence between the attenuated intensity and incident light intensity is easily differentiated from the cubic dependence exhibited for a TPA/ESA dual mode mechanism. The later finding will prove to be extremely useful in subsequent experimental studies conducted by our group to aid in distinguishing the nature of NLO responses in nonlinear chromophores with TPA, RSA, and dual mode NLO mechanisms.

Lastly, it was successfully shown that the target chromophores **TPA-1**, **Re-1**, **Ru-1** and **Ir-1** all exhibit significant NLO activity. **TPA-1** successfully achieved two photon excitation to produce an excited state equivalent to excited states produced from one photon ground state excitation. Being a strictly TPA chromophore, **TPA-1** exhibited a quadratic dependence between the attenuated intensity and incident light intensity during the course of NLT experiments. Target metal-organic chromophores **Re-1**, **Ru-1** and **Ir-1** were shown to be successfully two photon excited to produce equivalent excited states to those produced by one photon ground state absorption. Additionally, all three complexes exhibited enhanced TPA/ESA dual mode nonlinear absorption. Confirmation of the dual mode nature of an enhanced nonlinear absorption mechanism was verified by not only a relative strengthening of the overall NLO response but also by a representative cubic dependence between the attenuated intensity and incident light intensity.

Experimental

Instrumentation

Nuclear Magnetic Resonance (NMR) spectra were obtained with either a Varian Gemini-300 or a Varian VXR-300. No significant difference in data quality or resolution was noted between these two instruments. Mass Spectrometry data was provided by the University of Florida Mass Spectrometry Services from a Bruker APEX II FTICR. UV-Visible absorption spectra were obtained on a Varian Cary 100 dual-beam spectrophotometer utilizing 1-cm quartz

cells. Corrected steady-state one photon emission spectra were obtained on a PTI Felix 32I fluorometer. Emission quantum yields were measured by relative actinometry with 9,10-diphenylanthracene in cyclohexane ($\Phi_{em} = 0.90$)[64] and $Ru(bpy)_3$ in water ($\Phi_{em} = 0.037$)[1, 65] as the actinometers for **TPA-1** and the metal complexes, respectively. Time-resolved emission decays were obtained with a Photochemical Research Associates FLT by time-correlated single photon counting utilizing 375 and 450 nm IBH NanoLEDs as excitation sources and monitored without filters. Two photon emission spectra were obtained on an in-house instrumented setup utilizing a Continuum Surelite II-10 Nd:YAG laser (355 nm, third harmonic of the 1064 nm fundamental) augmented with a Surelite OPO Plus (420-1600 nm wavelength range) as the sample excitation source and directed through an Acton Research SpectraPro 150 dual grating spectrograph to a Princeton Instruments PI-Max intensified CCD camera. Transient absorption spectra were obtained utilizing an in-house instrumented setup[74] utilizing a Quanta-Ray Nd:YAG laser (355 nm, third harmonic of 1064 nm fundamental) as the sample excitation source. Nonlinear absorption / transmittance spectra was obtained utilizing two optically similar in-house instrumented setups utilizing either a Quanta-Ray Nd:YAG laser (1064 nm fundamental) or the Continuum Surelite II-10 Nd:YAG laser augmented with a Surelite OPO Plus (420-1600 nm wavelength range) as a high intensity photon source. The laser source was attenuated by both fixed transmission and continuously variable neutral density filters to achieve the desired sample input energy and subsequently focused on the sample solution by 50.8 cm diameter plano-convex lens of either 10 cm (for Surelite/OPO setup) or 13 cm (Quanta-Ray 1064 nm setup). Change in transmittance as a function of laser power was monitored directly utilizing an Ophir Laserstar dual channel power meter configured with a pair of matching OPH PE10-SH V2 pyroelectric detectors (sensitivity range 10 μJ to 10 mJ).

Materials

Triphenylamine, 2-methyl-3-butyn-2-ol, *N*-bromosuccinimide, and 2-phenylpyridine were purchased from Acros Organics and used in the condition received. *Trans*-dichloro-bis(triphenylphosphine) palladium (II), *cis*-dichloro-bis(2,2'-bipyridine) ruthenium(II) dihydrate, $Re(CO)_5Cl$, and $IrCl_3$ hydrate were purchased from Strem Chemicals and used in the condition received. Trimethylsilylacetylene was purchased from GFS Chemicals and used in the condition received. 5,5'-dibromo-2,2'-bipyridine, 5,5'-trimethylsilylethynyl-2,2'-bipyridine, and 5,5'-diethynyl-2,2'-bipyridine were synthesized using a significantly modified literature preparation. Full synthetic details are provided for clarity. All other chemicals/solvents not mentioned above were purchased from commercial sources and used in the condition received.

Synthesis

Protonated 2,2'-bipyridine (1)[75]

Acetyl bromide (35.5 mL, 0.480 mol) was added dropwise (over a period of 30 minutes) into a solution containing 2,2'-bipyridine (15.0 g, 0.096 mol) in 400 mL of MeOH. Upon addition of approximately 70% of the acetyl bromide, a pale yellow precipitate formed. The reaction solution was stirred for an additional hour, filtered, and the precipitate was washed with cold acetone yielding 27.46 g (91.7%) of **1**. The NMR spectrum values were identical to values found in the literature.[75] ^{1}H-NMR (300 MHz, D_20) δ 7.80 (m, 2H), 8.30 (m, 4H), 8.71 (dt, 2H). ^{13}C (75.4 MHz, D_20) δ 124.04, 127,36, 143.61,146.01, 147.12.

5,5'-Dibromo-2,2'-bipyridine (2)[75, 76]

Protonated bipyridine **1** (5.0 g, 0.015 mol) and Br_2 (11.3 g, 0.071 mol) were combined in a stainless steel pressure reaction vessel that was fitted with a Teflon sleeve and gasket. The apparatus was sealed pressure tight and heated to 180 °C for 4 days. Heat was removed and the reaction vessel was allowed to cool to room temperature. The reaction vessel was placed on ice

for 15 minutes before opening to ensure internal vessel pressure was eliminated. The dark orange material was removed and placed on a glass dish overnight to allow excess Br_2 to evaporate. The remaining solid was stirred in 1 M NaOH solution to deprotonate followed by extraction with $CHCl_3$. The fractions were combined, dried with $MgSO_4$ and the chloroform was removed under vacuum yielding a light tan solid. The solid was added to 40 ml of acetone and stirred for 30 minutes. The solid which did not dissolve was vacuum filtered yielding 5,5'-dibromo-2,2'-bipyridine as a white solid. The product was washed with two 10 mL aliquots of cold acetone and allowed to dry, yielding pure 5,5'-dibromo-2,2'-bipyridine (1.48 g, 4.69 mmol, 31.2%). The NMR spectrum values were identical to values found in the literature.[75, 76] ^{1}H-NMR (300 MHz, $CDCl_3$) δ 7.93 (qd, 2H), 8.29 (dd, 2H), 8.70 (dd, 2H). ^{13}C (75.4 MHz, $CDCl_3$) δ 121.45, 122.22, 139.60, 150.28 153.66.

Bis-5,5'-trimethylsilylethynyl-2,2'-bipyridine [75, 76]

5,5'-Dibromo-2,2'-bipyridine (1.60 g, 5.10 mmol), trimethylsilylacetylene (2.00 g, 1.4 mL, 20.40 mmol), THF (10 mL), and i-Pr_2NH (10 mL) were combined and degassed under argon for 30 minutes. 5 mol% $Pd(PPh_3)_2Cl_2$ (0.180 g, 0.26 mmol) and 5 mol% CuI (0.05 g, 0.26 mmol) were added and the solution was degassed further for an additional 5 minutes. The reaction then heated to 70 °C and refluxed under an argon balloon for 17 hrs. The solution was allowed to cool and filtered through a bed of sand/celite to remove CuI and ammonium bromide salts. The solution was vacuum evaporated to remove THF and i-Pr_2NH. The resulting solid was taken up in $CHCl_3$, washed with H_2O, dried with $MgSO_4$, and solvent removed under vacuum. The solid was purified by flash chromatography on silica gel with 50:1 hexane-ethyl acetate solution yielding bis-5,5'-trimethylsilylethynyl-2,2'-bipyridine as a flaky light tan solid (1.61 g, 4.61 mmol, 90.5%). The NMR spectrum values were identical to values found in the literature.[75, 76]

^{1}H-NMR (300 MHz, $CDCl_3$) δ 0.27 (s, 9H), 7.86 (dd, 1H), 8.36 (dd, 1H), 8.72 (dd, 1H). ^{13}C (75.4 MHz, $CDCl_3$) δ -0.18, 99.46, 101.74, 120.33, 120.47, 139.77, 152.06, 154.19.

5,5'-Diethynyl-2,2'-bipyridine [75, 76]

5,5'-Trimethylsilylethynyl-2,2'-bipyridine (0.43 g, 1.23 mmol) was dissolved in a solution containing 20 mL THF and 10 mL MeOH. Sodium hydroxide (8ml, 1 M) was added and the reaction stirred at room temperature for 4 hrs. The solution was vacuum evaporated to remove THF and MeOH. The remaining slurry was diluted with 20 mL of H_2O and extracted three times with $CHCl_3$. The extract was dried with $MgSO_4$ and vacuum evaporated to yield (0.23 g, 1.13 mmol, 91%) of pure 5,5'-diethynyl-2,2'-bipyridine as shiny cooper colored flakes that are very electrostatic. The NMR spectrum values were identical to values found in the literature.[75, 76] ^{1}H-NMR (300 MHz, $CDCl_3$) δ 3.30 (s, 2H), 7.90 (dd, 2H), 8.39 (dd, 2H), 8.78 (dd, 2H). ^{13}C (75.4 MHz, $CDCl_3$) δ 80.90, 81.80, 119.80, 120.79, 140.27, 152.50, 154.50.

4-Bromo-N,N-diphenylaniline (3)[77]

Methylene chloride (25 mL) was cooled to 0 °C and flushed with Ar for 20 min. *N*-bromosuccinimide (NBS) (3.60 g, 20.4 mmol) was added and the solution was allowed to stir for 5 min. A pale yellow color was observed and a slight amount of NBS remained undissolved. Upon addition of triphenylamine (5.00 g, 20.4 mmol) the solution turned dark leafy green and a slight rise in temperature was noted. Within 5 min. the majority of the remaining NBS entered into solution. The solution was allowed to slowly warm to room temperature and stirred overnight. The reaction mixture was added to 150 ml of water and the organic layer was separated, dried over $MgSO_4$, and evaporated under reduced pressure to yield a viscous oil with a slight green tint. 20 ml of MeOH was added to the oil and rapidly stirred. The MeOH developed a light blue tint and the product precipitated as an off-white solid. The solid was washed two

additional times with fresh MeOH. Inspection by TLC (silica, 100% hexane) showed the solid contained a mixture of starting material and two other compounds believed to be the mono and dibromo species. Flash chromatography on silica gel with 100% hexane proved difficult due to ΔR_f values being < 0.10. Initial purification of the product for spectroscopic identification was by recrystallization from hexane over a period of two days to a white solid. (3.91 g, 12.1 mmol, 58.3%) Subsequent synthetic pathway modification eliminated the need to purify the product. In turn, all other preparations of this compound were used without further purification. The NMR spectrum values were identical to values found in the literature.[77] ^{1}H-NMR (300 MHz, $CDCl_3$) δ 7.00 (m, 2H), 7.07 (m, 6H), 7.21(m, 6H). ^{13}C (75.4 MHz, $CDCl_3$) δ 122.54, 123.20, 124.18, 125.18, 129.19, 137.92, 147.08, 147.68.

4-(4-(Diphenylamino)phenyl)-2-methyl-3-butyn-2-ol (4)[77]

4-Bromo-*N*,*N*-Diphenylaniline **3** (6.50 g, 20.0 mmol), 2-methyl-3-butyn-2-ol (3.37g, δ = 0.860 g/ml, 40.0 mmol), 10 mL THF and 100 mL diisopropylamine were combined and degassed under argon for 30 minutes. $Pd(PPh_3)_2Cl_2$ (0.704 g, 0.10 mmol, 5 mol%) and CuI (0.16 g, 0.10 mmol, 5 mol%) were added and the solution was degassed further for an additional 5 minutes. The reaction then stirred at 70 °C under an argon balloon for 6 hrs. The solution was filtered through a bed of sand/celite to remove CuI and amine salts. The solvent was evaporated under vacuum to a minimum of solvent. The product was purified easily by flash chromatography on silica gel (ΔR_f values > 0.50) with 2:1 hexane-diethyl ether solution yielding pure 4-(4-(diphenylamino)phenyl)-2-methyl-3-butyn-2-ol **4** as a flaky light caramel colored solid (3.80 g, 11.6 mmol, 58.0%). The NMR spectrum values were identical to values found in the literature.[77] ^{1}H-NMR (300 MHz, $CDCl_3$) δ 1.60 (s, 6H), 2.11 (s, 1H), 6.96 (dd, 2H), 7.03 (dd,

2H), 7.07 (d, 4H), 7.25 (m, 6H). ^{13}C (75.4 MHz, $CDCl_3$) δ 31.55, 65.63, 82.18, 92.91, 115.60, 122.35, 123.41, 124.82, 129.33, 132.52, 147.18, 147.84.

4-Ethynyl-N,N-diphenylaniline (5)[77]

4-(4-(Diphenylamino)phenyl)-2-methyl-3-butyn-2-ol **4** (2.00 g, 6.10 mmol) was dissolved in 20 mL toluene. Solid KOH (2.50 g) was crushed inside a sealed and doubled plastic bag to maintain anhydrous conditions and added quickly to the reaction vessel. The solution was stirred at reflux for 8 hrs. The solution was vacuum evaporated to remove excess toluene. The remaining slurry was diluted with 20 mL of H_2O and extracted three times with $CHCl_3$. The extract was dried with $MgSO_4$ and vacuum evaporated. Flash chromatography on silica gel with 100% hexane yielded (1.27 g, 4.71 mmol, 77.2%) of 4-ethynyl-*N,N*-diphenylaniline as a fine yellow powder. The NMR spectrum values were identical to values found in the literature.[77] ^{1}H-NMR (300 MHz, $CDCl_3$) δ 3.02 (s, 1H), 6.95 (dd, 2H), 7.05 (m, 2H), 7.10 (m, 4H), 7.30 (m, 6H). ^{13}C (75.4 MHz, $CDCl_3$) δ 76.15, 83.91, 114.73, 122.03, 123.62, 125.03, 129.40, 133.04, 147.11, 148.34.

4,4'-(2,2'-bipyridine-5,5'-diylbis(ethyne-2,1-diyl))bis(N,N-diphenylaniline) (TPA-1) (6)

4-Ethynyl-*N,N*-diphenylaniline **5** (1.00 g, 3.70 mmol), 5,5'-dibromo-2,2'-bipyridine **2** (0.583 g, 0.185 mmol), THF (50 mL), and triethylamine (50 mL) were combined and degassed under argon for 30 minutes. $Pd(PPh_3)_2Cl_2$ (0.130 g, 0.185 mmol, 5 mol%) and CuI (0.035 g, 0.184 mmol, 5 mol%) were added and the solution was degassed further for an additional 5 minutes. The reaction was stirred at 70 °C under an argon balloon for 20 hrs. The solution was allowed to cool and filtered through a bed of sand/celite to remove CuI and amine salts. The solvent was then evaporated under vacuum. The resulting solid was taken up in $CHCl_3$, washed with H_2O, dried with $MgSO_4$, and solvent removed under vacuum. The solid was purified by flash chromatography on silica gel with 2:1 hexane/methylene chloride yielding pure **TPA-1** as a

bright yellow powder (0.641 g, 0.928 mmol, 50.1%). ^{1}H-NMR (300 MHz, $CDCl_3$) δ 7.03 (m, 2H), 7.14 (m, 4H), 7.29 (m, 4H), 7.41 (m, 4H), 7.90 (dd, 2H), 8.40 (dd, 2H), 8.78 (dd, 2H)7.90 (dd, 2H), 8.40 (dd, 2H), 8.78 (dd, 2H). ^{13}C (75.4 MHz, $CDCl_3$) δ 85.71, 94.27, 115.03, 120.50, 120.82, 121.93, 123.77, 125.18,129.44, 132.67, 139.06, 147.03, 148.43, 151.54, 153.81. MS calculated for $C_{50}H_{34}N_4$ 690.28, M+1 found 691.29.

Ru(TPA-1)(bpy)$_2^{2+}$·2PF$_6^-$ (Ru-1) (7)

cis–Ru(bpy)$_2$Cl$_2$ (0.133 g, 0.255 mmol) was dissolved in 20 mL of MeOH and refluxed under Ar for 2 hrs. Solution color turned a deep wine color immediately upon reflux. **TPA-1** (0.0160 g, 0.232 mmol) was dissolved in 5 mL THF and added via syringe and the solution was refluxed for an additional 18 hrs. Solution fluorescence subsided slowly over the first 8 hrs. Upon cooling to room temperature a saturated aqueous solution of NH_4PF_6 was added dropwise producing a brick red precipitate. Approximately 5 mL of NH_4PF_6 was added before precipitate no longer formed. The precipitate was filtered utilizing a medium porosity fritted filter. The product was reprecipitated by dissolving the product in a minimum of CH_2Cl_2 and adding dropwise slowly into 50 mL of diethyl ether. The precipitate was filtered as before, rinsed with three 10 mL aliquots of diethyl ether and dried yielding a dark red powder. The product was further purified on an alumina (6% H_2O added) column eluting with 4:1 CH_2Cl_2/CH_3CN. Pure metallated **Ru-1** (0.051g, 0.037 mmol, 16%) was obtained as a red powder. ^{1}H-NMR (300 MHz, $CDCl_3$) δ 6.91 (m, 4H), 7.08 (m, 12H), 7.27 (m, 12H), 7.49 (m, 4H), 7.57 (d, 2H), 7.71 (m, 4H), 8.08 (m, 6H), 8.50 (m, 6H). ^{13}C (75.4 MHz, $CDCl_3$) δ 78.91, 98.72, 113.88, 121.56, 125.36, 125.55, 126.65, 128.91,129.44, 130.69, 133.84, 139.23, 140.41, 147.63, 150.44, 152.87, 153.24, 154.00, 156.20, 158.15, 161.85. MS calculated for $C_{70}H_{50}N_8Ru$ (M -2PF$_6$) 1104.32, M found 1104.32.

$Re(TPA\text{-}1)(CO)_3Cl$ (Re-1) (8)

$Re(CO)_5Cl$ (0.121g, 0.276 mmol) and **TPA-1** (0.231g, 0.334 mmol) were combined in 40 ml of toluene and the solutions was deoxygenated with argon for 20 min then heated to reflux (110° C) with rapid stirring. Very quickly after the reaction temperature passed 100° C the bright blue-green fluorescence of **TPA-1** disappeared and was replaced by a bright reddish-pink solution which was not fluorescent. Heat was removed after 45 minutes when it was noted that all evidence of fluorescence was gone. Stirring was continued until well after the reaction solution reached room temperature. A small amount of bright red precipitate was observed prior to removal of the solvent. Solvent was evaporated under vacuum and the product was rinsed with fresh acetone until rinsing solvent remained clear. Pure metallated **Re-1** was recovered as a light red power (0.115g, 0.117 mmol, 42.4%). Multiple attempts to obtain a usable ^{13}C spectrum were unsuccessful (scan multiples of over 10,000 were tried) due to the product's limited solubility in all available NMR solvents. Photophysical data is included to supplement the characterization data for **Re-1**. ^{1}H-NMR (300 MHz, $CDCl_3$) δ 7.99 (d, 4H), 7.15 (m, 12H), 7.33 (m, 8H), 7.44 (m, 4H), 8.10 (m, 4H), 9.09 (bs, 2H). ^{13}C (75.4 MHz) δ (see above). $\lambda_{max}/\varepsilon_{max}$ 334 nm / 5.5 x 10^4 $M^{-1}cm^{-1}$, 460 nm / 4.9 x 10^4 $M^{-1}cm^{-1}$. λ_{em} 696 nm (ϕ_{fl} 0.0051). MS calculated for $C_{53}H_{34}ClN_4O_3Re$ (M) 996.19, M found 996.19.

$Ir_2(ppy)_4Cl_2$ (9)[78]

$IrCl_3$ (hydrate) (0.500g, 1.67 mmol), and 2-phenylpyridine, (1.00g, 6.44 mmol, δ = 1.086 g/mL), were dissolved in a mixture of 2-methoxyethanol (40 mL) and water (20 mL). The reaction mixture was refluxed at 110° C for 18 hrs. The product solution was cooled to room temperature at which time a fine yellow precipitate was formed. The precipitate was collected using vacuum filtration with a medium porosity glass fritted filter. The precipitate was washed

three times with each 95% ethanol (15 mL each) and acetone (30 mL). The crude yellow product was dissolved in 3 mL of CH_2Cl_2 and a layer of hexane was carefully added to top of the CH_2Cl_2 solution. After one hour at room temperature, the solution began to precipitate a fine bright yellow powder. The solution was cooled overnight. The final product was collected by vacuum filtration with a medium glass fritted filter as a bright yellow crystalline powder (0.695g, 0.648 mmol, 77.6%).

$Ir(TPA\text{-}1)(ppy)_2^+ \cdot PF_6^-$ (Ir-1) (10)

$Ir_2(ppy)_4Cl_2$ (0.164g, 0.153 mmol) and **TPA-1** (0.211g, 0.305 mmol) were added to 7 mL of 2-methoxyethanol. The starting materials were only slightly soluble. The reaction mixture was heated to 100° C along with rapid stirring under an argon atmosphere for a period of 26 hrs. Reaction progress was monitored over the reaction period utilizing TLC (silica, 100% CH_2Cl_2) and a UV lamp. It was noted that as the reaction proceeded, the solution turned a deep red and the fluorescence intensity decreased. The reaction was cooled to room temperature when fluorescence was no longer detected visually with a UV lamp and only a faint trace of fluorescent starting material remained on TLC. To the reaction mixture was added a saturated aqueous solution of NH_4PF_6 (approx 6 mL) and a bright red precipitate formed immediately. Stirring was continued for 30 minutes at which time 50 mL of water was added and stirred for an additional 15 minutes. The precipitate was collected by vacuum filtration with a medium glass fritted filter and dried overnight. The product was further purified by flash chromatography on neutral alumina using 100% CH_2Cl_2. First off the column was unreacted **TPA-1** starting material followed by product. The product eluted as a medium red band. Pure metallated **Ir-1** (0.304g, 0.255 mmol, 83.5%). was obtained after vacuum evaporation as a dark yellow powder. ^{1}H-NMR (300 MHz, $(CD_3)_2CO$) δ 6.29 (dd, 2H), 6.94 (m, 6H), 7.02 (m, 4H), 7.15 (m, 12H), 7.30 (m, 12H), 7.57 (dd, 2H), 7.79 (m, 4H), 8.00 (m, 4H), 8.12 (dd, 2H), 8.00 (d, 4H). ^{13}C (75.4

MHz, $(CD_3)_2CO$) δ 84.57, 99.00, 113.77, 121.00, 121.60, 123.70, 124.73, 125.55, 125.88, 126.02, 126.66, 127.29, 130.69, 131.47, 132.58, 133.89, 139.78, 141.91, 145.05, 147.64, 150.49, 150.66, 152.90, 154.85, 168.53. MS calculated for $C_{72}H_{50}N_6Ir$ (M -PF_6) 1191.37, M+ found 1191.37.

CHAPTER 4
CONCLUSION

In the preceding chapters, findings are presented from the study of the synthesis and photophysical investigation of a series of transition metal based metal-organic chromophores with the potential to exhibit an enhanced dual mode nonlinear optical mechanism. The methodology involved the combination of two photon absorption (TPA) as the excitation pathway followed by intersystem crossing to produce strongly absorbing triplet excited states capable of nonlinear absorption through an excited state absorption (ESA) mechanism

The initial focus of this project centered on the synthesis of the two photon active organic chromophore **TPA-1**. Utilizing known two photon structure-property architecture, the **TPA-1** chromophore was designed with electron donating triphenylamine end caps capable of producing a large two photon absorption cross section and linked with an electron accepting bipyridine core by highly polarizable acetylene linkages to produce a two photon active chromophore with a D-π-A-π-D architecture. Upon investigation of the photophysical characteristics of **TPA-1**, it was determined the chromophore exhibited strong ground state absorption over a wide spectral range with both one and two photon excitations as well as an emission quantum yield of unity. Further investigation of the nonlinear character of **TPA-1** revealed significant nonlinear absorbance and optical limiting from a two photon excitation source and a fast temporal profile of less than 5 ns.

For the subsequent synthetic portion of the project, complexation of the **TPA-1** chromophore with a series of transition metal based chromophores was undertaken. To achieve the final target metal-organic chromophores the $Re(CO)_3Cl$, $Ru(bpy)_2^{2+}$ and $Ir(ppy)_2^{+}$ moieties were complexed with **TPA-1** utilizing its bipyridine core by known reaction procedures. The resulting complexes **Re-1**, **Ru-1** and **Ir-1** were synthesized and photophysically characterized prior to the investigation for dual mode nonlinear absorption.

The next phase of research involved the development of an experimental apparatus capable of detecting nonlinear absorption. The desired capabilities of this nonlinear transmission (NLT) apparatus included the need to observe, acquire and record data of nonlinear response in a solution of known chromophore concentrations and be capable of comparing the data obtained to results obtained under similar experimental conditions for samples whose nonlinear character is well known. It was also desired to create an experimental technique that could utilize a broad spectrum of laser wavelengths as its excitation source. A survey of applicable nonlinear absorption characterization techniques and their needed equipment requirements led to the determination that a nonlinear transmission or optical limiting apparatus could be developed with the least amount of new equipment required. Testing of the NLT setup was performed utilizing a series of platinum-acetylide dimers (**Pt2-Ar**) that were synthesized by Dr Kye-Young Kim and compared to the NLO response found in **E1-DPAF**, for which nonlinear character is known.

It was concluded the NLT apparatus was able to detect and render data to depict the desired nonlinear responses of interest. With the current configuration of the NLT apparatus, a repeatable semi-quantitative representation of nonlinear response can be achieved. Ease of setup and data collection presents this nonlinear detection technique as an experiment that can be utilized with only a minimum of prior training and orientation on the apparatus. The quality of data gathered is excellent and very easy to compile into useable nonlinear absorption and optical limiting plots. Future use of this setup in conjunction with experiments capable of determining nonlinear absorptive cross sections will allow for quantitative comparisons of nonlinear data to results from other studies with little need for exhaustive model compound synthesis or standard sample preparations and comparisons.

The results from testing the NLT apparatus also led to the successful collection of nonlinear data for the **Pt2-Ar** series of platinum-acetylide dimers. Successful two photon excitation followed by excited state absorption was confirmed and verified. With the comparison of the **Pt2-Ar** series results to the model compound **E1-DPAF,** it was determined the **Pt2-Ar** series has a greater overall nonlinear response. The reason for this difference can be attributed to the variation in the core arylene units. This is logical since the TPA chromophore is identical for each complex in the series. With the TPA nonlinear excitation pathway identical for each compound, the differences seen are deemed to originate from the ESA active portion of the chromophore. Initial analysis of the preliminarily data found here points to the strength of triplet-triplet absorption as the main variable that correlates with the enhancement found in the nonlinear response in the **Pt2-Ar** series.

The final portion of this research incorporated nonlinear transmission techniques and apparatus to investigate the relative strength of an enhanced dual mode nonlinear response in the metal-organic complexes **Re-1**, **Ru-1**, and **Ir-1** which were synthesized earlier in this project. The goal of developing a series of metal-organic chromophores that exhibit dual mode nonlinear response utilizing both two photon excitation and excited state absorption was successfully realized. **TPA-1** was confirmed to elicit a robust two photon excitation capable of optical limiting by a two photon mechanism at 645 nm while maintaining excellent optical transparency at the two photon active wavelengths. Complexation of **TPA-1** with the $Re(CO)_3Cl$, $Ru(bpy)_2^{2+}$, and $Ir(ppy)_2^{+}$ moieties yielded the metal-organic complexes **Re-1**, **Ru-1** and **Ir-1** which were shown to enhance the nonlinear response of **TPA-1** with the addition of triplet-triplet absorption leading to of a excited state absorption (ESA) mechanism. Utilizing the NLT apparatus, a systematic study of the presence and relative strengths of dual mode nonlinear absorption in the

metal-organic series was successfully compared to solutions of C_{60} whose nonlinear characteristics have been previously studied.

In the process of conducting the nonlinear investigations, validation of the detection capability and establishment of the experimental reliability of the NLT apparatus was verified. It was also shown the NLT apparatus could be used to distinguish between a system having a single NLO mechanism and a dual mode TPA/RSA mechanism. Utilizing an established model developed to characterize NLO mechanisms in conjunction with data obtained during these investigations, the differentiation of a TPA only process from a dual mode mechanism was accomplished. A single NLO process, such as TPA or RSA exhibits a quadratic dependence between the attenuated intensity and incident light intensity and is easily differentiated from the cubic dependence of the attenuated intensity and incident light intensity for a TPA/ESA dual mode mechanism. The later finding will prove to be extremely useful in subsequent experimental studies conducted by our group. The ability to distinguishing the nature of an NLO response in nonlinear chromophores exhibiting a TPA, or RSA from a dual mode NLO mechanisms is a potentially powerful characterization tool.

APPENDIX A
^{1}H AND ^{13}C SPECTRA

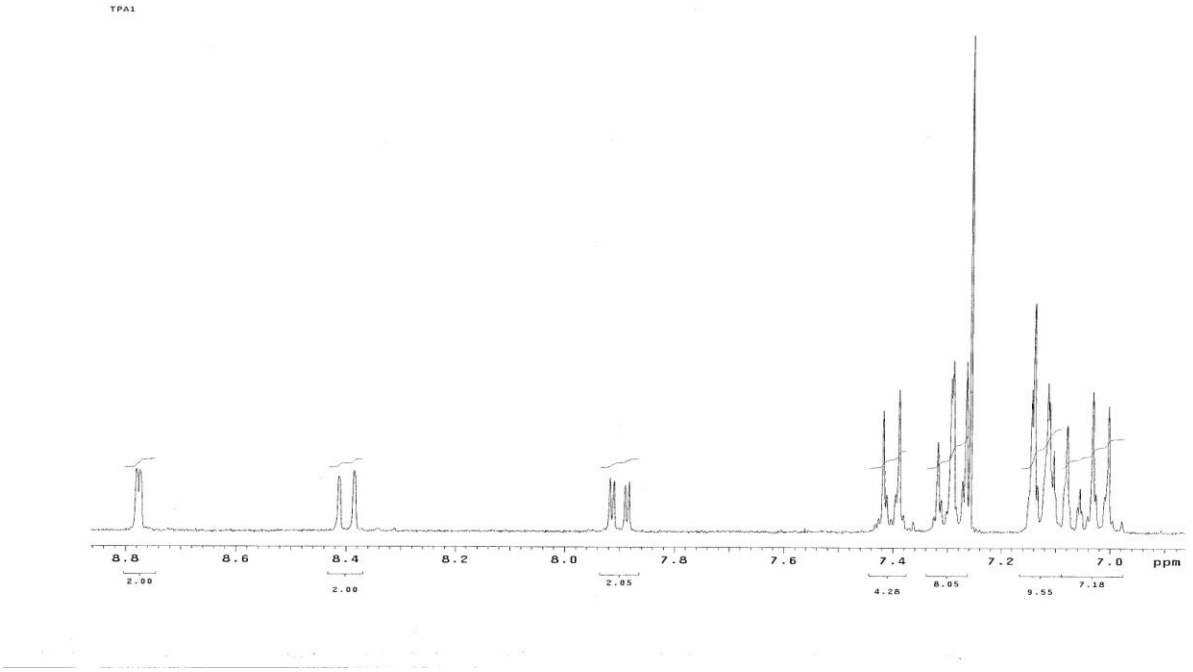

Figure A-1. ^{1}H NMR spectrum of **TPA-1** in CDCl3.

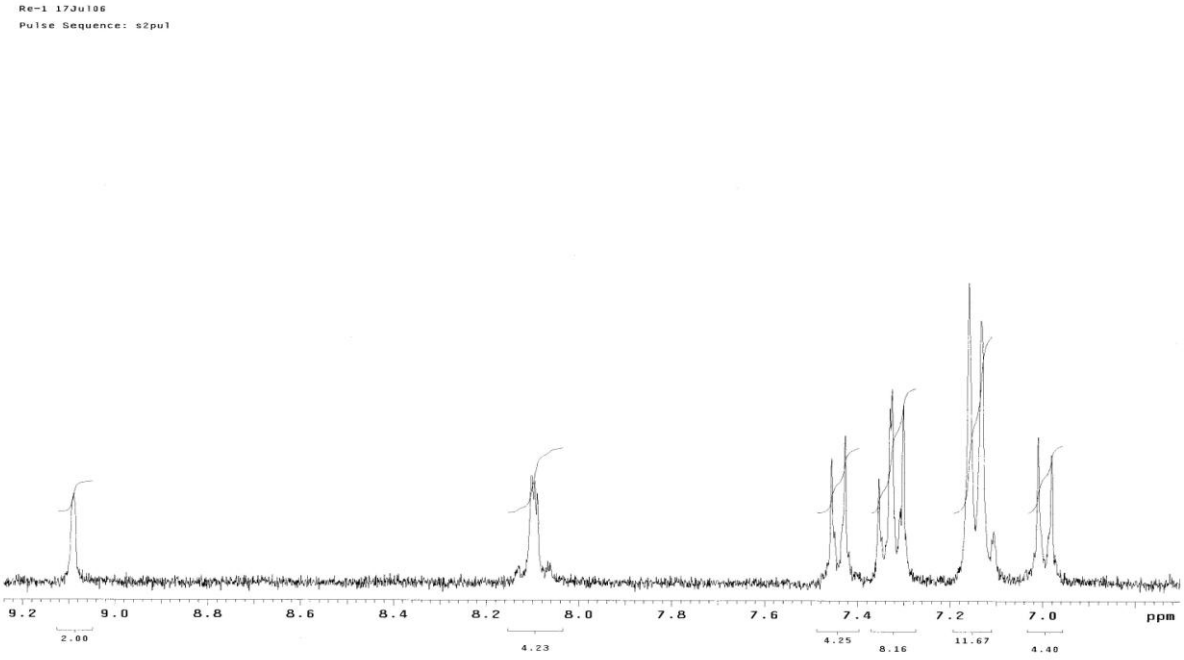

Figure A-2. ^{1}H NMR spectrum of **Re-1** in CD_2Cl_2.

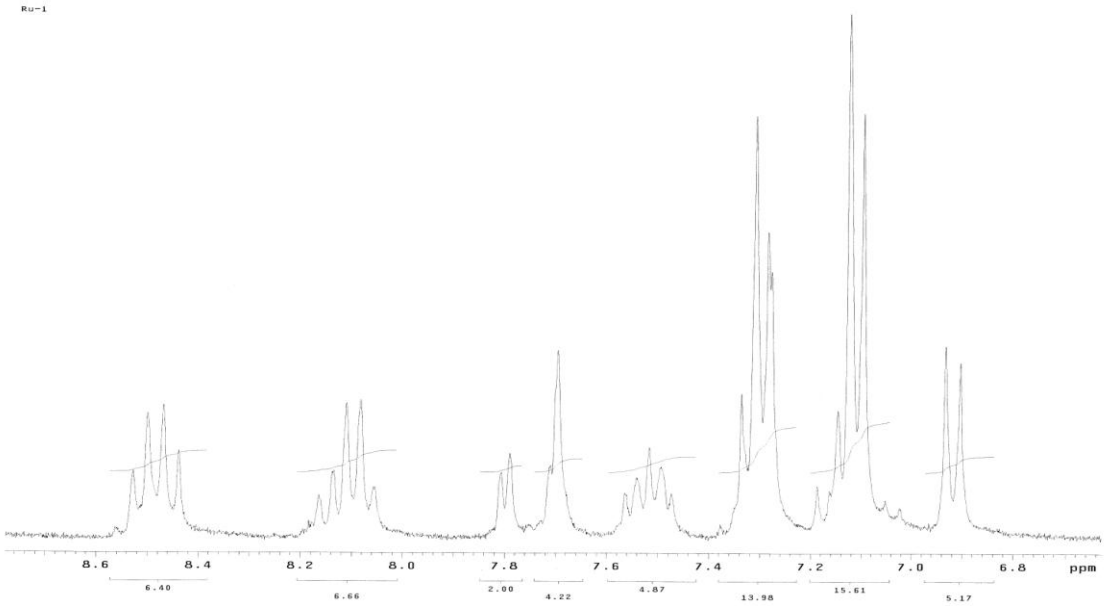

Figure A-3. ^{1}H NMR spectrum of **Ru-1** in CD_2Cl_2.

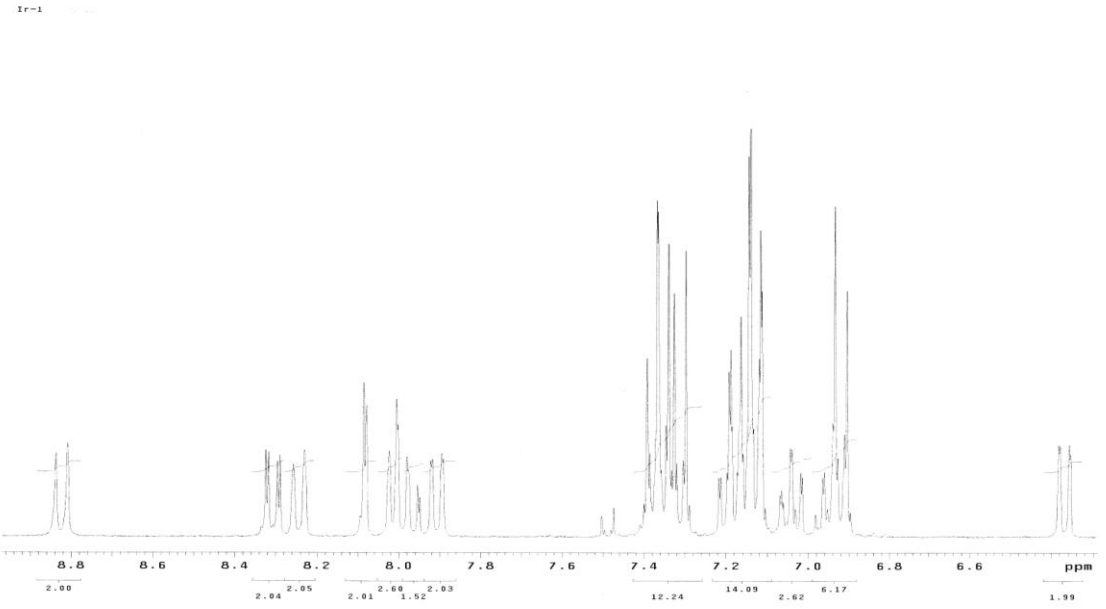

Figure A-4. ^{1}H NMR spectrum of **Ir-1** in CD_2Cl_2.

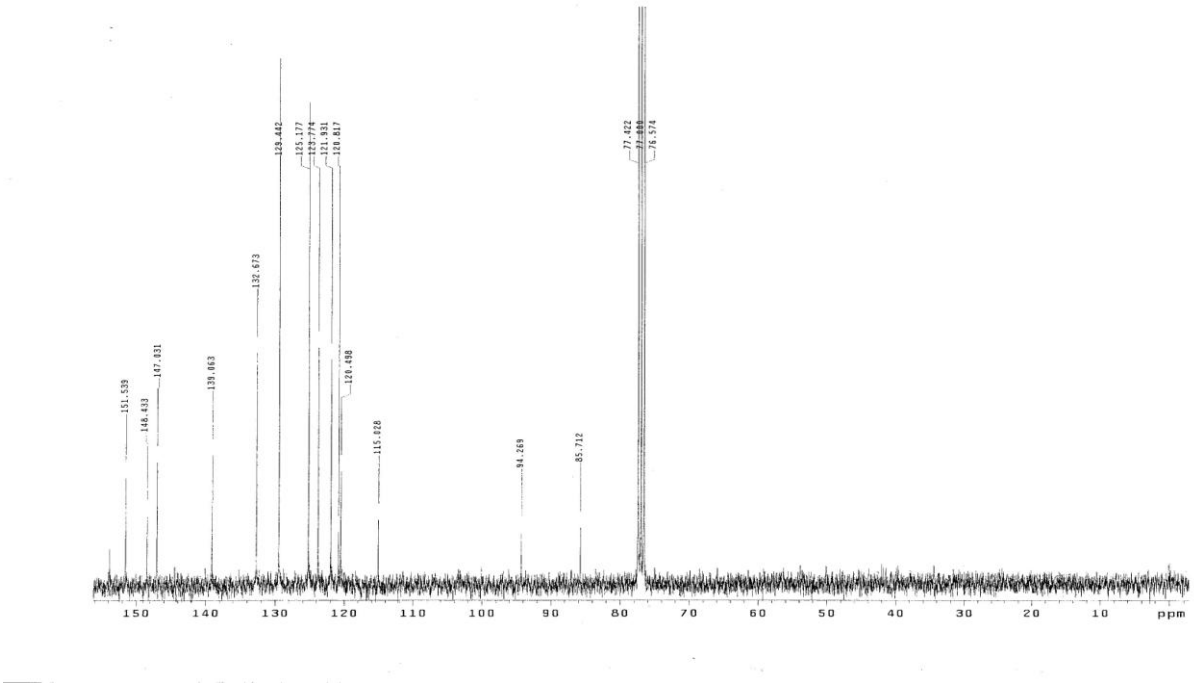

Figure A-5. ^{13}C NMR spectrum of **TPA-1** in $CDCl_3$.

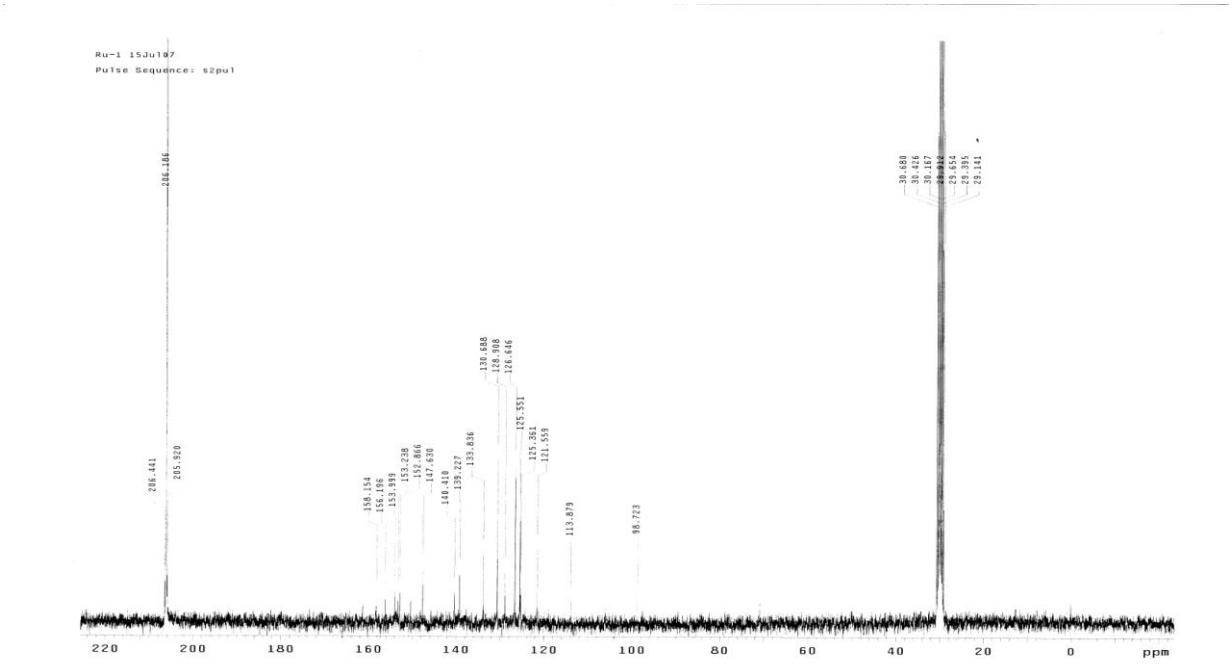

Figure A-6. ^{13}C NMR spectrum of **Ru-1** in $(CD_3)_2CO$.

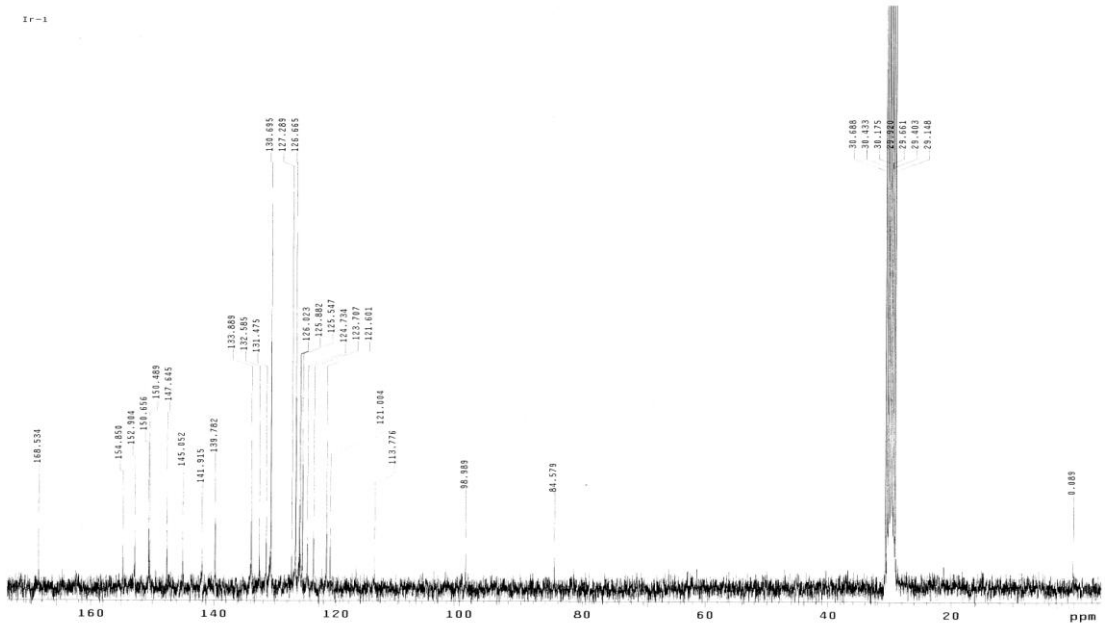

Figure A-7. ^{13}C NMR spectrum of **Ir-1** in CD_2Cl_2.

APPENDIX B
NONLINEAR TRANSMISSION MANUAL

Manual for Nonlinear Transmission

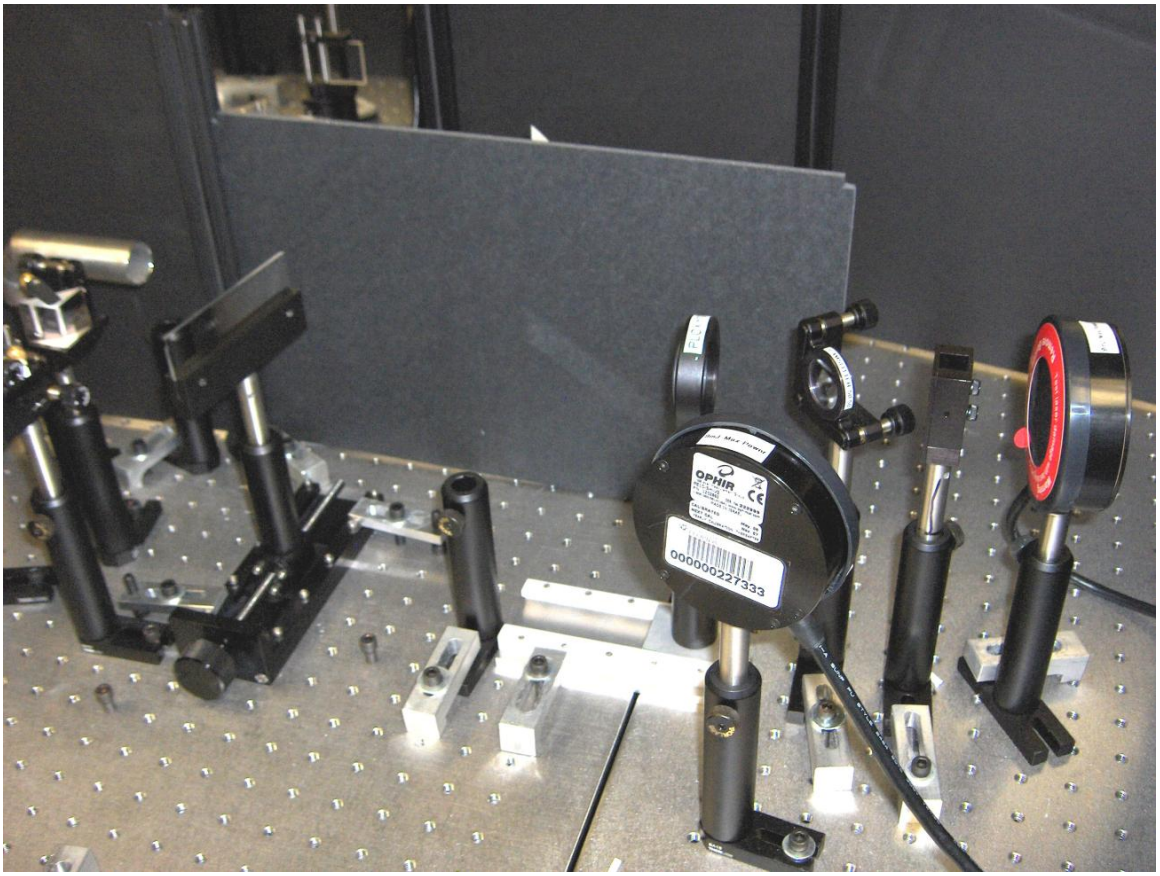

Prepared by John Peak

Department of Chemistry
University of Florida
September 2007

Safety Notes

- **If at any time you are unsure of how to operate or modify the instrument layout, contact the laser lab manager or Dr. Schanze.**
- **Always know where the laser beam path will travel. Never lean over or into an energized laser beam path.**
- **Proper eye protection is mandatory when the laser beam is energized. Ensure all reflected laser energy is suppressed prior to starting the experiment.**
- **Confirm all optics are clean and free of defects or damage prior to energizing the laser.**

Sample Preparation

Any solvent may be used effectively for this experiment, however ground state absorption of your solvent at the desired wavelength should be evaluated and minimized as much as possible. Solvent choice should be based on complete solvation of your sample. Incomplete solvation will lead to potentially unwanted optical scattering and reduction of sample transmission.

2 to 3 ml of solution is needed to perform this experiment and should not be prepared in the sample cell. There are two reasons for this: first, a blank solvent measurement in the sample cell being used is necessary to compensate for the optical effects of cell containing the solvent, and second, any undissolved sample on the surface of the cell has the potential to damage the cell during the experiment.

Laser Table Preparation

Remove all equipment and material that is not needed for the experiment from the vicinity of the laser beam path.

Remove all plastic bags from the prisms, lens and filters prior to turning on the laser and associated equipment.

Laser Wavelength Selection and Alignment

Quanta-Ray

Available wavelengths – 266, 355, 532, and 1064 nm.

If you need to change the laser wavelength, set the prism control rods to the proper configuration as listed below. These rods are located on the silver box at the front of the laser head. Never move the control rods when the laser is in operation. Prism 1 enables conversion of the 1064 nm fundamental to the second harmonic of 532 nm. Prism 2 allows generation of the third and fourth harmonics (355 and 266 nm respectively). Do not place Prism 2 in either the T or F positions if Prism 1 is not in the II position as this will damage Prism 2.

Wavelength / nm	Prism 1	Prism 2
1064	I	**O**
532	II	**O**
355	II	**T**
266	II	**F**

Figure B-1. Prism control rod configuration for wavelength selection (Quanta-Ray).

Remember that all wavelengths longer than the selected wavelength are emitted by the laser. Currently a dispersing prism is being utilized to separate wavelengths and multiple beam dumps are positioned to suppress unwanted wavelengths. If you are unsure how to properly isolate and utilize the wavelength you need for your experiment contact the laser lab manager or Dr. Schanze.

Alignment of the Quanta-Ray output beam should be perpendicular to the optical axis of the nonlinear transmission apparatus. Due to the high energy output of this laser, a glass slide

should be used to redirect a portion of the beam to the apparatus. A beam dump must be placed after the pickoff to capture the unused portion of the beam. In Figure B-2, a photo schematic depicting the main output beam, pickoff and beam dump is presented as a visual guide.

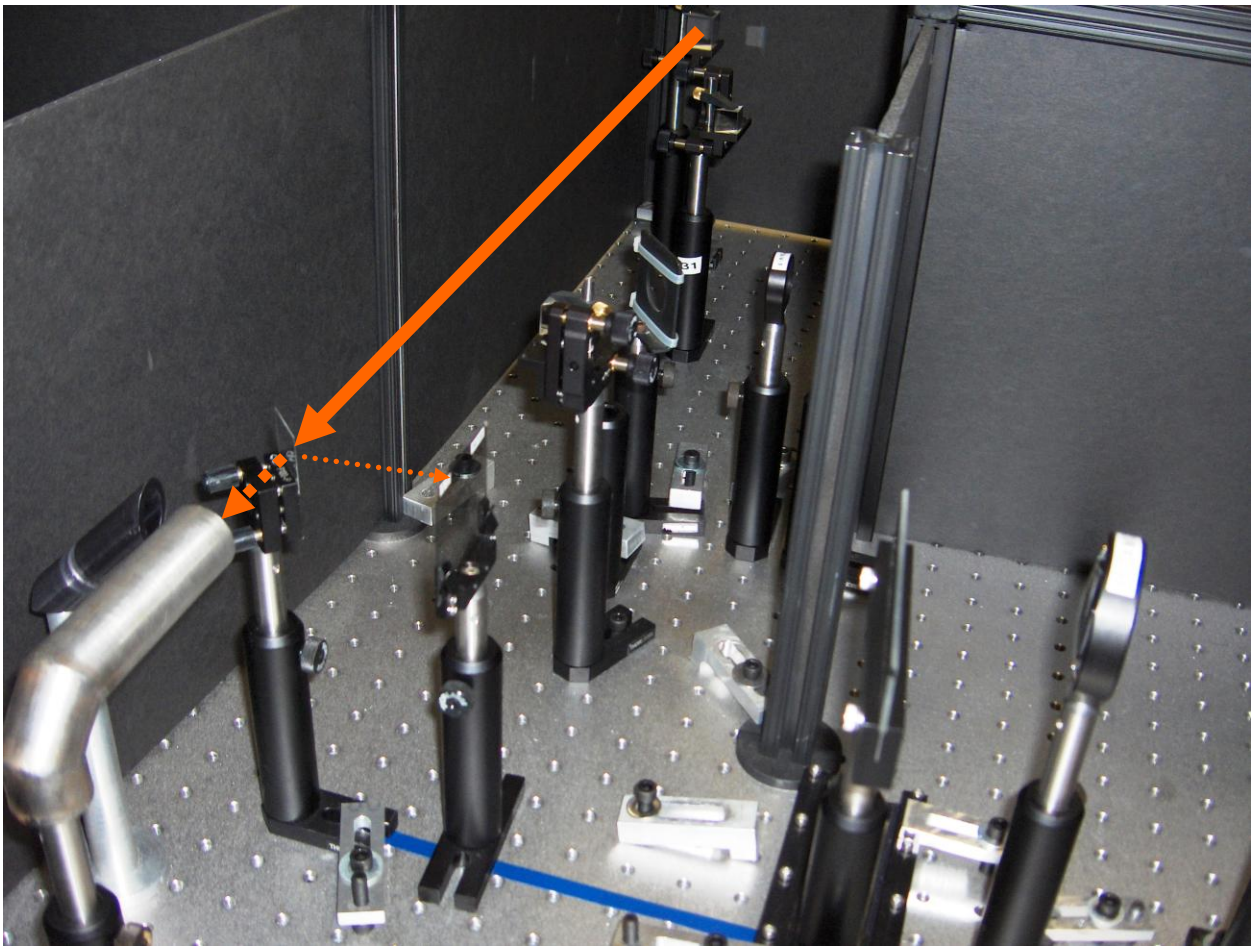

Figure B-2. Beam pickoff configuration for Quanta-Ray.

Surelite II/OPO

Laser output from the optical parametric oscillator (OPO) is divided into two different beams, the signal and idler. With respect to the direction of beam propagation, the left output is the signal and the right output is the idler. The available wavelengths from the signal output are approximately 420 to 570 nm and 600 to 1100 nm from the idler output. Energy output from the OPO is highly wavelength-dependant and it should be determined if enough output energy is

available at the desired wavelength prior to starting your experiment. Typical output energies needed range from 5 to 9 mJ.

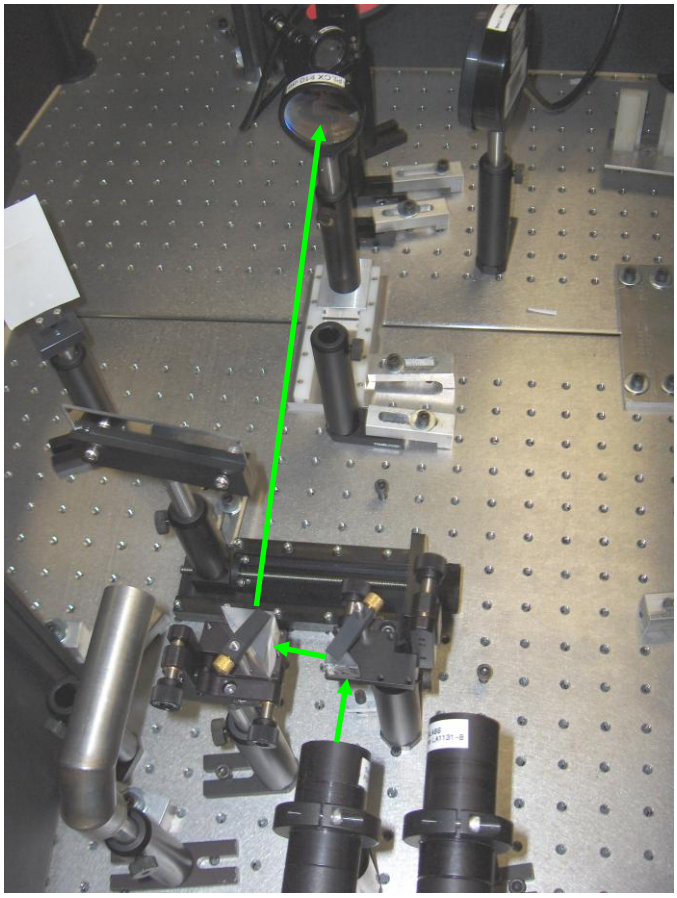

Figure B-3. Dual prism alignment for Surelite/OPO output.

Initial alignment of the OPO output beam to the nonlinear transmission apparatus is best accomplished by a pair of right angle prisms. This two-prism configuration allows for easier beam steering and aides in adjusting the output beams so they are parallel to the laser table. This configuration also simplifies switching from signal to idler beams since only the first prism needs to be moved to the appropriated output position.

Nonlinear transmission setup and alignment

Regardless of laser output (Quanta-Ray, or Surelite/OPO) the setup and alignment are similar. For this section, the laser source refers to the laser beam path as it exits the final turning

optic as described above in the laser wavelength selection and alignment section. To aid in the following alignment, a strip of colored tape may be placed on the surface of the laser table from the laser source to point beyond the estimated position of the sample holder and detector 2 (see Figure B-4) to help visualize the optical axis of the apparatus and aid in placement of the optics.

Setup

Refer to Figure B-4 for general configuration of apparatus setup.

(1) Measure the height from the laser source to the surface of the laser table. This will be the height above the table surface you will use to place all the other optics, filters and detectors for the setup.

(2) Place detector 2 along the optical axis at a distance of approximately 2 to 3 feet from the laser source at the height noted above. This distance should be sufficient to allow for proper placement of all the optics and minimize the setup footprint. A longer distance may be used if it is deemed necessary.

(3) Center the sample holder on the optical axis approximately 5 cm in front of detector 2.

(4) Place the focusing lens, centered on the beam path, in front of the sample holder at a distance equivalent to its focal length. Plano-convex lenses, 50.8 mm (2") in diameter, with focal lengths of 10 to 14 cm have been used effectively. Lenses of different focal lengths may be substituted; however caution should be exercised when utilizing shorter focal length lenses. Shorter focal lengths will significantly increase energy densities and damage to the sample cell will be more likely.

(5) Place a 50:50 or 30:70 beamsplitter 5 cm prior to the sample holder at a 45° angle to the optical axis and at the height of the laser source. The type of beamsplitter to be used is determined by the available energy from the laser and the desired input energy to the sample.

(6) Position detector 1 10 cm from the beamsplitter perpendicular to the optical axis of the apparatus. It is important to position both detectors at equal distances from the beamsplitter and focusing lens. By making these distances equivalent, the spot size hitting each detector will be equivalent and data gathered will be much more consistent.

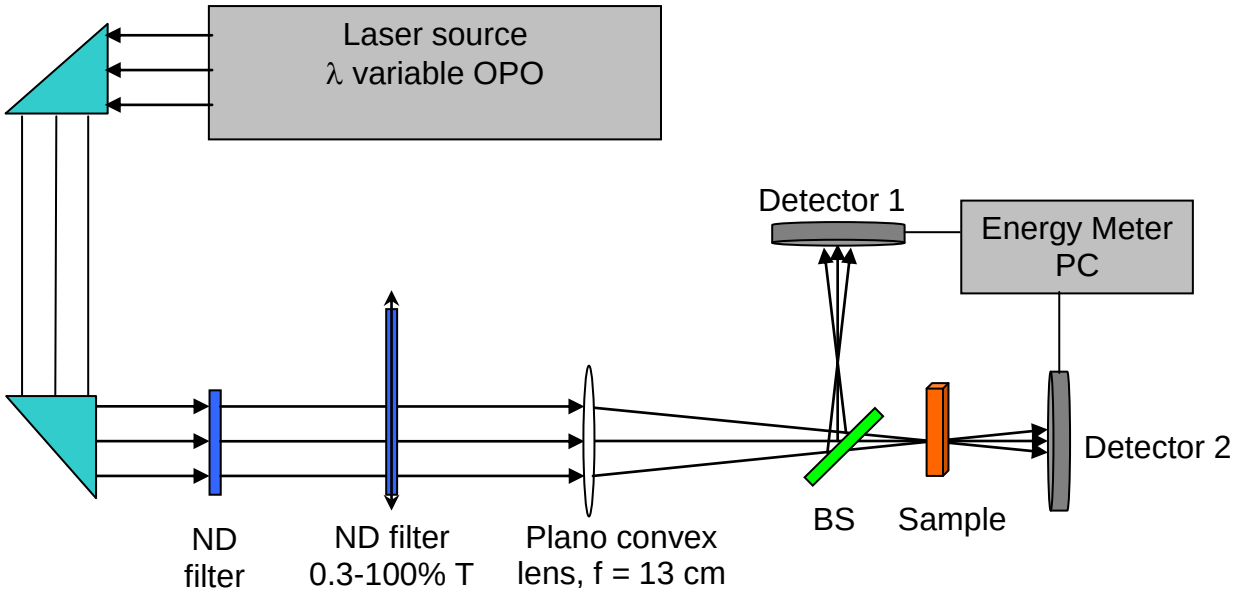

Figure B-4. General schematic diagram of nonlinear transmission setup.

(7) A continuously variable neutral density filter mounted on a single-axis translation stage is placed prior to the focusing lens. **Note**: a significant amount of laser energy is reflected from the ND filter's front face and this energy should be redirected into a dump by slightly rotating the filter off-axis (~10°). The filter and beam can be clearly seen in Figure B-3.

Alignment

During alignment, the laser power should be set at just over threshold power to minimize the potential of equipment damage. Eye protection should be worn anytime the laser is energized.

(1) Adjust the laser source beam optics (prisms or pickoff) to ensure the beam is parallel to the laser table and at a constant height over the course of the setup.

(2) Adjustment of the beamsplitter and detector 1 may be needed to place the reflected energy on the exact center of detector 1. Inspect the size of the laser spot hitting detector 1. The spot should not be larger than one-half the available area of the detection pad.

(3) Adjust the focusing lens and/or the sample holder placement as needed to position the beam focus on the exact center of the sample holder (front to back). Burn paper can be used as a guide to position the focus. An alternate method is to place a cell containing a fluorescent dye solution in the sample holder which will allow for a visual alignment of the focus.

(4) Adjust the position of detector 2 and inspect the size of the laser spot hitting the detection pad. The spot should not be lager than one-half the available area of the detection pad. Recheck the distance of detectors 1 and 2 from the beamsplitter to ensure they are equal.

Energy meter setup

Prior to operation, familiarize yourself with the operation of the LaserStar dual channel energy meter by reading the operators manual. **Note**: the PE10-V2 pyroelectric detector heads have a sensitivity range of 10 μJ to 9 mJ. Laser energies in excess of 9 mJ will damage the detectors.

All applicable operating software for the energy meter is installed on the laser lab laptop and can be accessed on the desktop with the StarCom32 icon. Installation instructions are available in operators manual. An RS-232 to USB converter is supplied for computer connection. The appropriate driver software must be installed to use this connector. The disk is stored in the LaserStar file and should be returned after installation.

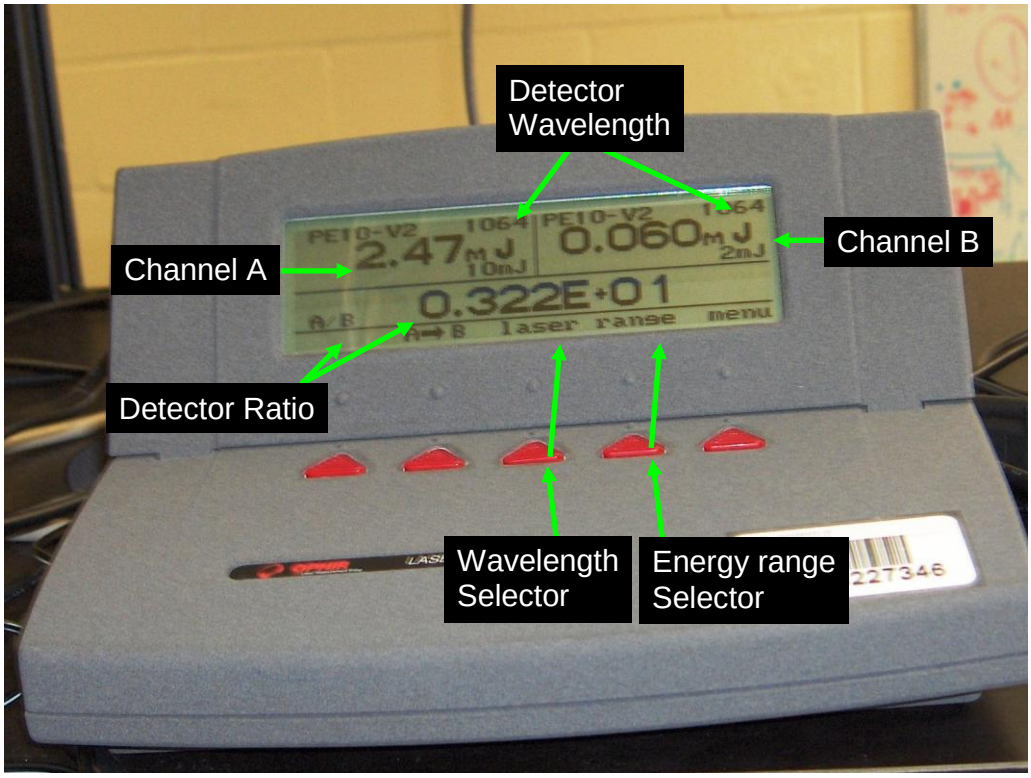

Figure B-5. LaserStar energy meter.

(1) With the energy meter off, connect detector 1 as channel A and detector 2 as channel B.

(2) Connect the energy meter to the computer utilizing the RS-232/USB connector.

(3) Turn energy meter on. Channels A and B should read zero, if not then recycle power.

(4) Select the StarCom32 icon on the computer desktop.

(5) From the drop down menu, choose the connect function.

(6) Select ratio A/B from the drop down menu.

(7) On the energy meter, select the wavelength for each detector that matches the wavelength to be used (see Figure B-5, middle red button). Press esc when complete.

(8) Select the detector energy range most appropriate for each detector (see Figure B-5, second red button from right). Each range represents the maximum energy to be read. The ranges 200 μJ, 2 mJ and 10 mJ are the three most common ranges you will use.

The nonlinear transmission apparatus is now aligned and configured for data acquisition.

Performing the nonlinear experiment

Startup

With the variable neutral density filter completely out of the beam path, adjust the laser power to the highest energy desired for the experiment. Detector 2 is reading the actual energy the sample cell will be exposed to and caution must be used to not exceed 9 mJ during this adjustment. The ratio value observed on the energy meter should remain a constant value; if it is not; recheck the beam alignment and detector distances. You may notice the amount of energy redirected by the beamsplitter does not represent the ratio value expected (i.e. 50:50) but this is normal. The beamsplitters will redirect different amounts of energy depending on the wavelength being used and its orientation in the beam path. This difference does not necessitate readjustment. If more energy is needed to the sample, replace the beamsplitter with one that has a higher throughput value.

Block the laser source and reposition the variable neutral density filter into the beam path. Leave the beam block in place until data acquisition is desired. For the Surlite/OPO the manual shutter works the best for this step. A beam dump works best for the Quanta-Ray.

Collecting data

(1) Place a sample cell (due to their expense, quartz is not needed) containing solvent in the sample holder. 2 to 3 ml of solution is optimum. Take note of which side is facing the laser source, as you will want to configure you sample solution in the same manner.

(2) Remove the beam block and press "start" on the computer.

(3) Move the variable neutral density filter across the beam path using the adjustment knob on the bottom of the translation stage. **Note**: watch the energy readout closely and BEFORE the readings reach their maximum range value, press stop on the program. Select a new range and press start when the reading stabilizes. Unless you press the clear tab, data will continue to be added to the current data file. Repeat this as often as needed to achieve the desired range of data.

(4) When the desired range of data is collected, press stop. Replace the beam block. Immediately save the data file using the drop down menu under file. If the data is not saved soon after acquisition, the meter may reset automatically and the data will be lost. For a solvent, no nonlinear response should be present and a constant ratio will be presented (see Figure B-6). The average ratio will be annotated at the top of the data page. For the example below the ratio is 0.291. This will be the factor you will use to convert the Channel A readings to input energy to your sample.

(5) Reset the neutral density filter and press clear on the program.

(6) Remove the solvent from the sample cell and replace with a sample of known concentration. 2 to 3 ml of solution is sufficient for measurement.

(7) Repeat steps 1 through 4.

For samples that exhibit a nonlinear response, a data plot similar to Figure B-7 will be collected. Remember that the ratio found for the solvent-only sample is the conversion factor that is used for input energy calculation.

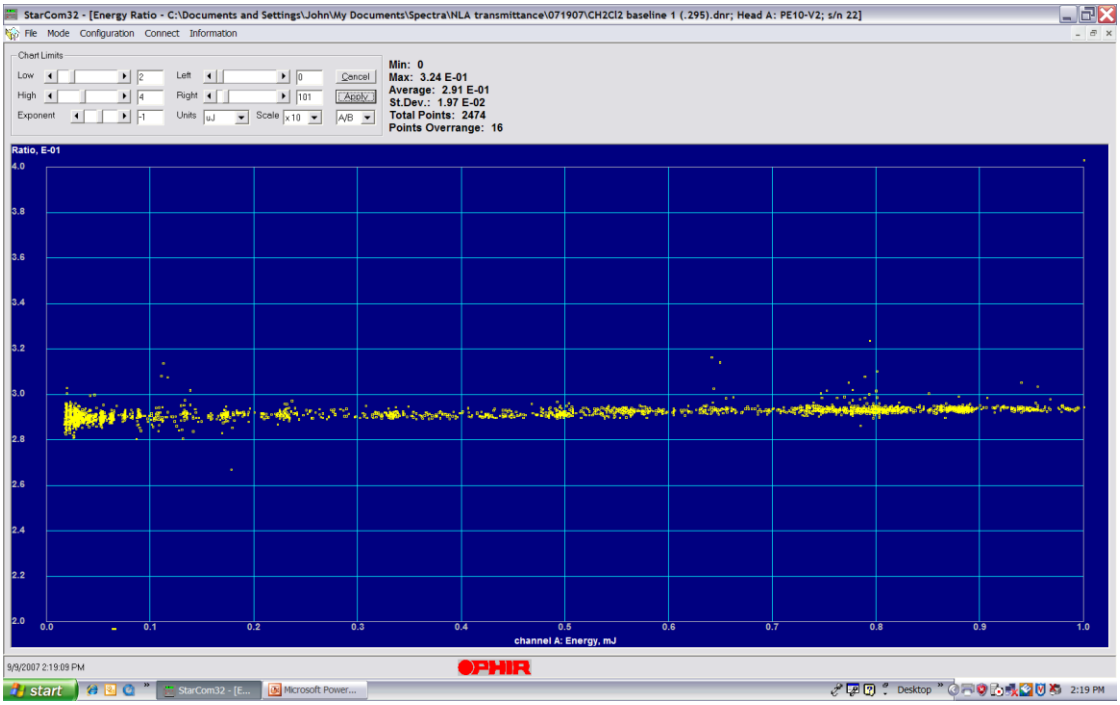

Figure B-6. Example of data acquired from a CH_2Cl_2 solvent only sample.

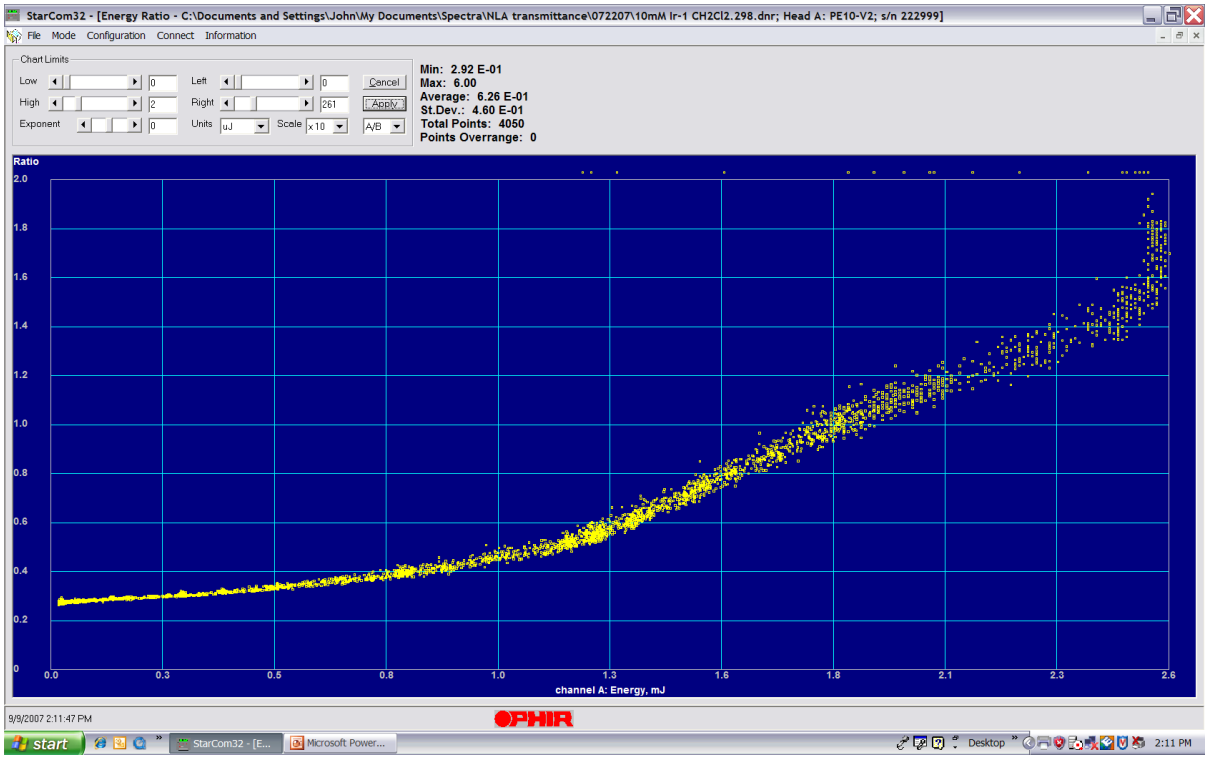

Figure B-7. Example data for a sample exhibiting a nonlinear response.

Shut down

(1) Power down laser. If unsure of laser power down sequence, contact the laser lab manager prior to starting the experiment for a full laser operation orientation.

(2) Turn off energy meter. Disconnect both detectors and computer interface. Return the energy meter, power cord, and cables to the cabinet drawer marked "energy meter."

(3) Cover all optics and filters with plastic bags.

(4) Clean experiment area, remove and properly dispose of all samples and return sample cells.

Plotting data

The data file generated from the Ophir StarCom32 software will be saved as a .dnr file and is easily imported directly into a graphing program such as Sigmaplot. The raw data contains two rows, one for each channel. The first row is channel A which represents detector 1 and the second row is channel B and represents detector 2.

The following is an example of how to create a plot of input energy versus output energy.

(1) Insert a blank column after channel A.

(2) Select quick transform from the drop down menu. Enter col(2) = col(1) / 0.291 then press run. The correction factor 0.291 is the correction factor found earlier and is used here only as an example. It is important that you use the proper value as found for your experiment. Col(2) will contain the energy values equivalent to the energy input to the sample corrected for the solvent and the cell.

(3) Column 3 contains the actual energy transmitted through the sample and can be used directly as the energy output values.

(4) Create a graph selecting column 2 as the x-axis and column 3 as the y-axis. Repeat as necessary for solvent and samples data. The graph should resemble Figure B-8.

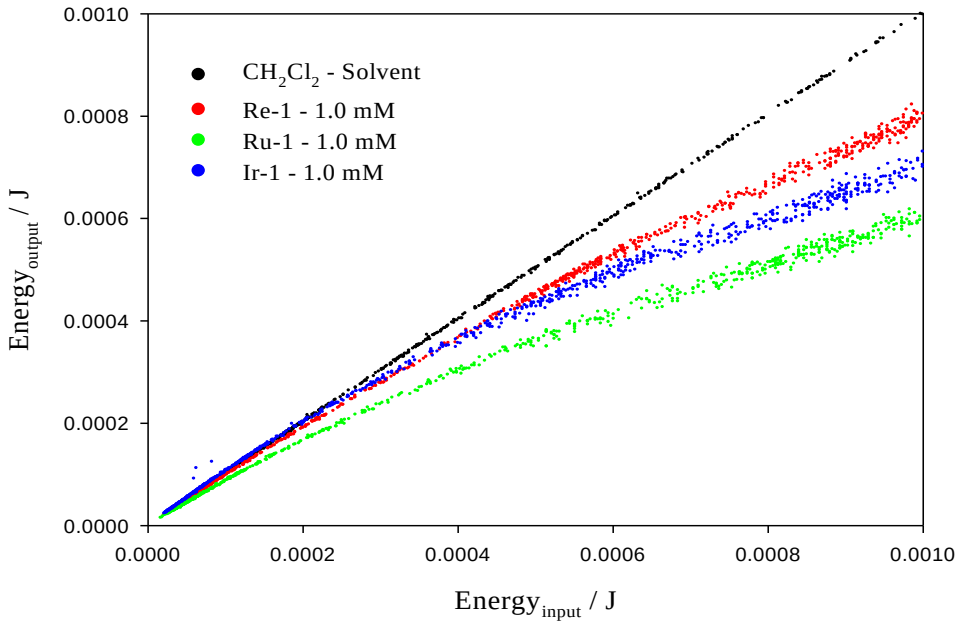

Figure B-8. Sample graph of nonlinear absorbance data.

When the graph is complete, the solvent data will represent 100% transmittance and be presented as a straight line (line of constant slope). For samples that exhibit a nonlinear response, the data points will deviate from "linear" and will present a line with a changing slope. For samples that do not exhibit 100% transmittance from the start of the experiment but have initial absorbance that is linear, the slope will be constant but offset from the solvent line.

The following is an example of how to create a plot of transmission (y-axis) versus input energy (x-axis).

(1) Insert a blank column after channel A.

(2) Select quick transform from the drop down menu. Enter col(2) = col(1) / 0.291, press run. Col(2) will then contain the energy values equivalent to the energy input to the sample corrected for the solvent and the cell.

(3) Select quick transform from the drop down menu. Enter col(4) = col(3) / col(2), press run.

(4) Column 4 represents transmission through the sample.

(5) Create a graph selecting column 2 as the x-axis and column 4 as the y-axis. Repeat as necessary for solvent and sample data. The graph should resemble Figure B-9. Often the input energy is plotted on a logarithmic scale to better represent the nonlinear nature of the data.

When the graph is complete, the solvent data will represent 100% transmittance and be presented as a straight line (line of zero slope). For samples that exhibit a nonlinear response, the data points will deviate from "linear" and will present as a line with a changing slope. For samples which do not present 100% transmittance from the start of the experiment but have initial absorbance that is linear, the slope will initially be zero and originating from a value equal to the initial transmittance then deviate as the transmission becomes nonlinear.

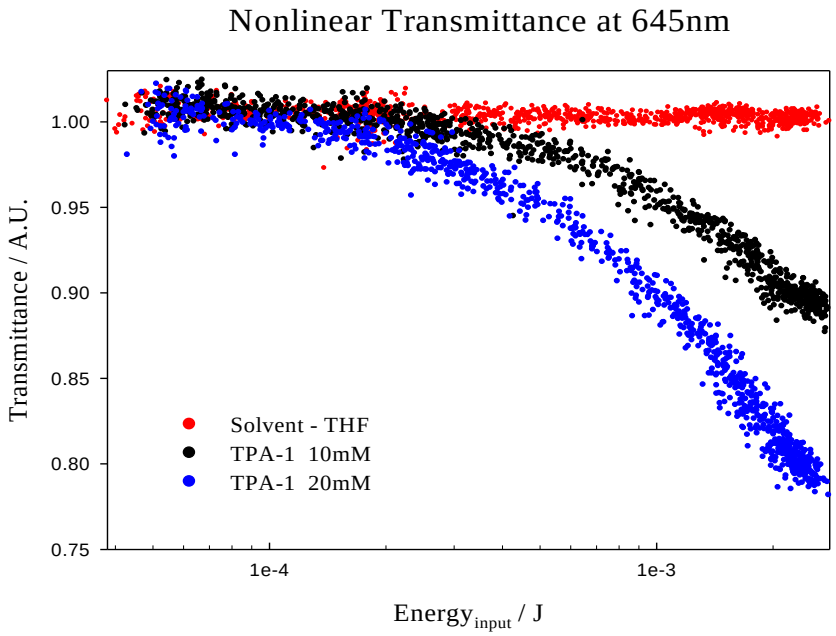

Figure B-9. Sample graph of nonlinear transmission data.

LIST OF REFERENCES

1. Kim, K.-Y.; Farley, R. T.; Schanze, K. S., An iridium(III) complex that exhibits dual mechanism nonlinear absorption. *Journal of Physical Chemistry B* **2006,** 110, (35), 17302-17304.

2. Balzani, V.; Moggi, L.; Manfrin, M. F.; Bolletta, F., Quenching and sensitization processes of coordination-compounds. *Coordination Chemistry Reviews* **1975,** 15, (4), 321-433.

3. Crosby, G. A., Spectroscopic investigations of excited-states of transition-metal complexes. *Accounts of Chemical Research* **1975,** 8, (7), 231-238.

4. Dearmond, M. K.; Myrick, M. L., The life and times of $[Ru(bpy)_3]^{2+}$ - Localized orbitals and other strange occurrences. *Accounts of Chemical Research* **1989,** 22, (10), 364-370.

5. Juris, A.; Balzani, V.; Barigelletti, F.; Campagna, S.; Belser, P.; Vonzelewsky, A., Ru(II) polypyridine complexes - photophysics, photochemistry, electrochemistry, and chemi-luminescence. *Coordination Chemistry Reviews* **1988,** 84, 85-277.

6. Kalyanasundaram, K., Photophysics, Photochemistry and solar-energy conversion with tris(bipyridyl)ruthenium(II) and its analogs. *Coordination Chemistry Reviews* **1982,** 46, (OCT), 159-244.

7. Meyer, T. J., Excited-state electron-transfer. *Progress in Inorganic Chemistry* **1983,** 30, 389-440.

8. Braterman, P. S.; Heath, G. A.; Yellowlees, L. J., Absorption and emission in tris(2,2'-bipyridyl)ruthenium(II) - Effects of excited-state asymmetry. *Journal of the Chemical Society-Dalton Transactions* **1985**, (6), 1081-1086.

9. Cunningham, G. B.; Li, Y.; Liu, S.; Schanze, K. S., Photoluminescence and Electroluminescence of d^6 metal-organic conjugated oligomers: correlation of photophysics and device performance. *Journal of Physical Chemistry B* **2003,** 107, (46), 12569-12572.

10. Du, H.; Fuh, R. C. A.; Li, J. Z.; Corkan, L. A.; Lindsey, J. S., PhotochemCAD: A computer-aided design and research tool in photochemistry. *Photochemistry and Photobiology* **1998,** 68, (2), 141-142.

11. Crosby, G. A.; Demas, J. N., Measurement of photoluminescence quantum yields. Review. *Journal of Physical Chemistry.* **1971,** 75, (8), 991-1024.

12. Hager, G. D.; Crosby, G. A., Charge-transfer excited-states of ruthenium(II) complexes.1. Quantum yield and decay measurements. *Journal of the American Chemical Society* **1975,** 97, (24), 7031-7037.

13. Hager, G. D.; Watts, R. J.; Crosby, G. A., Charge-transfer excited states of ruthenium(II) complexes. II. Relation of level parameters to molecular structure. *Journal of the American Chemical Society* **1975,** 97, (24), 7037-42.

14. Harrigan, R. W.; Crosby, G. A., Variable temperature sample mount for luminescent powders. *Spectrochimica Acta Part A-Molecular Spectroscopy* **1970,** A 26, (11), 2225-&.

15. Lakowicz Joseph R., *Principles of Fluorescence Spectroscopy*. 2nd ed.; Kluwer Academic/Plenum: New York, 1999; p 698.

16. Wang, B.; Wasielewski, M. R., Design and synthesis of metal ion-recognition-induced conjugated polymers: An approach to metal ion sensory materials. *Journal of the American Chemical Society* **1997,** 119, (1), 12-21.

17. Liu, S.; Schanze, K. S., Solvent tuned excited state configuration mixing in a p-conjugated metal-organic oligomer. *Chemical Communications (Cambridge, United Kingdom)* **2004**, (13), 1510-1511.

18. Liu, Y.; Jiang, S. J.; Schanze, K. S., Amplified quenching in metal-organic conjugated polymers. *Chemical Communications* **2003**, (5), 650-651.

19. Whittle, C. E.; Weinstein, J. A.; George, M. W.; Schanze, K. S., Photophysics of diimine platinum(II) bis-acetylide complexes. *Inorganic Chemistry* **2001,** 40, (16), 4053-4062.

20. Wang, Y.; Liu, S.; Pinto, M. R.; Dattelbaum, D. M.; Schoonover, J. R.; Schanze, K. S., Excited-state structure and delocalization in Ruthenium(II)-bipyridine complexes that contain phenyleneethynylene substituents. *Journal of Physical Chemistry A* **2001,** 105, (49), 11118-11127.

21. Glusac, K. D.; Jiang, S.; Schanze, K. S., Photophysics of Ir(III) complexes with oligo(arylene ethynylene) ligands. *Chemical Communications (Cambridge, United Kingdom)* **2002**, (21), 2504-2505.

22. Ley, K. D.; Li, Y. T.; Johnson, J. V.; Powell, D. H.; Schanze, K. S., Synthesis and characterization of pi-conjugated oligomers that contain metal-to-ligand charge transfer chromophores. *Chemical Communications* **1999**, (17), 1749-1750.

23. Walters, K. A.; Dattelbaum, D. M.; Ley, K. D.; Schoonover, J. R.; Meyer, T. J.; Schanze, K. S., Photophysics of phenyleneethynylene metal-organic oligomers. Probing the lowest excited state by time-resolved IR spectroscopy. *Chemical Communications (Cambridge, United Kingdom)* **2001**, (18), 1834-1835.

24. Rogers, J. E.; Slagle, J. E.; McLean, D. G.; Sutherland, R. L.; Sankaran, B.; Kannan, R.; Tan, L. S.; Fleitz, P. A., Understanding the one-photon photophysical properties of a two-photon absorbing chromophore. *Journal of Physical Chemistry A* **2004,** 108, (26), 5514-5520.

25. Maury, O.; LeBozec, H., Molecular engineering of octupolar NLO molecules and materials based on bipyridyl metal complexes. *Accounts of Chemical Research* **2005,** 38, (9), 691-704.

26. Zheng, Q. D.; He, G. S.; Prasad, P. N., Novel two-photon-absorbing, 1,10-phenanthroline-containing pi-conjugated chromophores and their nickel(II) chelated complexes with quenched emissions. *Journal of Materials Chemistry* **2005,** 15, (5), 579-587.

27. Bhawalkar, J. D.; He, G. S.; Prasad, P. N., Nonlinear multiphoton processes in organic and polymeric materials. *Reports on Progress in Physics* **1996,** 59, (9), 1041-1070.

28. Ehrlich, J. E.; Wu, X. L.; Lee, I. Y. S.; Hu, Z. Y.; Rockel, H.; Marder, S. R.; Perry, J. W., Two-photon absorption and broadband optical limiting with bis-donor stilbenes. *Optics Letters* **1997,** 22, (24), 1843-1845.

29. Marius Albota, D. B., Jean-Luc Brédas, Jeffrey E. Ehrlich, Jia-Ying Fu, Ahmed A. Heikal, Samuel E. Hess, Thierry Kogej, Michael D. Levin, Seth R. Marder, Dianne McCord-Maughon, Joseph W. Perry, Harald Röckel, Mariacristina Rumi, Girija Subramaniam, Watt W. Webb, Xiang-Li Wu, and Chris Xu, Design of organic molecules with large two-photon absorption cross sections. *Science* **1998,** 281, 1653-1656.

30. McKay, T. J.; Bolger, J. A.; Staromlynska, J.; Davy, J. R., Linear and nonlinear optical properties of platinum-ethynyl. *Journal of Chemical Physics* **1998,** 108, (13), 5537-5541.

31. McKay, T. J.; Staromlynska, J.; Davy, T. R.; Bolger, J. A., Cross sections for excited-state absorption in a Pt: ethynyl complex. *Journal of the Optical Society of America B-Optical Physics* **2001,** 18, (3), 358-362.

32. Reinhardt, B. A.; Brott, L. L.; Clarson, S. J.; Dillard, A. G.; Bhatt, J. C.; Kannan, R.; Yuan, L. X.; He, G. S.; Prasad, P. N., Highly active two-photon dyes: Design, synthesis, and characterization toward application. *Chemistry of Materials* **1998,** 10, (7), 1863-1874.

33. Staromlynska, J.; McKay, T. J.; Bolger, J. A.; Davy, J. R., Evidence for broadband optical limiting in a Pt: ethynyl compound. *Journal of the Optical Society of America B-Optical Physics* **1998,** 15, (6), 1731-1736.

34. Silly, M. G.; Porres, L.; Mongin, O.; Chollet, P. A.; Blanchard-Desce, M., Optical limiting in the red-NIR range with soluble two-photon absorbing molecules. *Chemical Physics Letters* **2003,** 379, (1-2), 74-80.

35. Drobizhev, M.; Karotki, A.; Rebane, A.; Spangler, C. W., Dendrimer molecules with record large two-photon absorption cross section. *Optics Letters* **2001,** 26, (14), 1081-1083.

36. Kannan, R.; He, G. S.; Lin, T. C.; Prasad, P. N.; Vaia, R. A.; Tan, L. S., Toward highly active two-photon absorbing liquids. Synthesis and characterization of 1,3,5-triazine-based octupolar molecules. *Chemistry of Materials* **2004,** 16, (1), 185-194.

37. Sutherland, R. L.; Brant, M. C.; Heinrichs, J.; Rogers, J. E.; Slagle, J. E.; McLean, D. G.; Fleitz, P. A., Excited-state characterization and effective three-photon absorption model of two-photon-induced excited-state absorption in organic push-pull charge-transfer chromophores. *Journal of the Optical Society of America B-Optical Physics* **2005,** 22, (9), 1939-1948.

38. Gao, Y. W.; Potasek, M. J., Effects of excited-state absorption on two-photon absorbing materials. *Applied Optics* **2006,** 45, (11), 2521-2528.

39. Prasad P N. Williams D.J., *Introduction to Nonlinear Optical Effects in Molecules and Polymers*. Wiley: New York, 1991; p 307.

40. Powell, C. E.; Humphrey, M. G., Nonlinear optical properties of transition metal acetylides and their derivatives. *Coordination Chemistry Reviews* **2004,** 248, (7-8), 725-756.

41. Oudar, J. L.; Chemla, D. S., Hyperpolarizabilities of nitroanilines and their relations to excited-state dipole-moment. *Journal of Chemical Physics* **1977,** 66, (6), 2664-2668.

42. Chemla D.S. Zyss J., *Nonlinear Optical Properties of Organic Molecules and Ccrystals*. Academic Press: Orlando, 1987.

43. Dalton, L. R.; Harper, A. W.; Robinson, B. H., The role of London forces in defining noncentrosymmetric order of high dipole moment high hyperpolarizability chromophores in electrically poled polymeric thin films. *Proceedings of the National Academy of Sciences of the United States of America* **1997,** 94, (10), 4842-4847.

44. Liao, Y.; Eichinger, B. E.; Firestone, K. A.; Haller, M.; Luo, J. D.; Kaminsky, W.; Benedict, J. B.; Reid, P. J.; Jen, A. K. Y.; Dalton, L. R.; Robinson, B. H., Systematic study of the structure-property relationship of a series of ferrocenyl nonlinear optical chromophores. *Journal of the American Chemical Society* **2005,** 127, (8), 2758-2766.

45. Marder, S. R., Organic nonlinear optical materials: where we have been and where we are going. *Chemical Communications* **2006**, (2), 131-134.

46. Prasad, P. N.; Perrin, E.; Samoc, M., A coupled anharmonic oscillator model for optical nonlinearities of conjugated organic structures. *The Journal of Chemical Physics* **1989,** 91, (4), 2360.

47. McWilliams, P. C. M.; Soos, Z. G., Interchain dispersion and second hyperpolarizability of conjugated polymers. *The Journal of Chemical Physics* **1991,** 95, (3), 2127.

48. Karna, S. P.; Keshari, V.; Prasad, P. N., Geometrical Effect On The Nonlinear-Optical Properties Of Model Rigid-Rod Polymers - Ab-initio time-dependent coupled Hartree-Fock studies. *Chemical Physics Letters* **1995,** 234, (4-6), 390-394.

49. Tang, B. Z.; Xu, H.; Lam, J. W. Y.; Lee, P. P. S.; Xu, K.; Sun, Q.; Cheuk, K. K. L., C60-Containing poly(1-phenyl-1-alkynes): Synthesis, light emission, and optical limiting. *Chemistry of Materials* **2000,** 12, (5), 1446-1455.

50. Payne, D. J.; Hopkins, R. A.; Eilert, B. G.; Noojin, G. D.; Stolarski, D. J.; Thomas, R. J.; Cain, C. P.; Hengst, G. T.; Kennedy, P. K.; Jost, T. R.; Rockwell, B. A., Comparative study of laser damage threshold energies in the artificial retina. *Journal of Biomedical Optics* **1999,** 4, (3), 337-344.

51. Roach, W. P.; Johnson, T. E.; Rockwell, B. A., Proposed maximum permissible exposure limits for ultrashort laser pulses. *Health Physics* **1999,** 76, (4), 349-354.

52. Barat, K. Laser Pointer Safety. http://www.hps.org/hpspublications/articles/laser.html (July 2007),

53. Birge, R. R., Two-photon spectroscopy of protein-bound chromophores. *Accounts of Chemical Research* **1986,** 19, (5), 138-146.

54. Cho, B. R.; Son, K. H.; Lee, S. H.; Song, Y. S.; Lee, Y. K.; Jeon, S. J.; Choi, J. H.; Lee, H.; Cho, M. H., Two photon absorption properties of 1,3,5-tricyano-2,4,6-tris(styryl)benzene derivatives. *Journal of the American Chemical Society* **2001,** 123, (41), 10039-10045.

55. Li, F.; Song, Y. L.; Yang, K.; Liu, S. T.; Li, C. F.; Wu, Y. Q.; Zuo, X.; Yu, C. X.; Zhu, P. W., Determination of nonlinear absorption mechanisms using a single pulse width laser. *Journal of Applied Physics* **1997,** 82, (5), 2004-2006.

56. Sheikbahae, M.; Said, A. A.; Wei, T. H.; Hagan, D. J.; Vanstryland, E. W., Sensitive measurement of optical nonlinearities using a single beam. *IEEE Journal of Quantum Electronics* **1990,** 26, (4), 760-769.

57. Ganeev, R. A.; Ryasnyansky, A. I.; Kodirov, M. K.; Usmanov, T., Nonlinear optical characteristics of C-60 and C-70 films and solutions. *Optics Communications* **2000,** 185, (4-6), 473-478.

58. Beam Concentration. http://optics.mellesgriot.com/opguide/gb_2_3.htm

59. Rogers, J. E.; Slagle, J. E.; Krein, D. M.; Burke, A. R.; Hall, B. C.; Fratini, A.; McLean, D. G.; Fleitz, P. A.; Cooper, T. M.; Drobizhev, M.; Makarov, N. S.; Rebane, A.; Kim, K. Y.; Farley, R.; Schanze, K. S., Platinum acetylide two-photon chromophores. *Inorganic Chemistry* **2007,** 46, (16), 6483-6494.

60. Liu, Y.; Li, Y.; Schanze, K. S., Photophysics of p-conjugated oligomers and polymers that contain transition metal complexes. *Journal of Photochemistry and Photobiology, C: Photochemistry Reviews* **2002,** 3, (1), 1-23.

61. Walters, K. A.; Ley, K. D.; Cavalaheiro, C. S. P.; Miller, S. E.; Gosztola, D.; Wasielewski, M. R.; Bussandri, A. P.; van Willigen, H.; Schanze, K. S., Photophysics of p-conjugated metal-organic oligomers: Aryleneethynylenes that contain the (bpy)Re$(CO)_3$Cl chromophore. *Journal of the American Chemical Society* **2001,** 123, (34), 8329-8342.

62. Gillispie, G. D.; Lim, E. C., Energy-Gap Correlation of internal-conversion rates. *Chemical Physics Letters* **1979,** 63, (1), 193-198.

63. Wittmann, H. F.; Friend, R. H.; Khan, M. S.; Lewis, J., Optical spectroscopy of platinum and palladium-containing poly-ynes. *Journal of Chemical Physics* **1994,** 101, (4), 2693-2698.

64. Meech, S. R.; Phillips, D., Photophysics of some common fluorescence standards. *Journal of Photochemistry* **1983,** 23, (3), 193-217.

65. Harriman, A., Photochemistry of a surfactant derivative of tris(2,2'-Bipyridyl)Ruthenium(II). *Journal of the Chemical Society-Chemical Communications* **1977**, (21), 777-778.

66. Spangler, C. W., Recent development in the design of organic materials for optical power limiting. *Journal of Materials Chemistry* **1999,** 9, (9), 2013-2020.

67. Sun, Y. P.; Riggs, J. E.; Liu, B., Optical limiting properties of [60]fullerene derivatives. *Chemistry of Materials* **1997,** 9, (5), 1268-1272.

68. Tutt, L. W.; Kost, A., Optical limiting performance of C60 and C70 solutions. *Nature (London, United Kingdom)* **1992,** 356, (6366), 225-6.

69. McLean, D. G.; Sutherland, R. L.; Brant, M. C.; Brandelik, D. M.; Fleitz, P. A.; Pottenger, T., Nonlinear absorption study of a C-60-toluene solution. *Optics Letters* **1993,** 18, (11), 858-860.

70. Li, C. F.; Si, J. H.; Yang, M.; Wang, R. B.; Zhang, L., Excited-state nonlinear absorption in multi-energy-level molecular-systems. *Physical Review A* **1995,** 51, (1), 569-575.

71. Gvishi, R.; Narang, U.; Ruland, G.; Kumar, D. N.; Prasad, P. N., Novel, organically doped, sol-gel-derived materials for photonics: Multiphasic nanostructured composite monoliths and optical fibers. *Applied Organometallic Chemistry* **1997,** 11, (2), 107-127.

72. Joshi, M. P.; Mishra, S. R.; Rawat, H. S.; Mehendale, S. C.; Rustagi, K. C., Investigation of optical limiting in C-60 solution. *Applied Physics Letters* **1993,** 62, (15), 1763-1765.

73. Kost, A.; Tutt, L.; Klein, M. B.; Dougherty, T. K.; Elias, W. E., Optical limiting with C-60 in polymethyl methacrylate. *Optics Letters* **1993,** 18, (5), 334-336.

74. Wang, Y.; Schanze, K. S., Photochemical probes of intramolecular electron and energy transfer. *Chemical Physics* **1993,** 176, (2-3), 305-19.

75. Ley, K. D.; Whittle, C. E.; Bartberger, M. D.; Schanze, K. S., Photophysics of pi-conjugated polymers that incorporate metal to ligand charge transfer chromophores. *Journal of the American Chemical Society* **1997,** 119, (14), 3423-3424.

76. Romero, F. M.; Ziessel, R., Preparation of novel mixed tritopic oligopyridine ligands built with chelating spacers and using palladium(0) catalyzed coupling reactions. *Tetrahedron Letters* **1994,** 35, (49), 9203-9206.

77. Suh, S. C.; Suh, M. C.; Shim, S. C., Photoconductivity of 3,5-dinitrobenzoate of poly[1-phenyl-1-penten-3-yn-5-ol] (DN-PPPYO) blended with poly[4-(p-N,N-diphenylaminophenyl)-1-phenyl-1-buten-3-yne] (PPAPBEY) as a hole transporting polymer. *Macromolecular Chemistry and Physics* **1999,** 200, (9), 1991-1997.

78. Sprouse, S.; King, K. A.; Spellane, P. J.; Watts, R. J., Photophysical effects of metal-carbon.sigma. bonds in ortho-metalated complexes of iridium(III) and rhodium(III). *Journal of the American Chemical Society* **1984,** 106, (22), 6647-6653.

BIOGRAPHICAL SKETCH

Being born in Victorville, California and moving to Aviano, Italy at the age of seven weeks was a foreshadowing of things to come. As the son of a helicopter pilot in the United States Air Force, I was blessed to be able to see more of the world before I was ten than most people get to see in a lifetime. I spent most of my primary and secondary school years in Marion, Ohio and went on to accomplish my undergraduate and masters degrees at Wright State University in Dayton, Ohio. It was at Wright State where I developed a love for teaching and chemistry. My penchant for not making things easy took me into the United States Air Force. I earned my aeronautical rating as a navigator and what followed was a wonderful thirteen year flying career which brought me to many wonderful and not so wonderful places. I married at about the same time I started my aviation career and was blessed with two gorgeous children Cameron and Kelsey. Sadly, marriage ended at about the same time as flying but the change prompted my return to teaching and chemistry. I am fortunate to know that I will be returning to the United States Air Force Academy to teach, but more importantly I will be returning to be with my children.